COMBUSTION RESEARCH FACILITY

SAND2016-9411PE

Optical Diagnostics in Direct-Injection, Swirl-Supported Diesel Engine

Kan Zha, Ph.D.

Sandia National Laboratories

Sandia National Laboratories is a multi-program laboratory managed and operated by Sandia Corporation, a wholly owned subsidiary of Lockheed Martin Corporation, for the U.S. Department of Energy's National Nuclear Security Administration under contract DE-AC04-94AL85000

Background

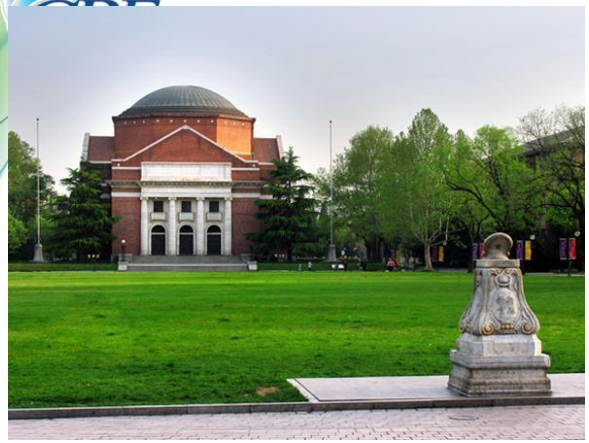

- B.S., Automotive Engineering 2004

  Tsinghua University, Beijing, P. R. China

- M.S., Ph.D., Mechanical Engineering 2013

  Wayne State University, Detroit, MI

- Post-doctoral Appointee 2013-Present

  Sandia National Laboratories, Livermore, CA

Outline

- **Motivation**
- High-speed in-cylinder soot optical thermometry
- Particle image velocimetry (PIV) inside an optical engine for swirl asymmetry quantification
- Quantification of in-cylinder mixture preparation with fuel tracer planar laser-induced fluorescence (PLIF) technique
- Research outlook

Motivation: why we need combustion to save the world?

Google pictures for noncommercial use

Combustion-driven power plants have competitively high capacity factor.

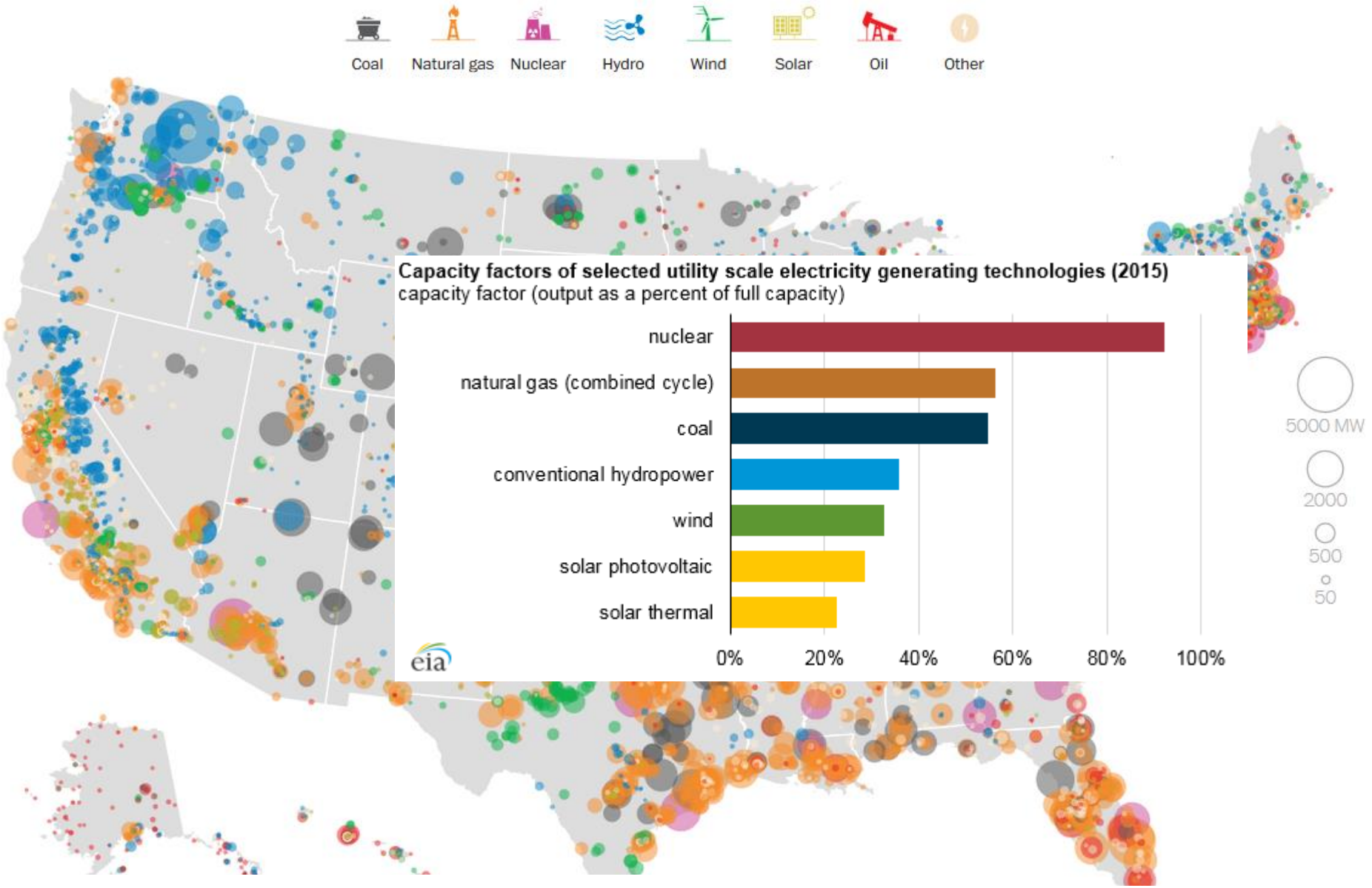

Downloaded from
https://www.washingtonpost.com/graphics/national/power-plants/

Plant capacity by power source in megawatts

Industrial processes (such as steelmaking, forging, glassmaking) still need combustion.

Google pictures for noncommercial use

Internal Combustion Engines (ICEs) will remain the dominant transportation powerplant for several more decades to come.

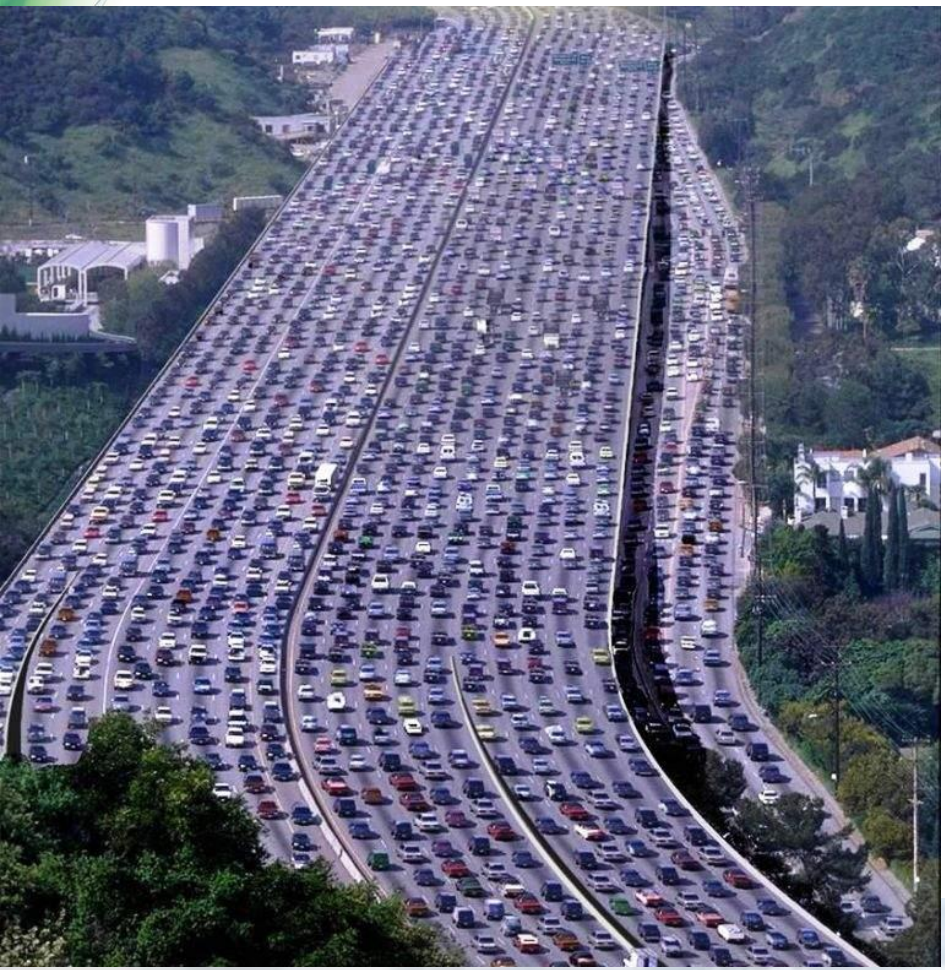

Google pictures for noncommercial use

Advanced Internal Combustion Engines Technical Barriers

Why in-cylinder combustion is one of the most challenging environment to investigate in the world?

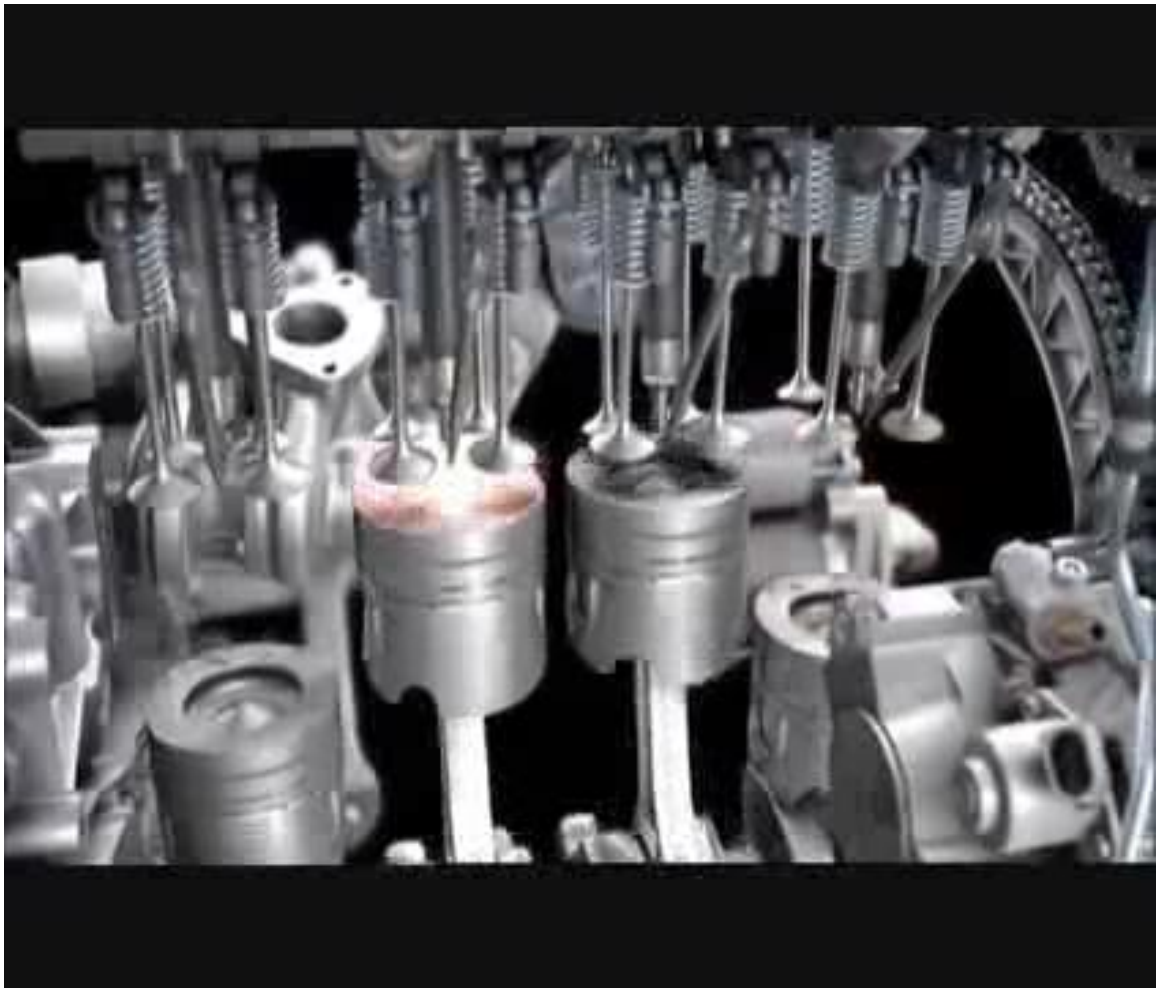

Adapted from video: https://www.youtube.com/watch?v=48EllCCGxu8

Why in-cylinder combustion is one of the most challenging environment to investigate in the world?

- For each cycle, a limited time is allowed for combustion to complete!

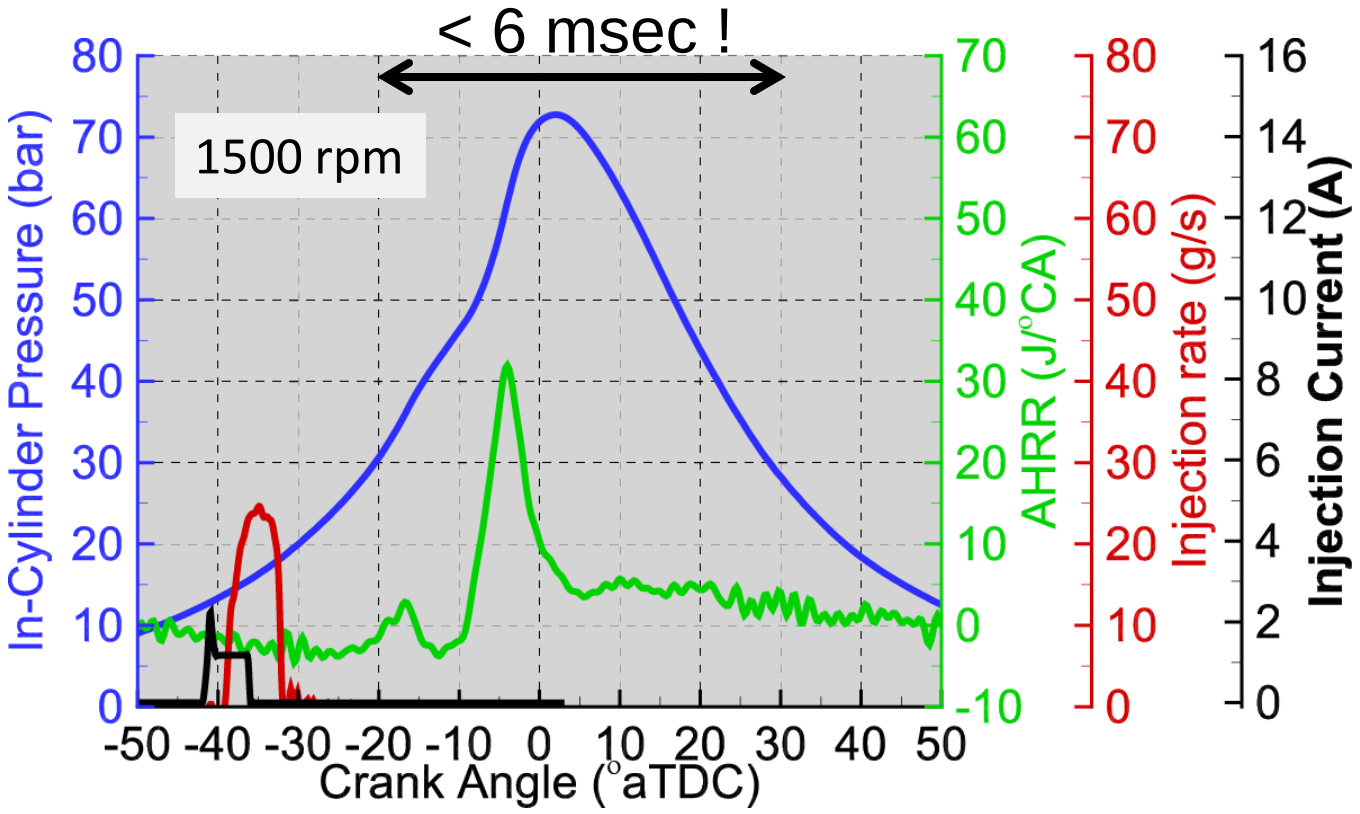

Why in-cylinder combustion is one of the most challenging environment to investigate in the world?

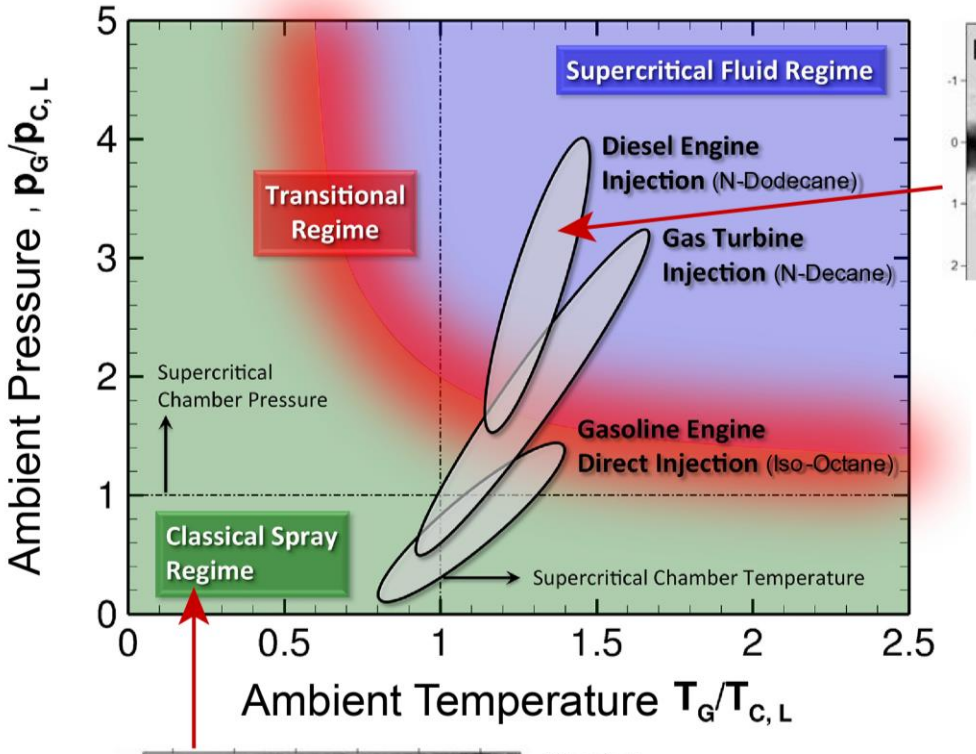

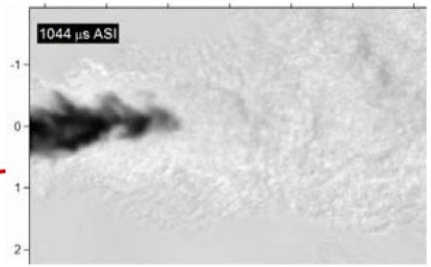

Diffusion dominated mixing (supercritical fluid)

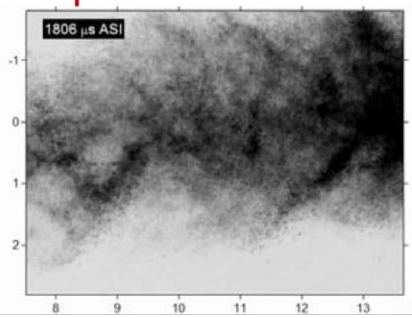

Classical atomization and spray dynamics

- Multi-physics, multi-scale
- Single/two-phase flows
- Turbulence-chemistry-radiation coupled
- Transient three-dimensional
- Rapid periodic swings of pressure and temperature

[1] Adapted from R. N. Dahms and J. C. Oefelein. On the transition between two-phase and single-phase interface dynamics in multicomponent fluids at supercritical pressures. Physics of Fluids, 25: 092103, 2013

Advanced ICEs Efficiency Scientific & Engineering Challenges

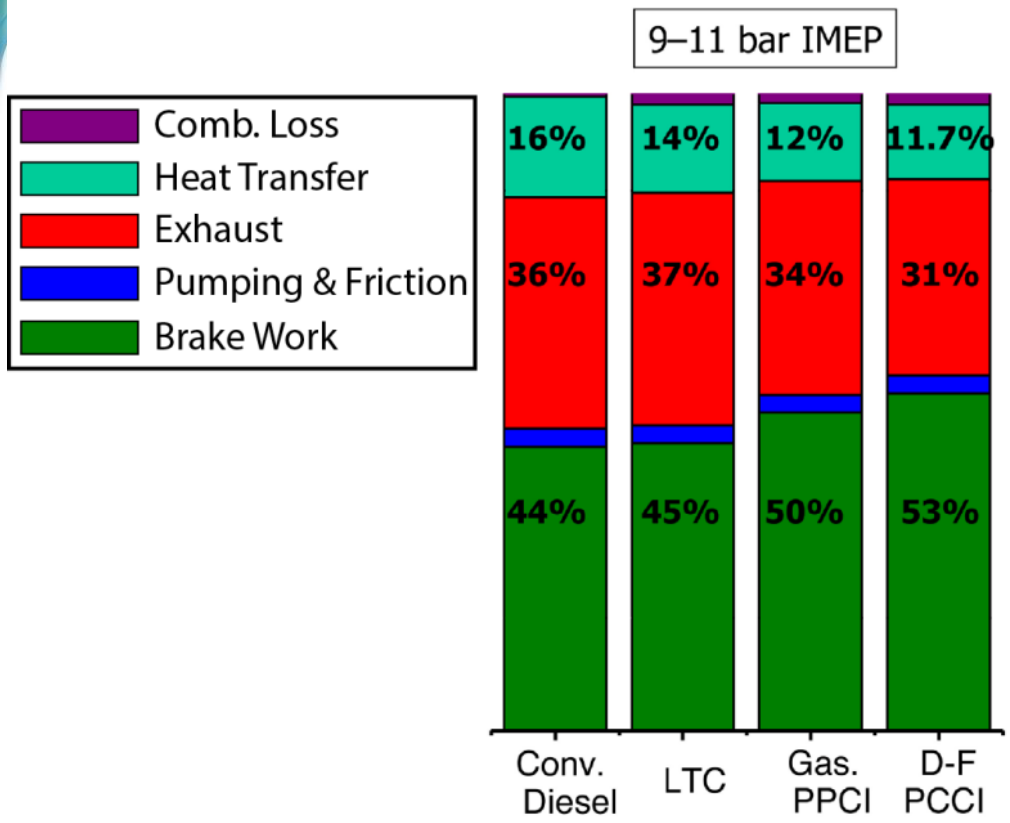

[2] Adapted from David Foster (UW), Transportation Combustion Engine Efficiency Colloquium, 2010 and Paul C. Miles (Sandia), SAND2013-7374c

Heat Transfer

Flow
- Mean flows (Swirl, Tumble)
- Turbulence

Temperature & Composition
- CR
- Lambda
- EGR
- Combustion Phasing/Duration
- Soot radiation

Chamber Geometry
- Chamber shape
- Bowl shape (re-entrant, shallow bowl)

Exhaust Losses

Work Extraction
- Combustion Phasing/Duration
- Charge Composition (lean, EGR)

Linked to Heat Transfer
- Interacts with gas properties to impact work extraction

Why optical diagnostics are needed for advanced combustion research?

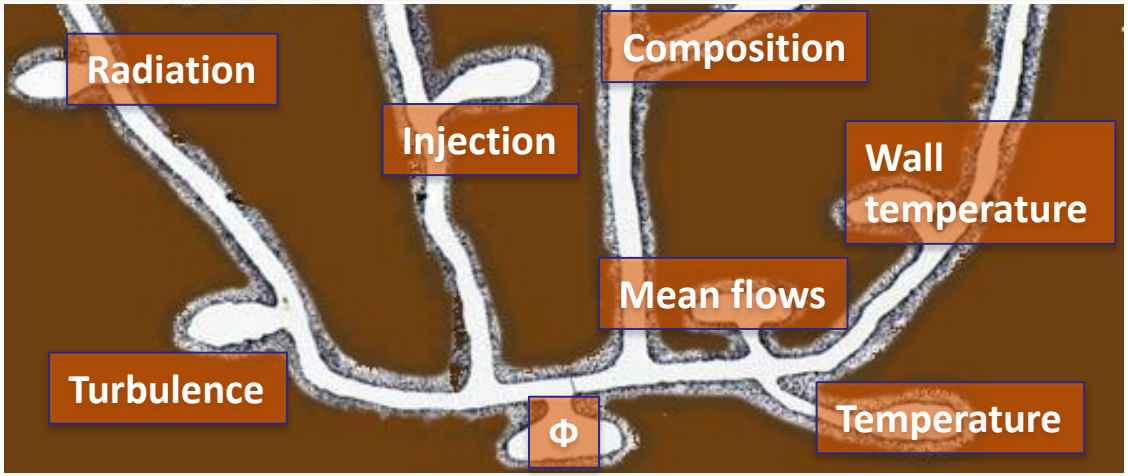

[3] Adapted from K. Dean Edwards, et. al., Defining engine efficiency limits, 17th DEER Conference, 2011

Bowditch piston with transparent windows allows optical access to the combustion chamber while engine is in operation.

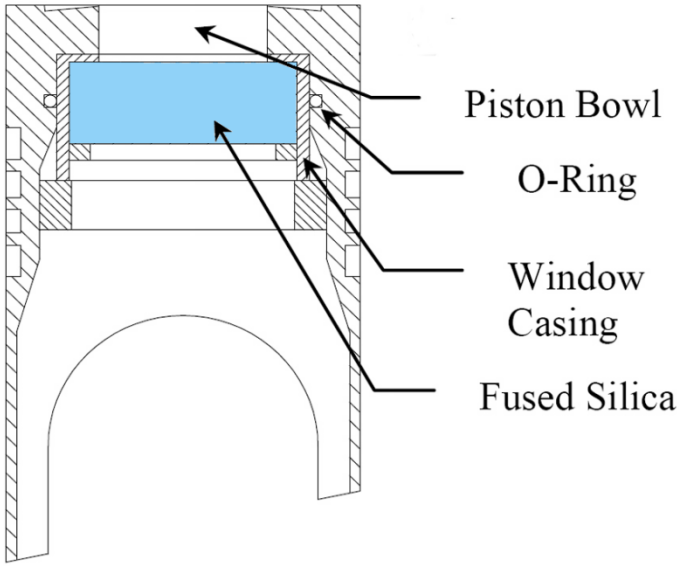

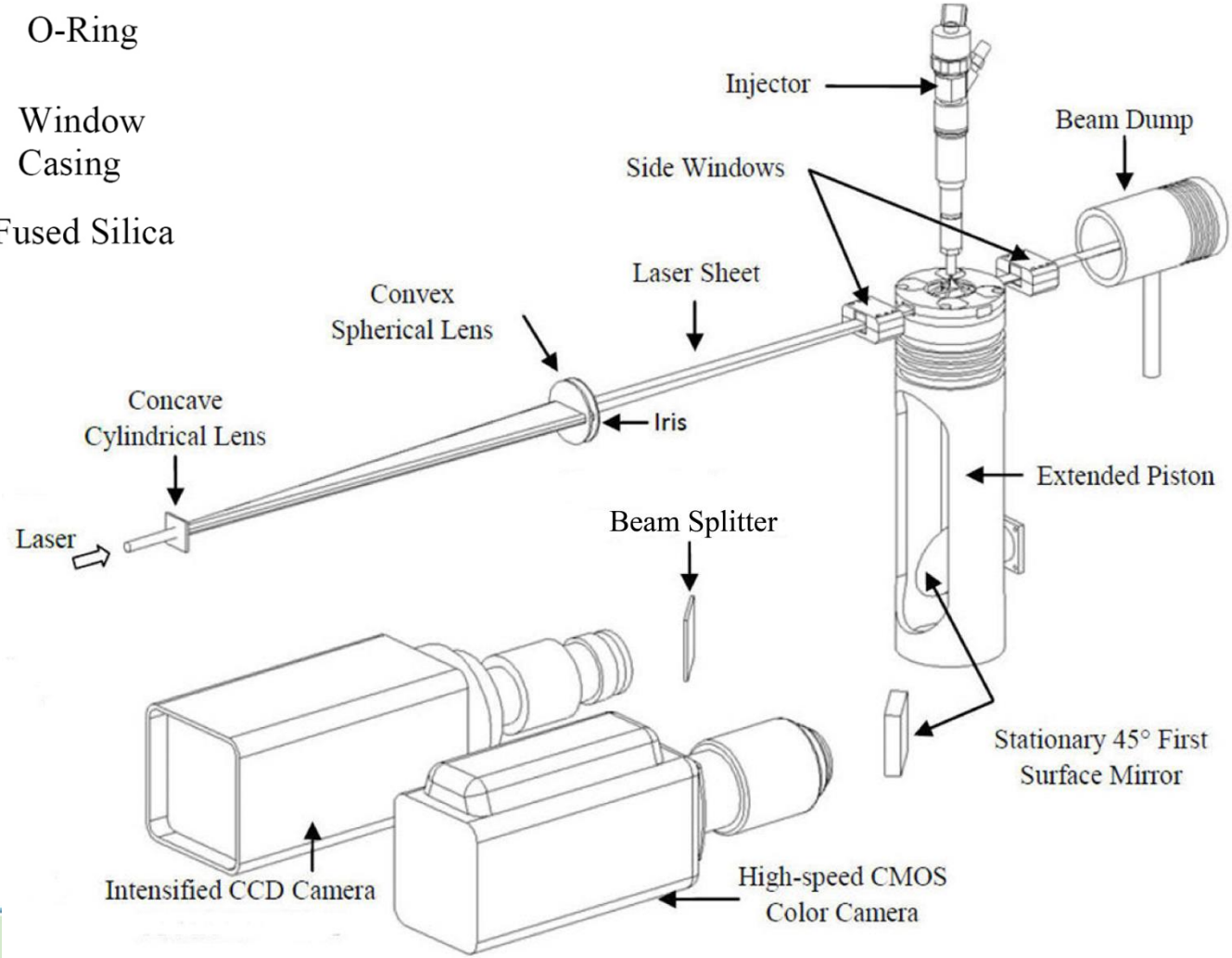

Optical diagnostics provides non-intrusive in-situ measurements of in-cylinder combustion processes.

- Help understand combustion processes in a fundamental level.
- Help identify the root cause for combustion-related problems.
- Create a reliable database for CFD simulation.

Outline

- Motivation
- **High-speed in-cylinder soot optical thermometry**
- Particle image velocimetry (PIV) inside an optical engine for swirl asymmetry quantification
- Quantification of in-cylinder mixture preparation with fuel tracer planar laser-induced fluorescence (PLIF) technique
- Research outlook

Soot is favorable in fuel rich environment, and also temperature sensitive. In-cylinder temperature history is necessary to quantify.

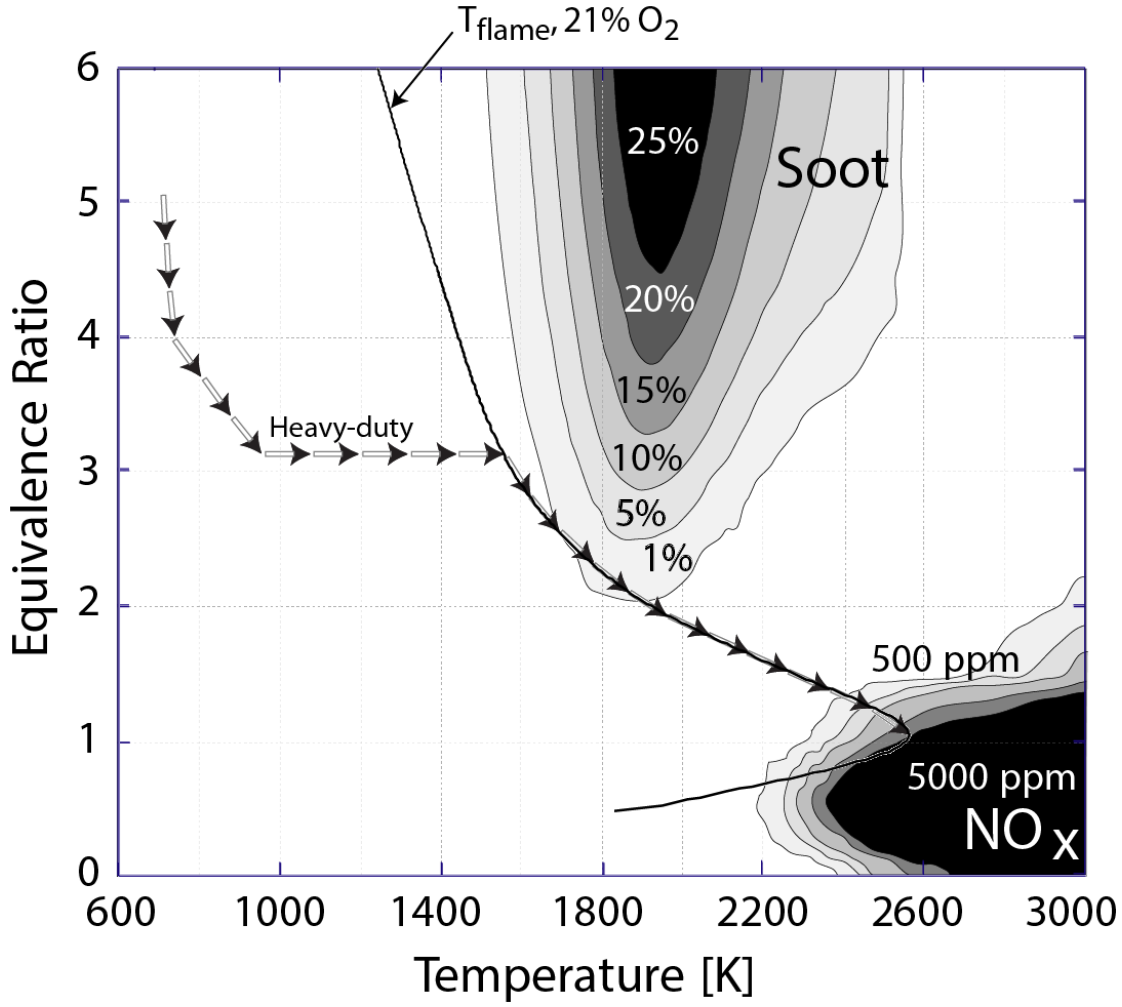

[4] Adapted from Paul Miles (Sandia), 3rd International Symposium on Homogeneous Charge Compression Ignition (HCCI), 2006

Low Temperature Diagnostic Facilities

- State-of-the-art facilities for the study of fundamental problems in internal combustion.
- One-of-a-kind optical engine within climatic chamber provides unique means of investigating effects of extreme temperatures.
- Allows application of optical diagnostics to practical combustion system.
- $2 million+ investment in capital equipment. (US DoD)

Optical Access

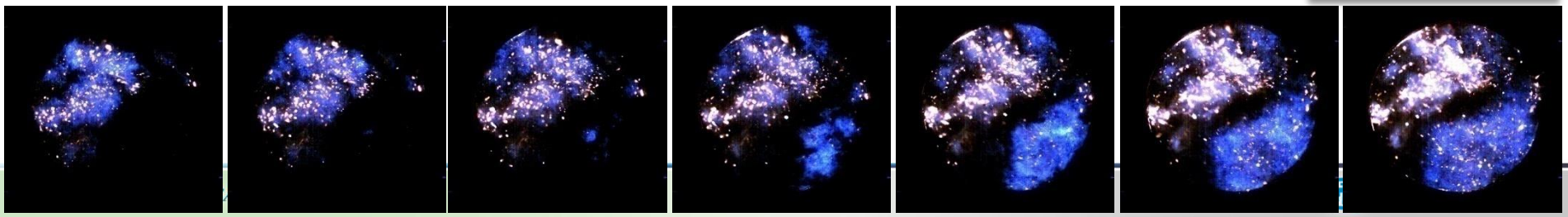

What is two-color optical pyrometry ?

Radiation of soot is modeled as blackbody radiation $E_{b,\lambda}$ weighed by $\varepsilon_{\lambda,KL}$ emissivity of soot

$$E_{soot,\lambda} = \varepsilon_{\lambda,KL} \cdot E_{b,\lambda} = \varepsilon_{\lambda,KL} \cdot \frac{C_1}{\lambda^5 \left[\exp\left(\frac{C_2}{\lambda T_{soot}} \right) - 1 \right]} = \frac{C_1}{\lambda^5 \left[\exp\left(\frac{C_2}{\lambda T_a} \right) - 1 \right]}$$

Soot Temperature Apparent Temperature

Soot emissivity model proposed by Hottel and Broughton [5]:

$$\varepsilon_{\lambda,KL} = 1 - \exp\left(-\frac{KL}{\lambda^{\alpha}} \right)$$

K: function of soot optical properties, and is proportional to the soot volume fraction.
L: path length of radiating media.

Recommended value:
α=1.39 for visible wavelengths λ<800 nm
α=0.95 for infrared wavelengths λ>800 nm
In a recent application, α=1.22-0.245*ln(λ[μm]) proposed by Musculus [6].

[5] Hottel, H.C. and Broughton, F.P., "Determination of True Temperature and Total Radiation from Luminous Gas Flames" Industrial and Engineering Chemistry Analytical Edition, **4**, pp. 166-175, 1932
[6] Musculus, M. P. B., 2005, "Measurements of the Influence of Soot Radiation on In-Cylinder Temperatures and Exhaust NOx in a Heavy-Duty DI Diesel Engine", *SAE Technical Paper* 2005-01-0925, DOI:10.4271/2005-01-0925

$$\varepsilon_{\lambda,KL} = 1 - \exp\left(-\frac{KL}{\lambda^{\alpha}}\right) = \frac{\exp\left(\frac{C_2}{\lambda T_{soot}}\right) - 1}{\exp\left(\frac{C_2}{\lambda T_a}\right) - 1}$$

$$KL = -\lambda^{\alpha} \ln\left[1 - \frac{\exp\left(\frac{C_2}{\lambda T_{soot}}\right) - 1}{\exp\left(\frac{C_2}{\lambda T_a}\right) - 1}\right]$$

The unknown product KL can be eliminated by rewriting the above equation for two specific wavelengths, λ1, λ2, and Ta1, Ta2 under the assumption that KL is the same for both wave bands.

$$-\lambda_1^{\alpha_1} \ln\left[1 - \frac{\exp\left(\frac{C_2}{\lambda_1 T_{soot}}\right) - 1}{\exp\left(\frac{C_2}{\lambda_1 T_{a_1}}\right) - 1}\right] = -\lambda_2^{\alpha_2} \ln\left[1 - \frac{\exp\left(\frac{C_2}{\lambda_2 T_{soot}}\right) - 1}{\exp\left(\frac{C_2}{\lambda_2 T_{a_2}}\right) - 1}\right]$$

Soot temperature T_{soot} can then be solved implicitly, and the back substitution of soot temperature T_{soot} yields product KL .

Previous application of this technique used narrow band pass filters to isolate the two wavelengths, the complex optics alignment is an issue.

Two-Color Pyrometry Implementation on High-speed Color Camera with Wide-band Bayer Filter

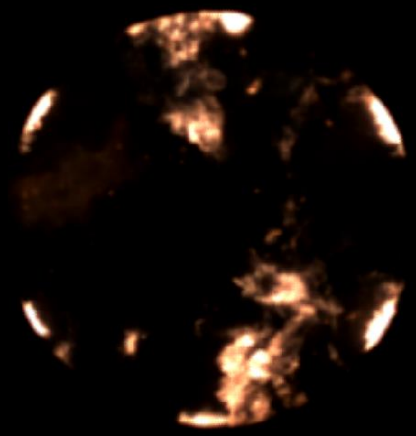

Pixel Count

Red

Green

Blue

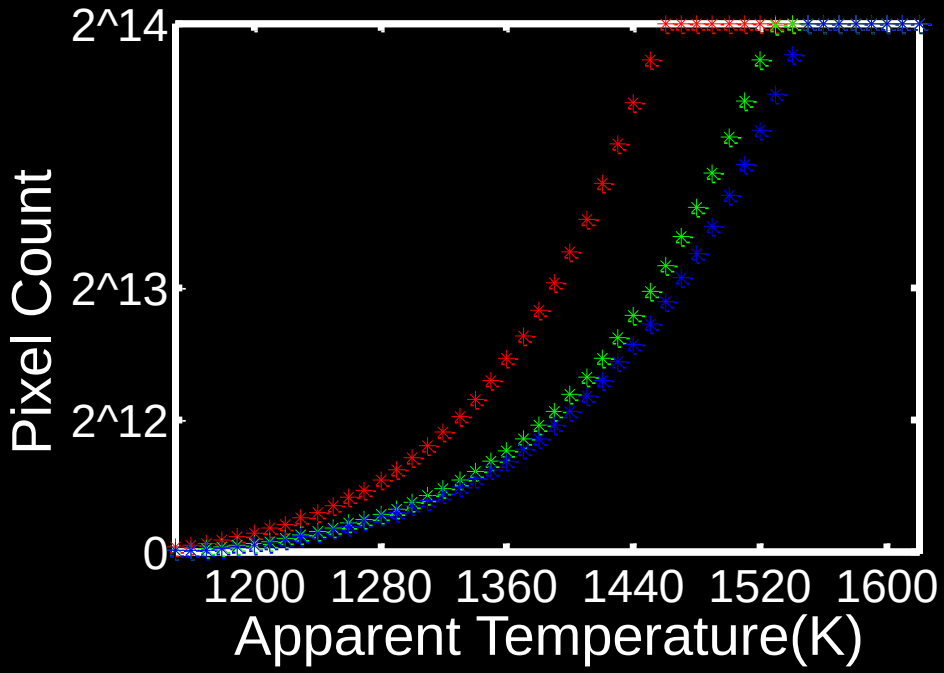

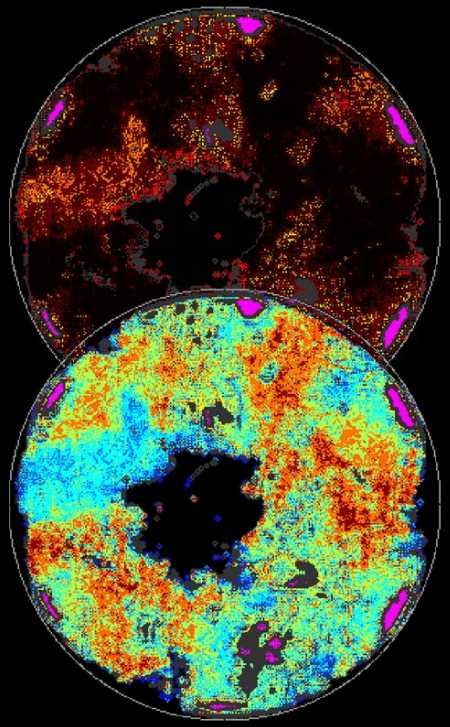

Soot KL

Soot T

Apparent Temperature(K) T_a

Optical System Response Coefficient

$$\int \frac{Q \cdot C_1 \cdot d\lambda}{\lambda^5 \left[\exp\left(\frac{C_2}{\lambda T_a} \right) - 1 \right]} = \int \left[1 - \exp\left(-\frac{KL}{\lambda^\alpha} \right) \right] \cdot \frac{Q \cdot C_1 \cdot d\lambda}{\lambda^5 \left[\exp\left(\frac{C_2}{\lambda T} \right) - 1 \right]}$$

Bayer Filter and Linear Demosaicing Algorithm

Color Filter Array

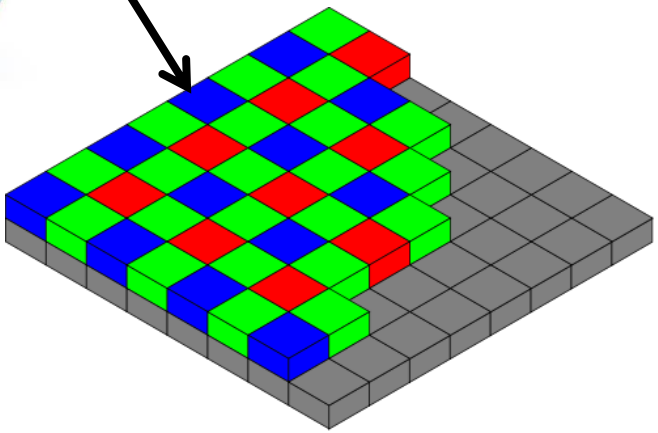

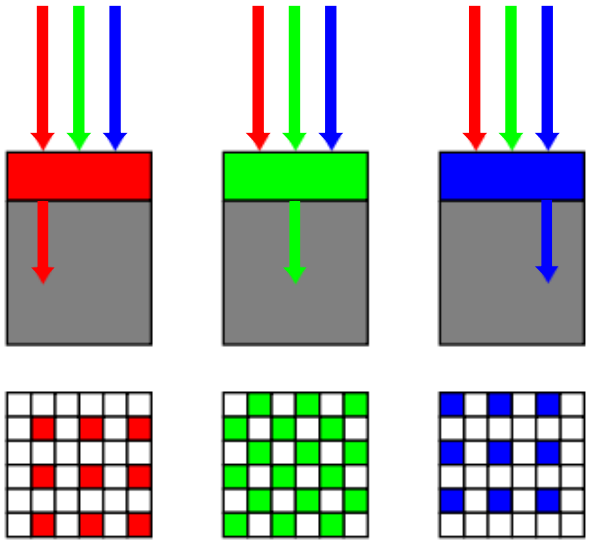

http://en.wikipedia.org/wiki/Bayer_filter

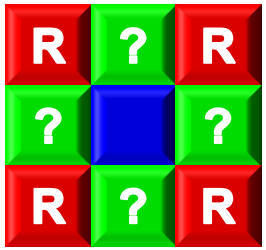

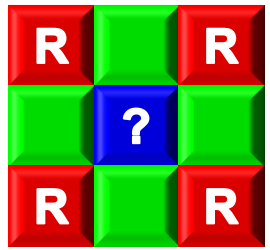

Two cases for interpolate red pixel count on blue / green pixels.

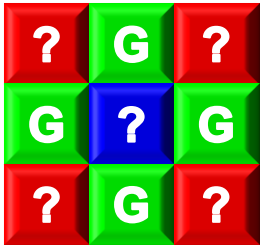

Every red / blue pixel is surrounded by four green pixels.

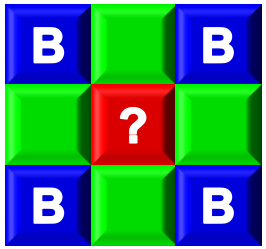

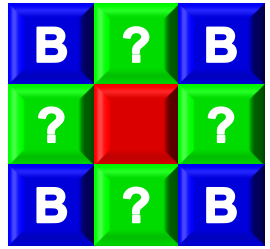

Two cases for interpolate blue pixel count on red / green pixels.

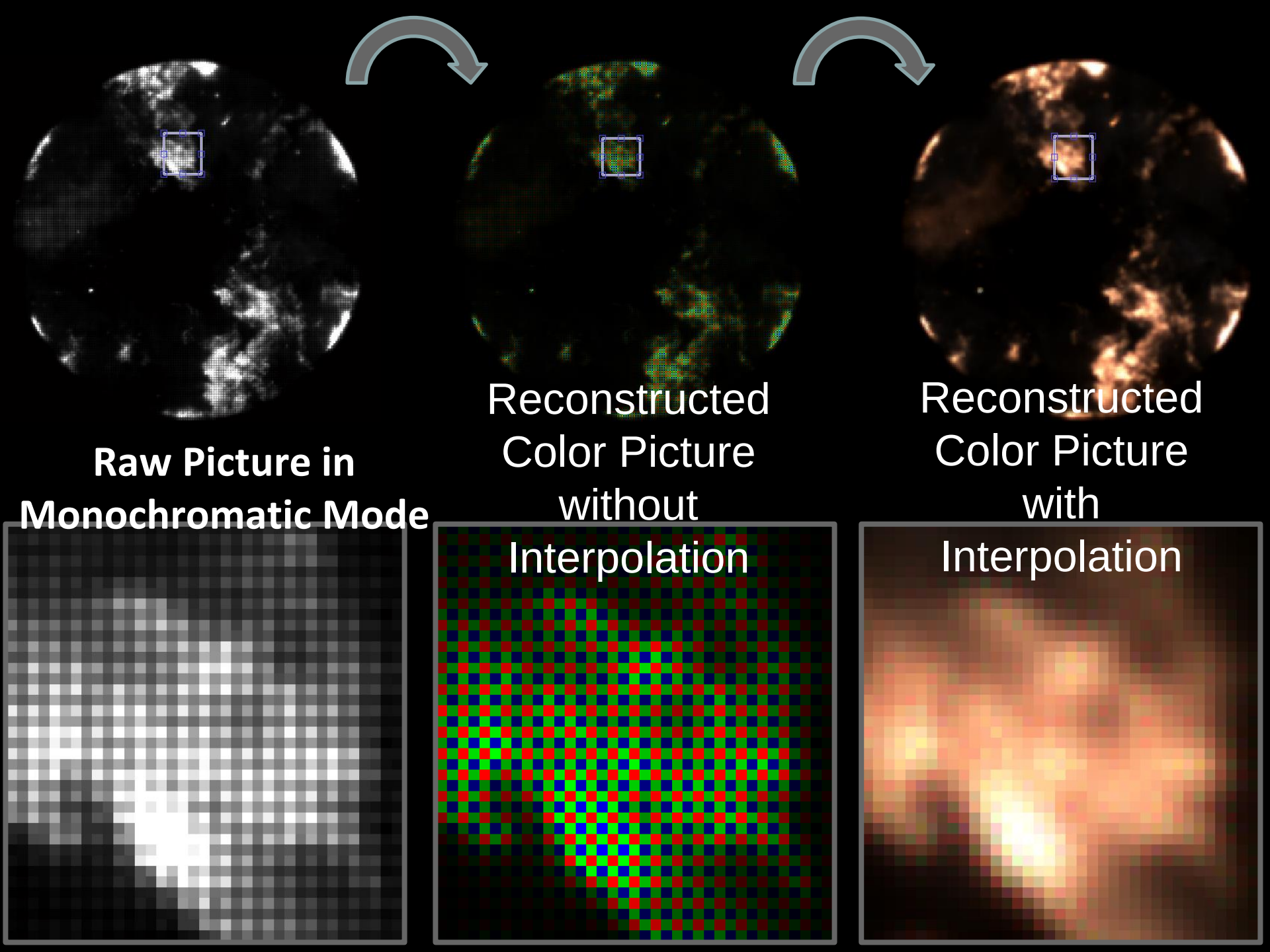
Raw Picture in Monochromatic Mode
Reconstructed Color Picture without Interpolation
Reconstructed Color Picture with Interpolation

Light Source from Halogen Light Bulb

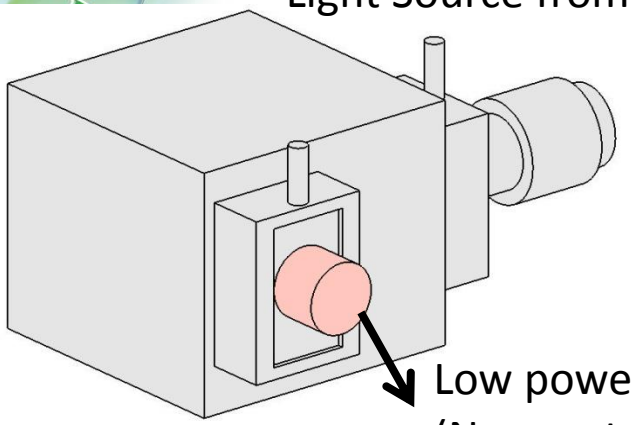

Light Source from Halogen Light Bulb

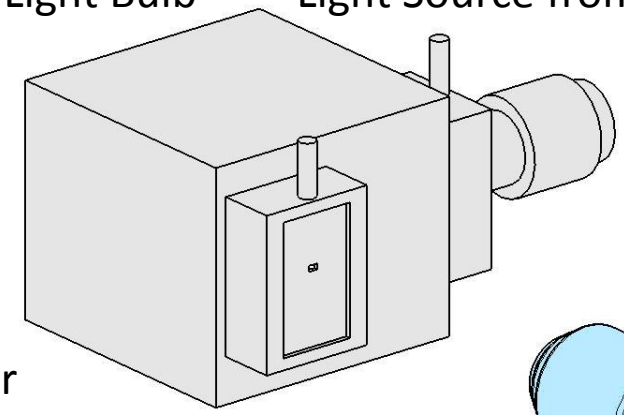

Slit Width = 150µm

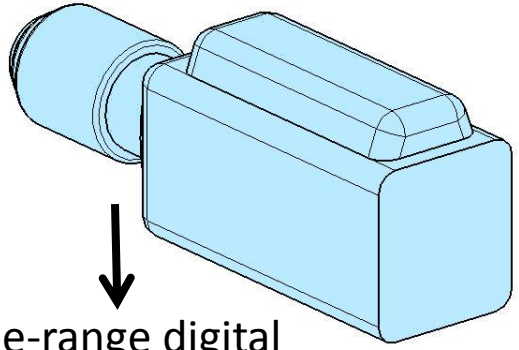

Low power detector
(Newport, 918D-UV-OD3)

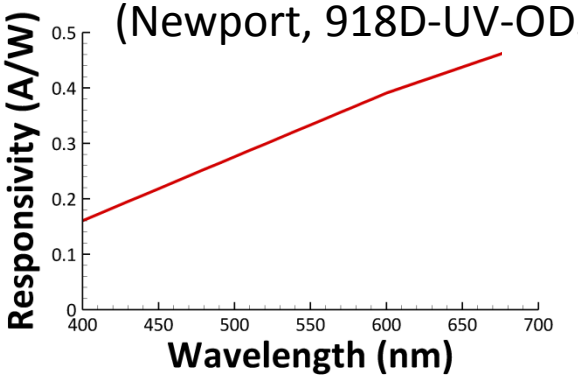

High-speed visible-range digital color camera (Phantom v7.3)

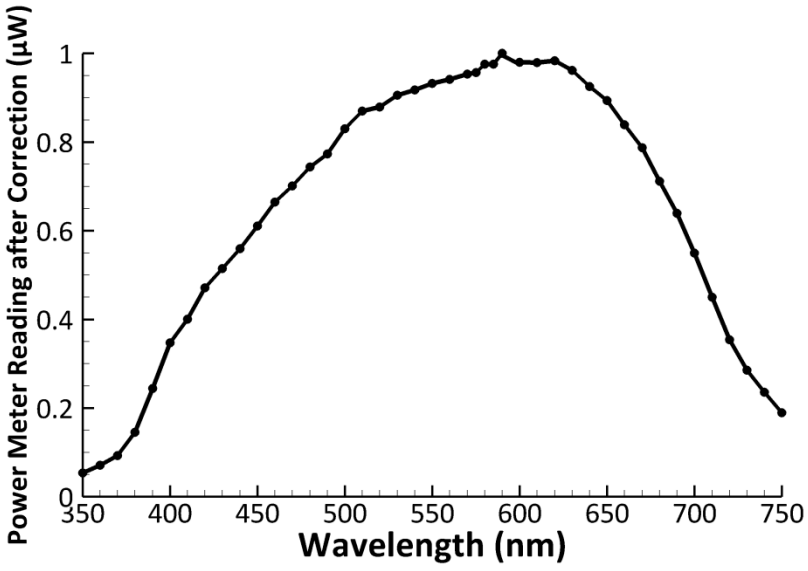

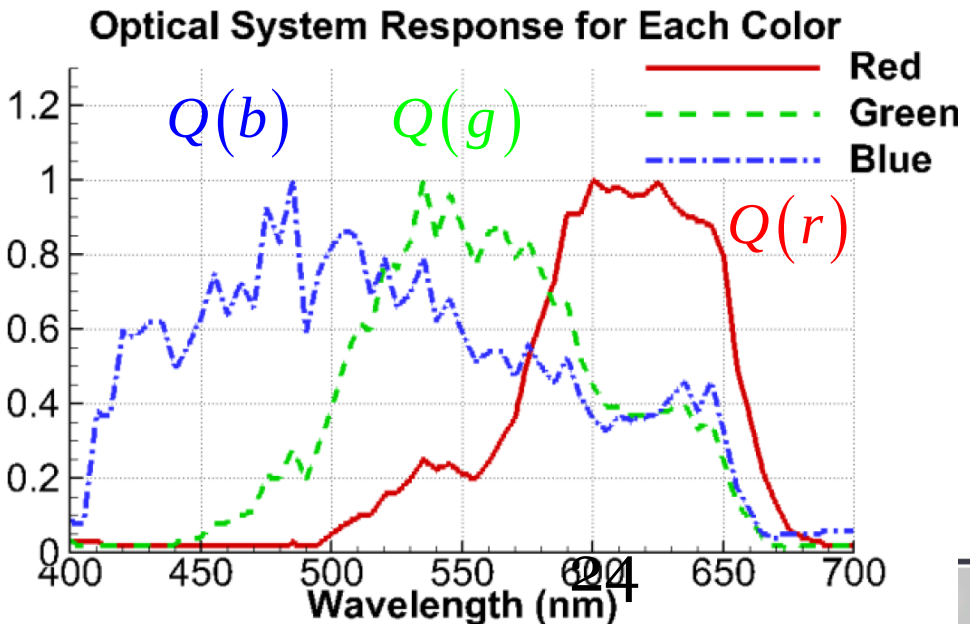

Pixel count sampled by each color channel is proportional to the black body irradiation weighed by "Optical System Response" $Q_{*,\lambda}$ along the optical path.

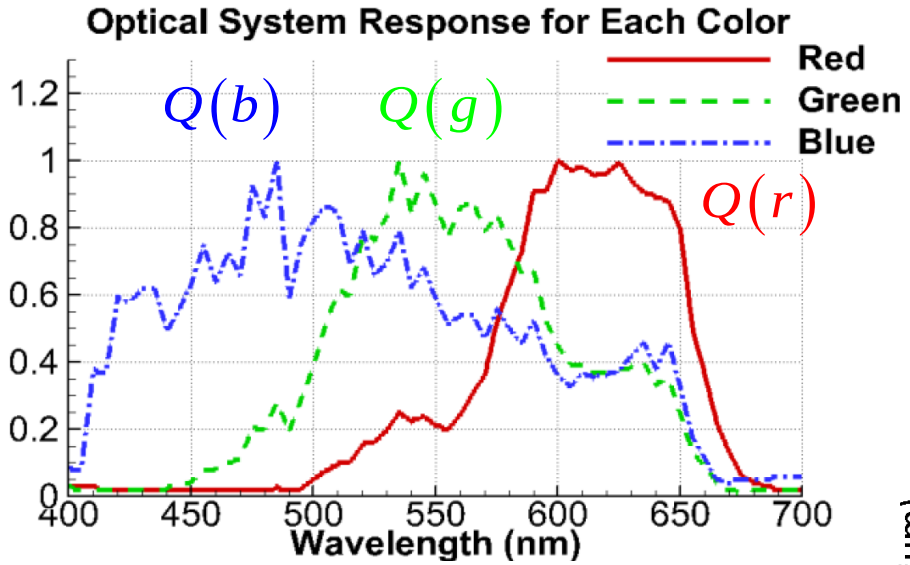

$$\int \left(E_{b,\lambda} \cdot Q_{*,\lambda} \right) d\lambda = \int \frac{Q_{*,\lambda} \cdot C_1}{\lambda^5 \left[\exp\left(\frac{C_2}{\lambda \cdot T_a} \right) - 1 \right]} d\lambda$$

Spectral Emissive Power $\left[\frac{W}{m^2 \cdot \mu m} \right]$

$$E_{b,\lambda} = \frac{C_1}{\lambda^5 \left[\exp\left(\frac{C_2}{\lambda T} \right) - 1 \right]}$$

Wavelength [μm]

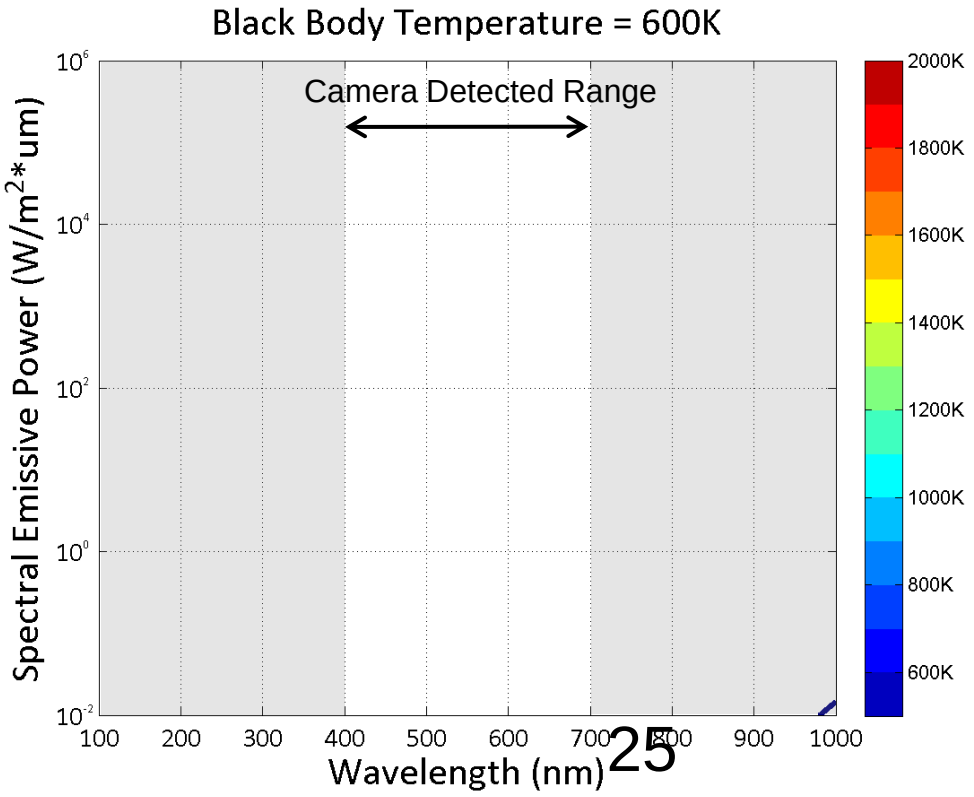

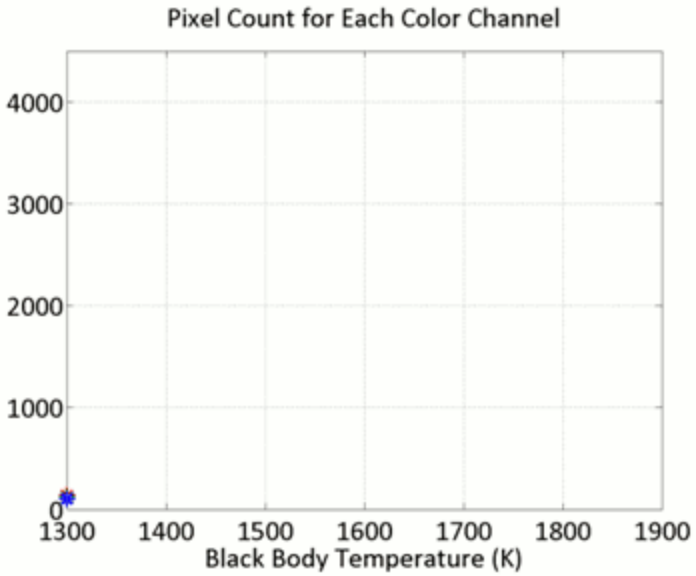

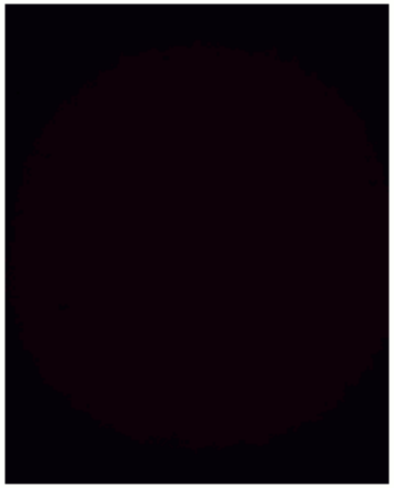

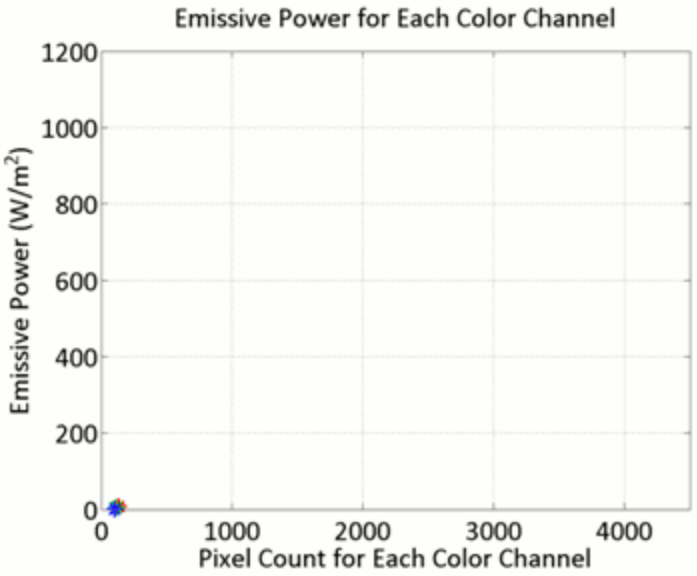

$$\int \left(E_{b,\lambda} \cdot Q_{*,\lambda} \right) d\lambda = \int \frac{Q_* \cdot C_1}{\lambda^5 \left[\exp\left(\frac{C_2}{\lambda \cdot T_a} \right) - 1 \right]} d\lambda$$

Camera Characterization

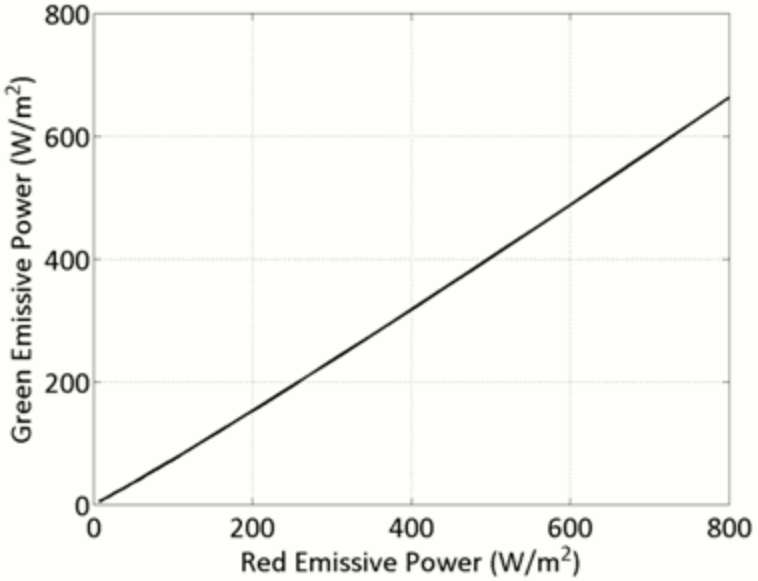

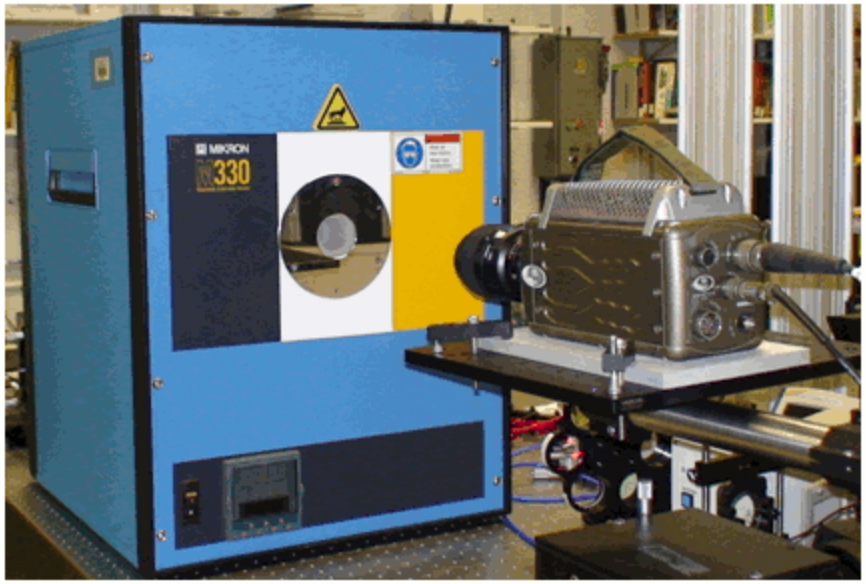

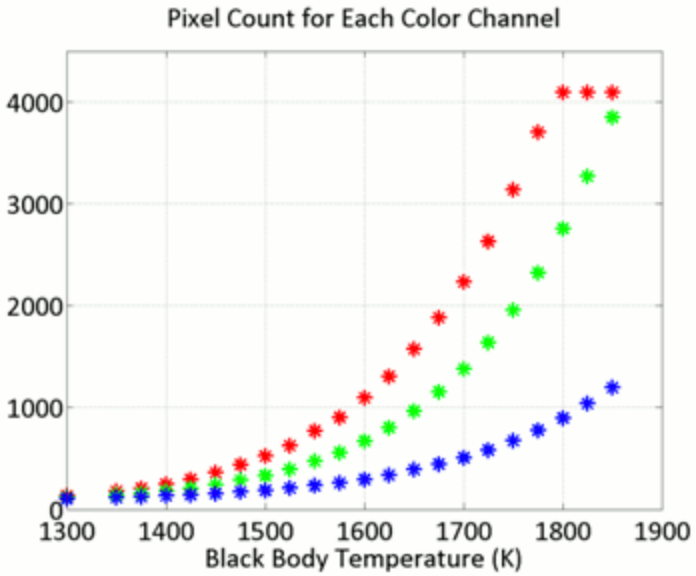

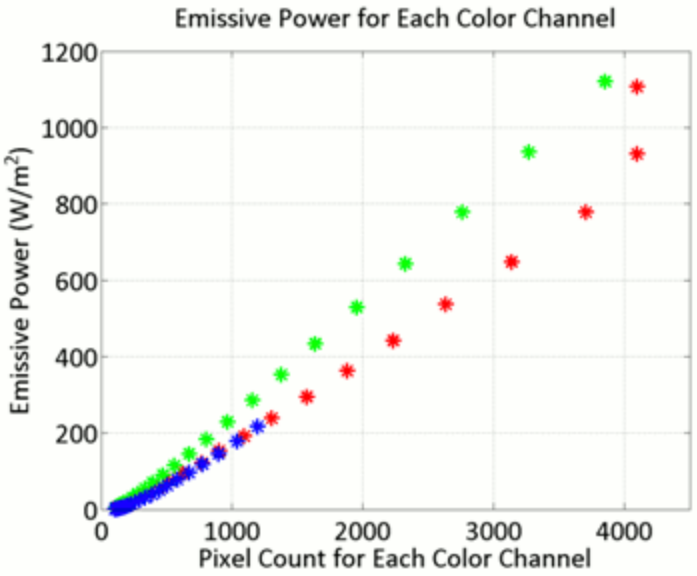

$$\int \left(E_{b,\lambda} \cdot Q_{*,\lambda} \right) d\lambda = \int \frac{Q_* \cdot C_1}{\lambda^5 \left[\exp\left(\frac{C_2}{\lambda \cdot T_a} \right) - 1 \right]} d\lambda$$

Camera Characterization

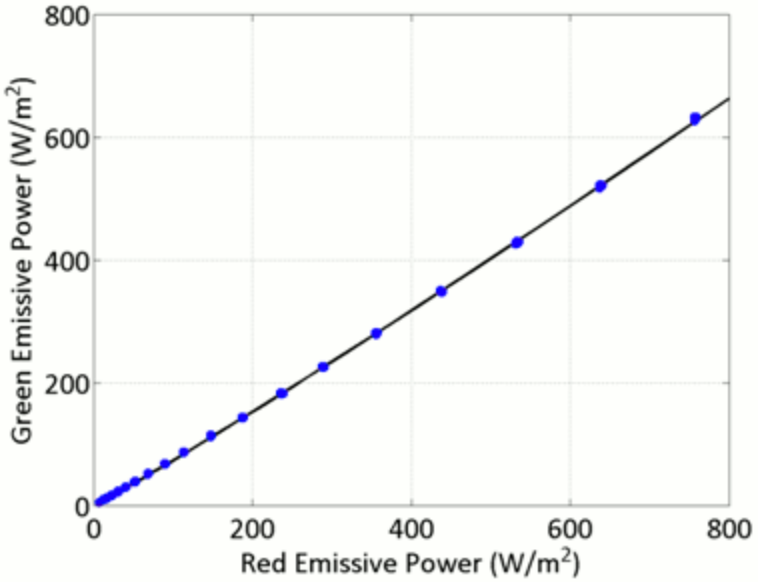

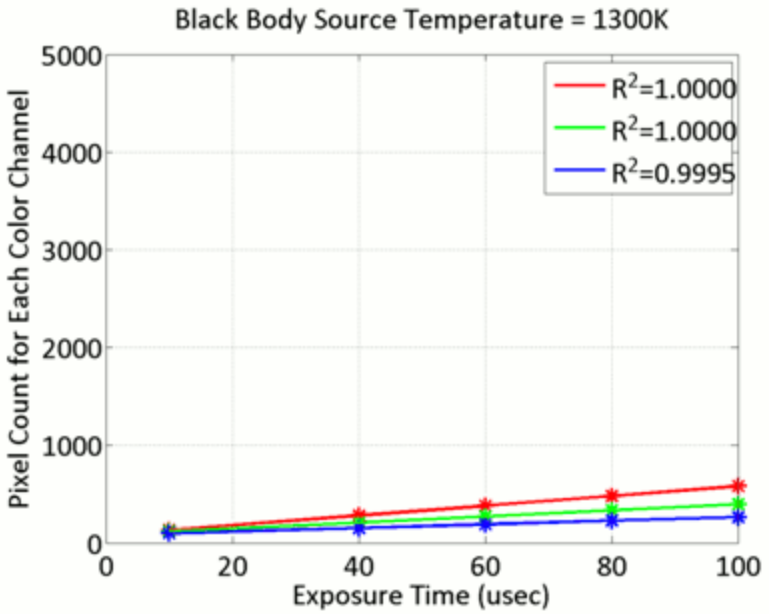

Two-Color Solution Domain Upper Bound Calculation: Adiabatic Gas Temperature Simulation

- Single-zone, adiabatic HCCI reactor (CHEMKIN Pro v15112)
- n-Heptane, Detailed Mechanism, Version 3.1 published by Lawrence Livermore National Laboratory
- Compression ratio = 15
- Connecting rod length-to-stroke ratio＝1.65
- Inlet temperature = 310 K @ 1 atm

$$\varepsilon_{\lambda,KL} = 1 - \exp\left(-\frac{KL}{\lambda^{\alpha}}\right)$$

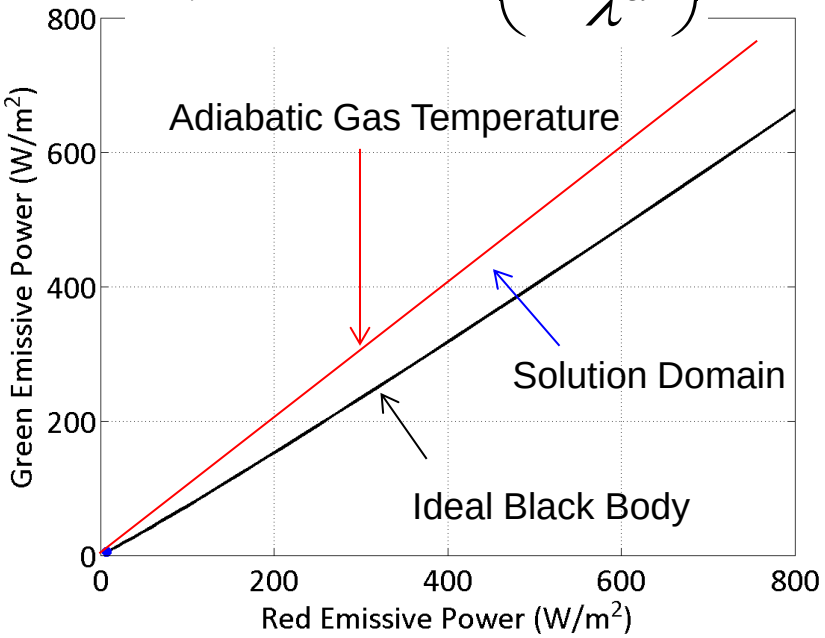

Φ = 1.06 for max temperature

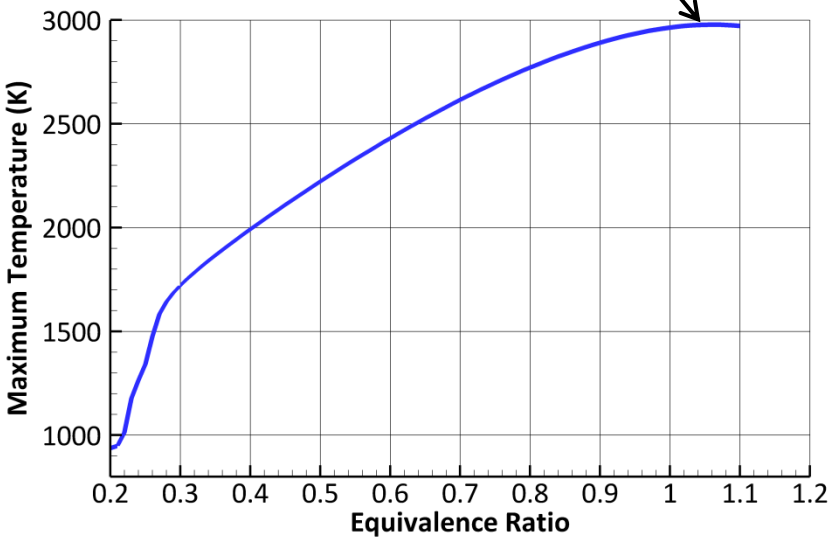

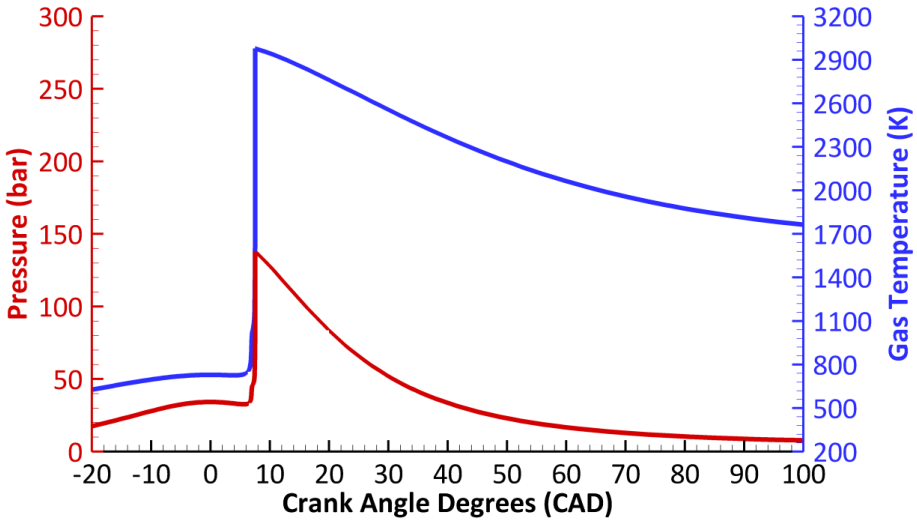

Two equations with two unknown variables, T and KL

$$\int \frac{Q(red)\cdot C_1}{\lambda^5\left[\exp\left(\frac{C_2}{\lambda T_a(red)}\right)-1\right]}d\lambda = \int\left[1-\exp\left(-\frac{KL}{\lambda^{\alpha}}\right)\right]\cdot\frac{Q(red)\cdot C_1}{\lambda^5\left[\exp\left(\frac{C_2}{\lambda T}\right)-1\right]}d\lambda$$

$$\int \frac{Q(green)\cdot C_1}{\lambda^5\left[\exp\left(\frac{C_2}{\lambda T_a(green)}\right)-1\right]}d\lambda = \int\left[1-\exp\left(-\frac{KL}{\lambda^{\alpha}}\right)\right]\cdot\frac{Q(green)\cdot C_1}{\lambda^5\left[\exp\left(\frac{C_2}{\lambda T}\right)-1\right]}d\lambda$$

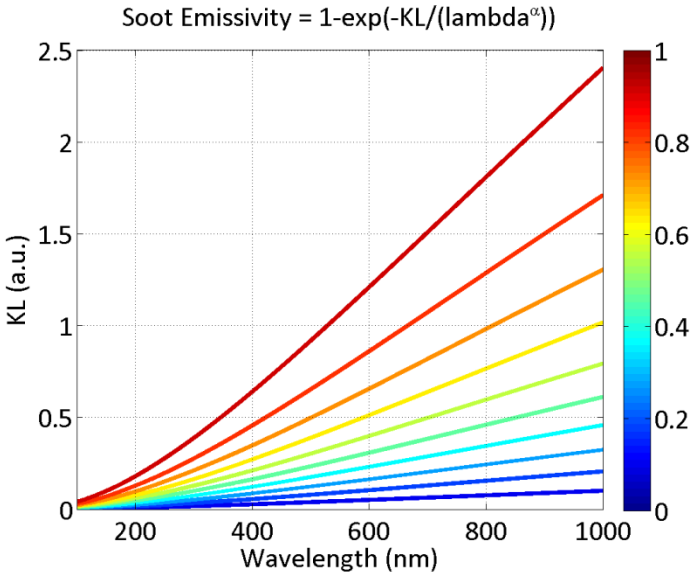

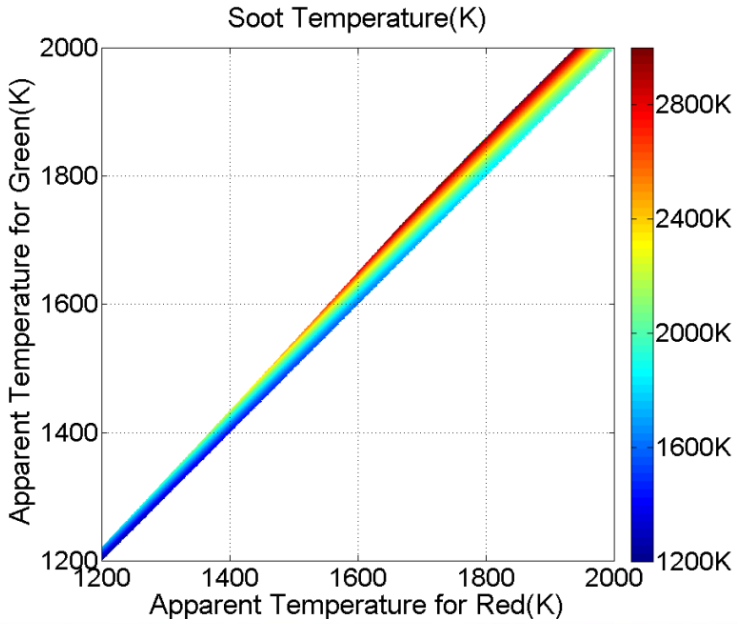

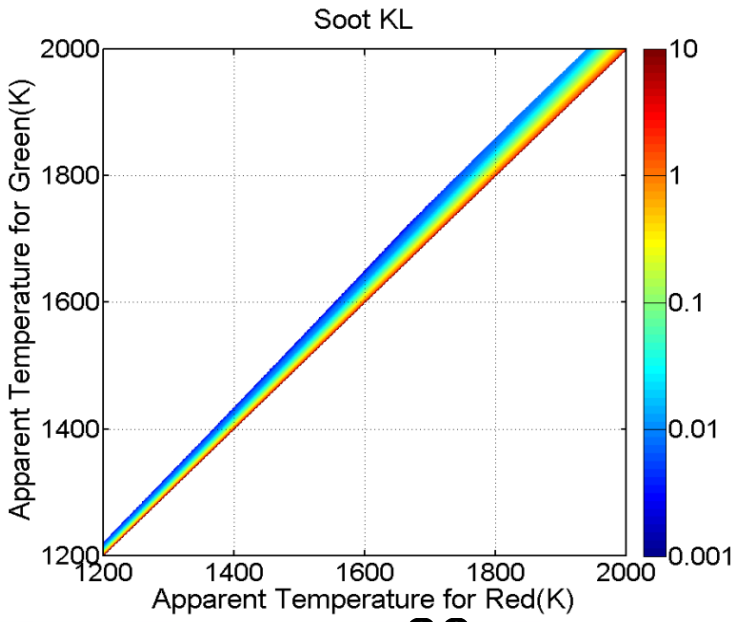

Comparison of Soot Evolution inside an Diesel Engine Fueled with Biodiesel Blend and ULSD

Optically accessible engine	AVL SCRE5402
Intake system	naturally aspirated
Exhaust gas recirculation	no
Bore x Stroke	85 x 90 mm
Swept Volume	510 cm^3
Compression Ratio (nominal)	15:1
Engine Speed	1200 rpm
Injection System	Common Rail CP1
Injection Pressure	600 bar
Injector Number of Holes, Type	5 holes, VCO
Hole Diameter	180 µm
Hole Included Angle	142˚
Fuel	ULSD

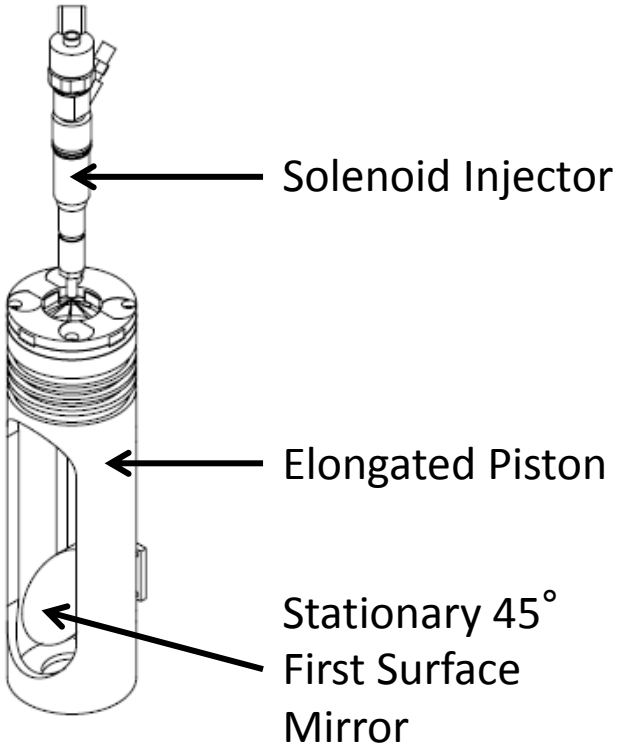

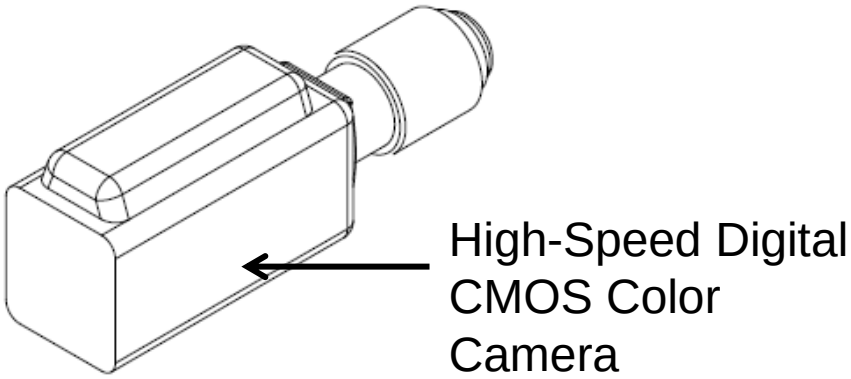

ULSD

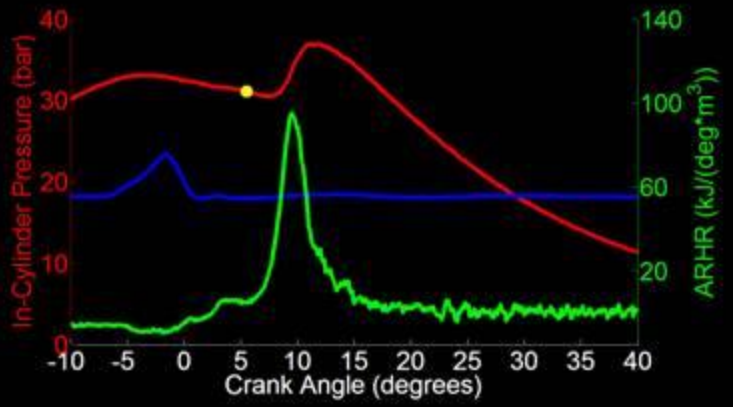

B20

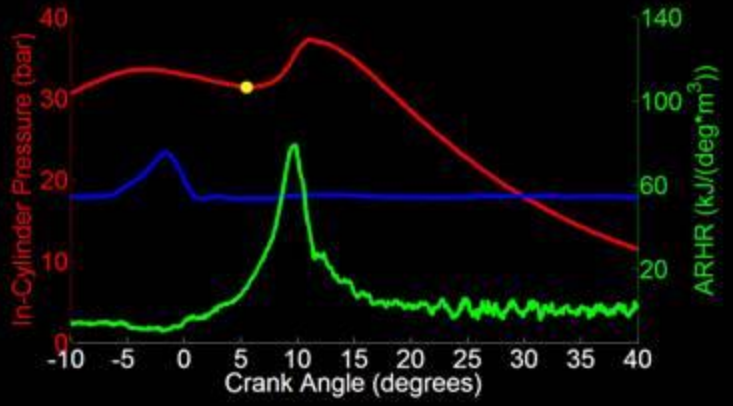

Soot Temperature

2400K
2300K
2200K
2100K
2000K
1900K
1800K
1700K

KL

1
0.31
0.1
0.03
0.01

Soot Temperature

2400K
2300K
2200K
2100K
2000K
1900K
1800K
1700K

KL

1
0.31
0.1
0.03
0.01

5.5 °CA aTDC

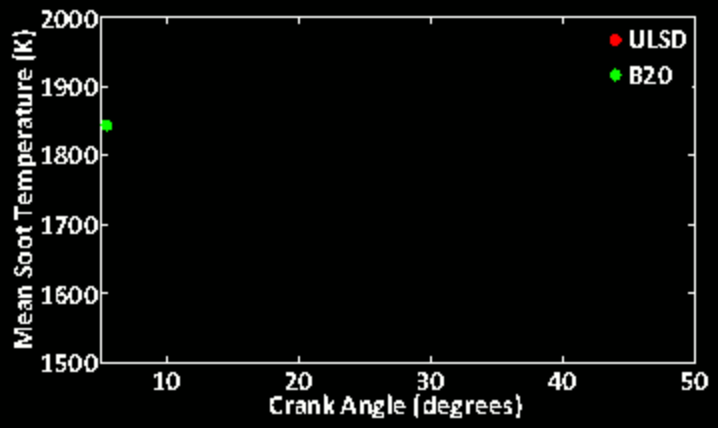
Mean Soot Temperature (K)
2000
1900
1800
1700
1600
1500
10
20
30
40
50
Crank Angle (degrees)
ULSD
B20

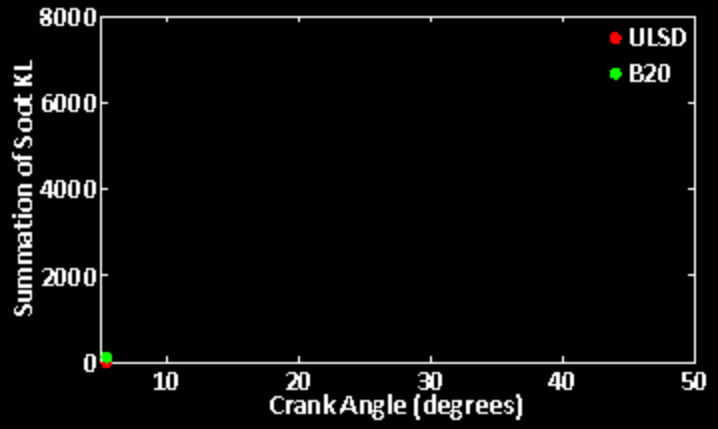
Summation of Soot KL
8000
6000
4000
2000
0
10
20
30
40
50
Crank Angle (degrees)
ULSD
B20

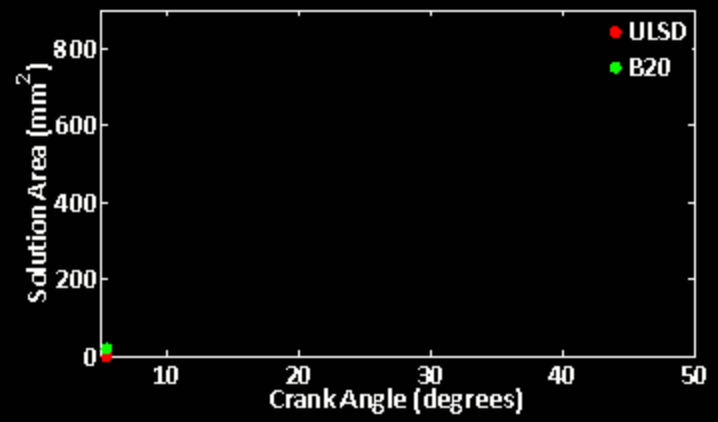
Solution Area (mm^2)
800
600
400
200
0
10
20
30
40
50
Crank Angle (degrees)
ULSD
B20

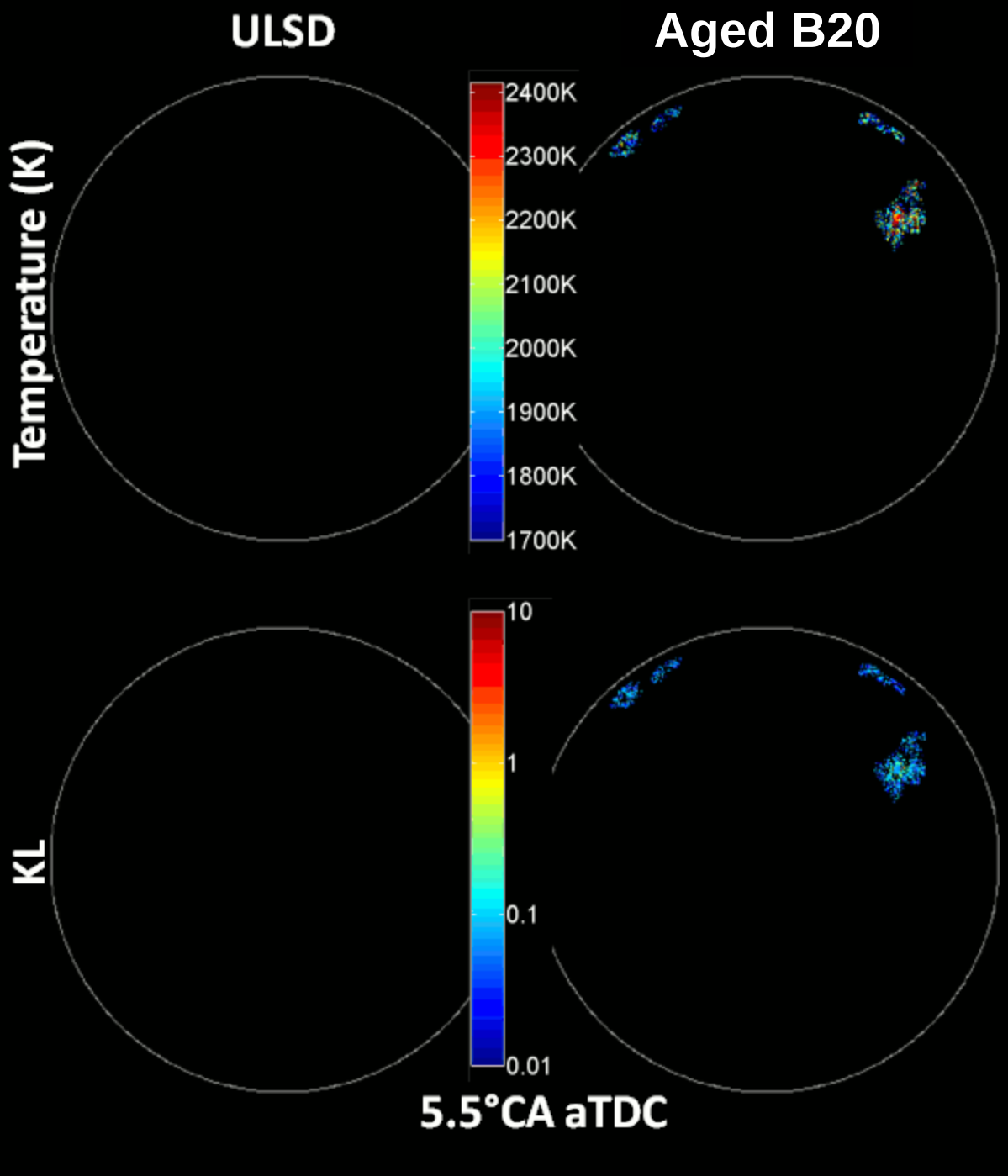
ULSD
Aged B20
Temperature (K)
2400K
2300K
2200K
2100K
2000K
1900K
1800K
1700K
KL
10
1
0.1
0.01
5.5°CA aTDC

Discrepancy exists between measured and simulated soot temperature & KL, any problems in soot radiation interpretation?

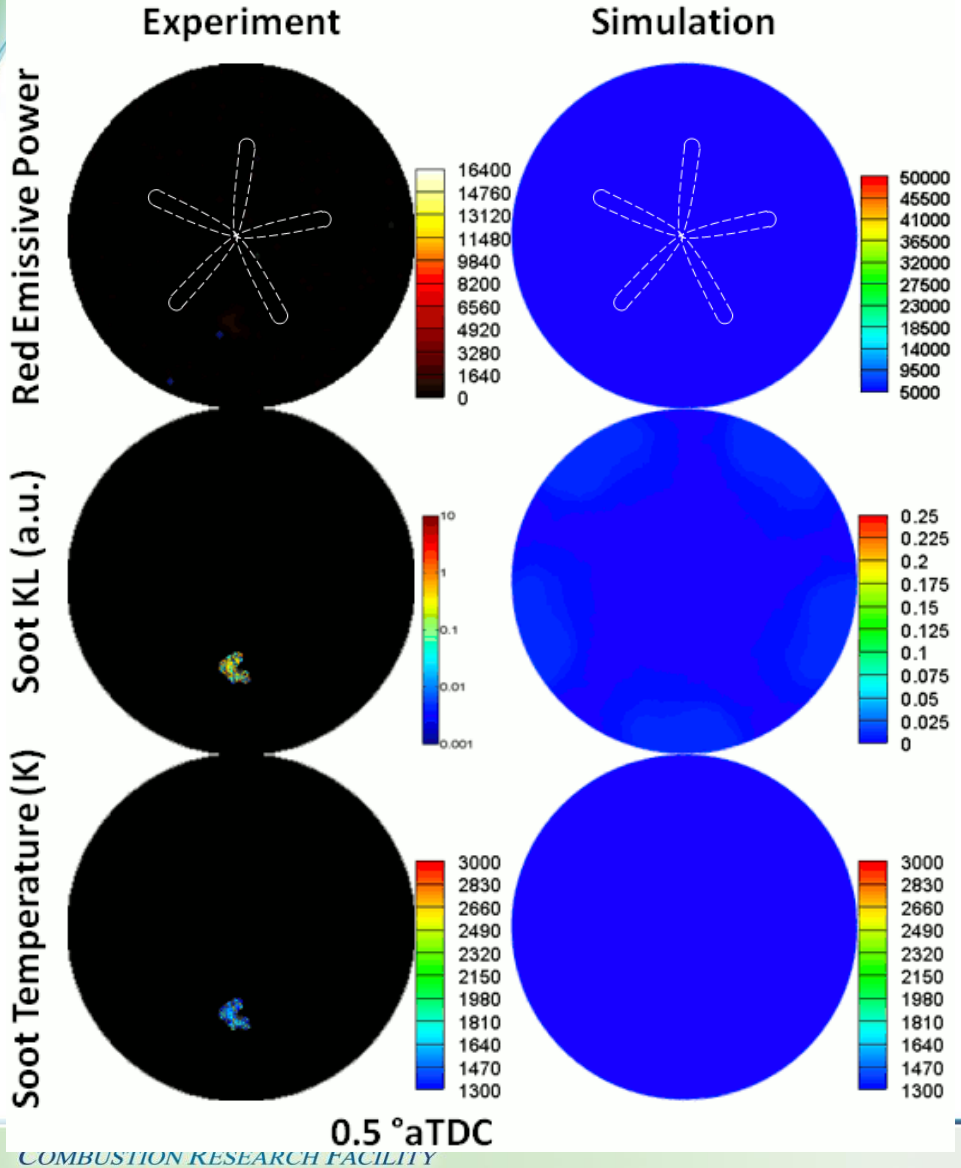

- Chemical kinetic-coupled CFD package (FORTE, Reaction Design), reduced n-Heptane mechanism, two-step empirical soot model.
- Two effective single wavelengths (λred=601.05nm λgreen=548.88nm) are calculated from measured "optical system response curve".
- Line-of-sight integration for soot radiation.
- Simulated two-color thermometry over-estimates soot temperature by 10%-20% in most crank angle intervals.
- Simulation overestimates soot KL exhibit from 3°aTDC until 45°aTDC.

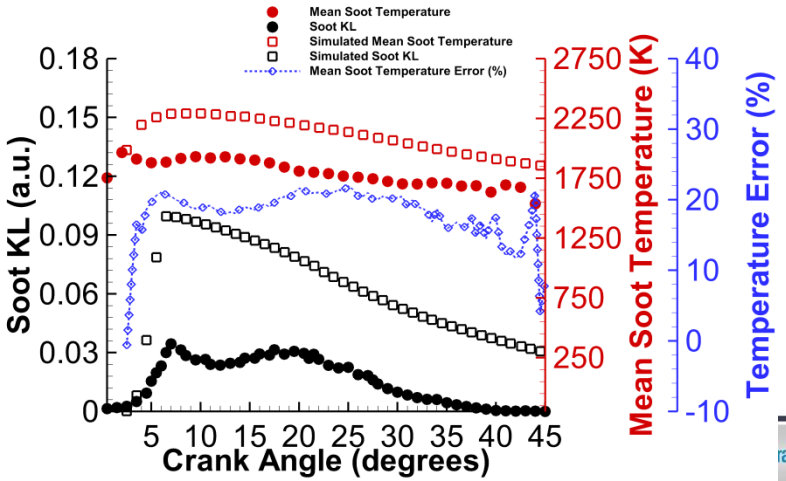

- Soot radiation is composed of two terms: soot emissivity model and Planck distribution term;
- All the coefficients in the Planck distribution term are well known.
- The accuracy of unknown soot temperature depends on the accuracy of soot emissivity model.

$$E_{soot,\lambda} = \varepsilon_{\lambda,KL} \cdot E_{b,\lambda} = \left[1 - \exp\left(-\frac{KL}{\lambda^{\alpha}}\right)\right] \cdot \frac{C_1}{\lambda^5 \left[\exp\left(\frac{C_2}{\lambda T_{soot}}\right) - 1\right]}$$

- An inherent assumption of the classic two-color method is that the product KL is the same for two specific wavelengths, λ1, λ2. The validity of this assumption is examined in a detailed analytical and experimental investigation of the soot emissivity model.

$$-\lambda_1^{\alpha_1} \ln\left[1 - \frac{\exp\left(\frac{C_2}{\lambda_1 T_{soot}}\right) - 1}{\exp\left(\frac{C_2}{\lambda_1 T_{a_1}}\right) - 1}\right] = -\lambda_2^{\alpha_2} \ln\left[1 - \frac{\exp\left(\frac{C_2}{\lambda_2 T_{soot}}\right) - 1}{\exp\left(\frac{C_2}{\lambda_2 T_{a_2}}\right) - 1}\right]$$

Question: is product KL the same for two specific wavelengths, λ1, λ2 ?

Soot Emissivity Model Analysis

$$\tau_{soot} = 1 - \alpha_{soot} - \rho_{soot}$$

Neglect soot reflectivity $\rho_{soot} \approx 0$ in micro scale investigation, equation is simplified as:

$$\tau_{soot} = 1 - \alpha_{soot} \qquad (1)$$

According to Beer's Law, which describes light attenuation in a gaseous media:

$$\frac{I}{I_0} = \tau_{soot} = \exp\left(-\beta_{soot} L\right) \qquad (2)$$

According to Kirchhoff's Law which equates emissivity to absorptivity under thermal equilibrium:

$$\varepsilon_{soot} = \alpha_{soot} = 1 - \tau_{soot} \qquad (3)$$

With equation (2),

$$\varepsilon_{soot} = 1 - \exp\left(-\beta_{\lambda} L\right)$$

τ_{soot} : soot transmissivity
α_{soot} : soot absorptivity
ρ_{soot} : soot reflectivity
β_{λ} : extinction coefficient

$$\beta_\lambda = \sigma_{s\lambda} + \kappa_\lambda = \int_0^\infty C_{sca} n(a) da + \int_0^\infty C_{abs} n(a) da$$

If the soot cloud is composed of a large amount of spherical particles of radius, a, a particle distribution function $n(a)$ is introduced to describe the number of particles as a function of the particle radius.

$$Q_{sca} = \frac{C_{sca}}{\pi a^2} = \frac{8}{3}\left|\frac{m^2-1}{m^2+2}\right|^2 x^4$$

size parameter: $x = 2\pi a / \lambda$

complex index of refraction: $m = n - ik$

If soot particles are extremely small, then the size parameter x becomes very small, and the process is described by the Rayleigh scattering regime, as occurs with typical gases. Scattering term can be ignored [10]:

$$Q_{sca} = \frac{C_{sca}}{\pi a^2} \approx 0 \qquad \beta_\lambda \approx \kappa_\lambda$$

For a cloud of nonuniform-size small particles, extinction coefficient:

$$Q_{abs} = \frac{C_{abs}}{\pi a^2} = -4\Im\left\{\frac{m^2-1}{m^2+2}\right\} x = -4\Im\left\{\frac{m^2-1}{m^2+2}\right\}\frac{2\pi a}{\lambda}$$

$$\beta_\lambda \approx \pi\int_0^\infty Q_{abs} a^2 n(a) da = -4\Im\left\{\frac{m^2-1}{m^2+2}\right\}\int_0^\infty \frac{2\pi a}{\lambda}\pi a^2 n(a) da$$

[7] Modest, Michael F., "RADIATIVE HEAT TRANSFER", Academic Press, 2013.

Soot volume fraction is:

$$f_v = \int_0^{\infty} \left(\frac{4}{3} \pi a^3 \right) n(a)\, da$$

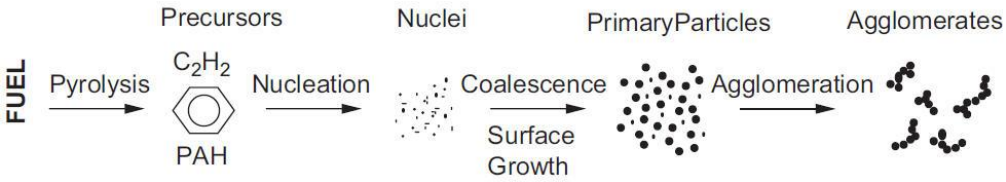

Schematic diagram of the steps in the soot formation process from gas phase to solid agglomerated particles. [11]

Soot extinction coefficient reduces to:

$$\beta_\lambda = -6\pi \Im\left\{ \frac{m^2 - 1}{m^2 + 2} \right\} \frac{f_v}{\lambda} = -\frac{6\pi \Im(m)\, f_v}{\lambda}$$

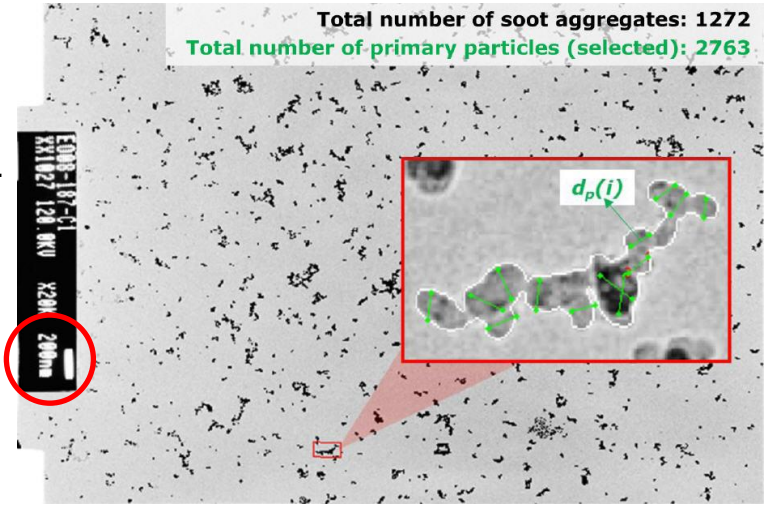

An example for automated boundary detection of soot aggregates (below as black areas) and manual selection of primary particles (green lines within the red-colored rectangular box) for a sample TEM image. [12]

Soot emissivity reduces to:

$$\varepsilon_{soot} = \alpha_{soot} = 1 - \exp\left(\frac{6\pi \Im(m)\, f_v L}{\lambda} \right)$$

Considering the scattering effect:

$$\varepsilon_{soot} = \alpha_{soot} = 1 - \exp\left((\rho_{sa} + 1) \frac{6\pi \Im(m)\, f_v L}{\lambda} \right)$$ Or:

$$\varepsilon_{soot} = \alpha_{soot} = 1 - \exp\left(\frac{6\pi \Im(m)\, f_v L}{\lambda^{\alpha}} \right)$$

ρ_{sa}

Ratio of scattering to absorption

[8] Tree, D. R. and Svensson, K. I., 2007, "Soot processes in compression ignition engines", *Progress in Energy and Combustion Science* **33**(3), pp.272-309

[9] Kook, S. and Pickett, L. M., 2012, "Soot Volume Fraction and Morphology of Conventional, Fischer-Tropsch, Coal-Derived, and Surrogate Fuel at Diesel Conditions", *SAE Int. J. Fuels Lubr.* 5(2), pp.647-664

Use α proposed by Musculus [6] to work with the following equation [13],

$$\varepsilon_{soot} = 1 - \exp\left(-\frac{g f_v L}{\lambda^{\alpha}}\right) \qquad \alpha = 1.22 - 0.245 \cdot \left(\ln \lambda[\mu m]\right)$$

If α accurately quantifies the soot scattering effect, the g factor is proportional to $\Im(m)$, $g = -6\pi\Im(m)$

With re-formulation of soot emissivity model, two-color method changes to:

$$\int \frac{Q(red)\cdot C_1}{\lambda^5\left[\exp\left(\frac{C_2}{\lambda T_a(red)}\right)-1\right]} d\lambda = \int \left[1-\exp\left(-\frac{KL}{\lambda^{\alpha}}\right)\right] \cdot \frac{Q(red)\cdot C_1}{\lambda^5\left[\exp\left(\frac{C_2}{\lambda T}\right)-1\right]} d\lambda$$

$$\int \frac{Q(green)\cdot C_1}{\lambda^5\left[\exp\left(\frac{C_2}{\lambda T_a(green)}\right)-1\right]} d\lambda = \int \left[1-\exp\left(-\frac{KL}{\lambda^{\alpha}}\right)\right] \cdot \frac{Q(green)\cdot C_1}{\lambda^5\left[\exp\left(\frac{C_2}{\lambda T}\right)-1\right]} d\lambda$$

[6] Musculus, M. P. B., 2005, "Measurements of the Influence of Soot Radiation on In-Cylinder Temperatures and Exhaust NOx in a Heavy-Duty DI Diesel Engine", *SAE Technical Paper* 2005-01-0925, DOI:10.4271/2005-01-0925
[10] Gray, W. A. and Muller, R., Engineering Calculations in Radiative Heat Transfer, Permagon Press, 1974.

Use α proposed by Musculus [6] to work with the following equation [21],

$$\varepsilon_{soot} = 1 - \exp\left(-\frac{g f_v L}{\lambda^{\alpha}}\right) \qquad \alpha = 1.22 - 0.245 \cdot \left(\ln \lambda[\mu m]\right)$$

If α accurately quantifies the soot scattering effect, the g factor is proportional to $\Im(m)$, $g = -6\pi\Im(m)$

With re-formulation of soot emissivity model, two-color method changes to:

$$\int \frac{Q(red)\cdot C_1}{\lambda^5\left[\exp\left(\frac{C_2}{\lambda T_a(red)}\right)-1\right]} d\lambda = \int \left[1-\exp\left(-\frac{g_{red} f_v L}{\lambda^{\alpha}}\right)\right] \cdot \frac{Q(red)\cdot C_1}{\lambda^5\left[\exp\left(\frac{C_2}{\lambda T}\right)-1\right]} d\lambda$$

$$\int \frac{Q(green)\cdot C_1}{\lambda^5\left[\exp\left(\frac{C_2}{\lambda T_a(green)}\right)-1\right]} d\lambda = \int \left[1-\exp\left(-\frac{g_{green} f_v L}{\lambda^{\alpha}}\right)\right] \cdot \frac{Q(green)\cdot C_1}{\lambda^5\left[\exp\left(\frac{C_2}{\lambda T}\right)-1\right]} d\lambda$$

[6] Musculus, Mark P.B., "Measurements of the Influence of Soot Radiation on In-cylinder Temperatures and Exhaust NOx in a Heavy-Duty DI Diesel Engine" SAE Technical Papers, 2005, 2005 SAE World Congress
[10] Gray, W. A. and Muller, R., Engineering Calculations in Radiative Heat Transfer, Permagon Press, 1974.

Soot Emissivity Model Calibration Against a Flat Flame

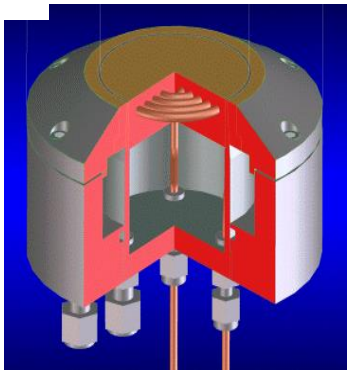

http://www.flatflame.com/

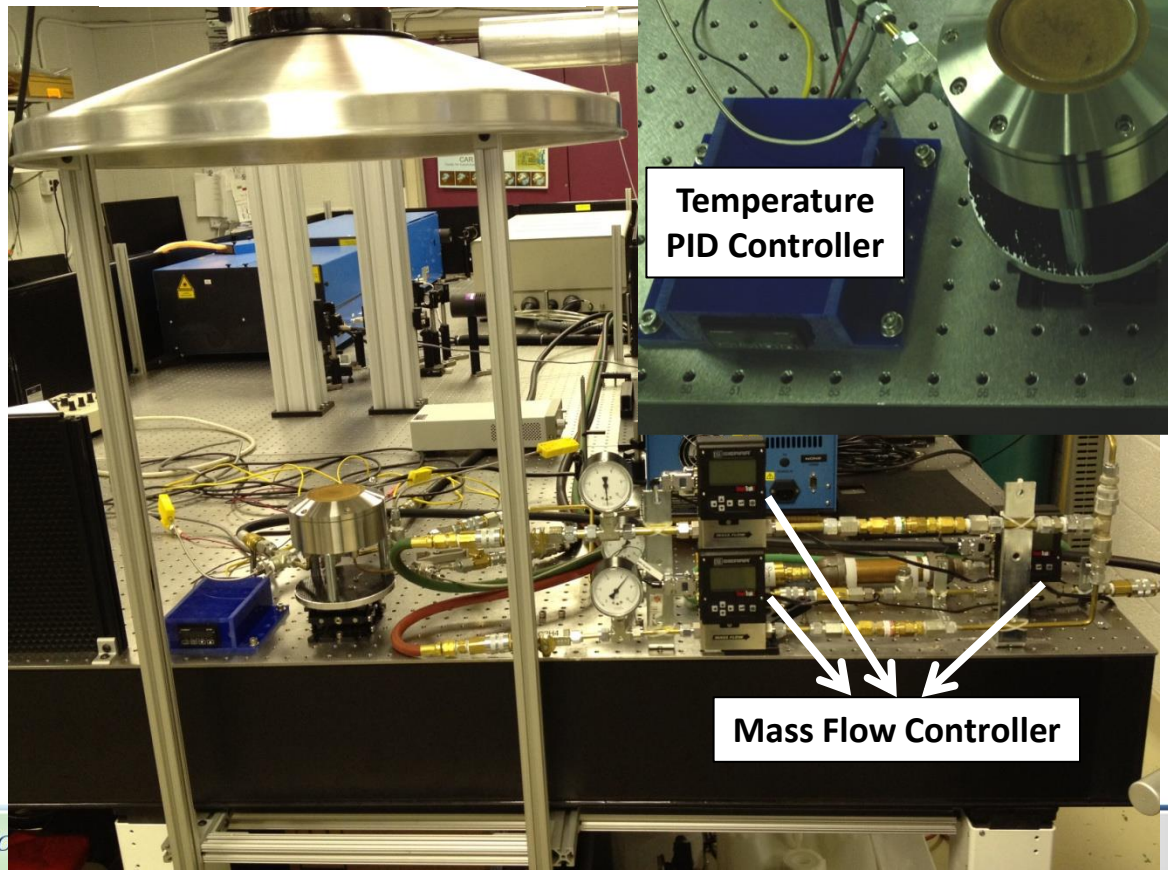

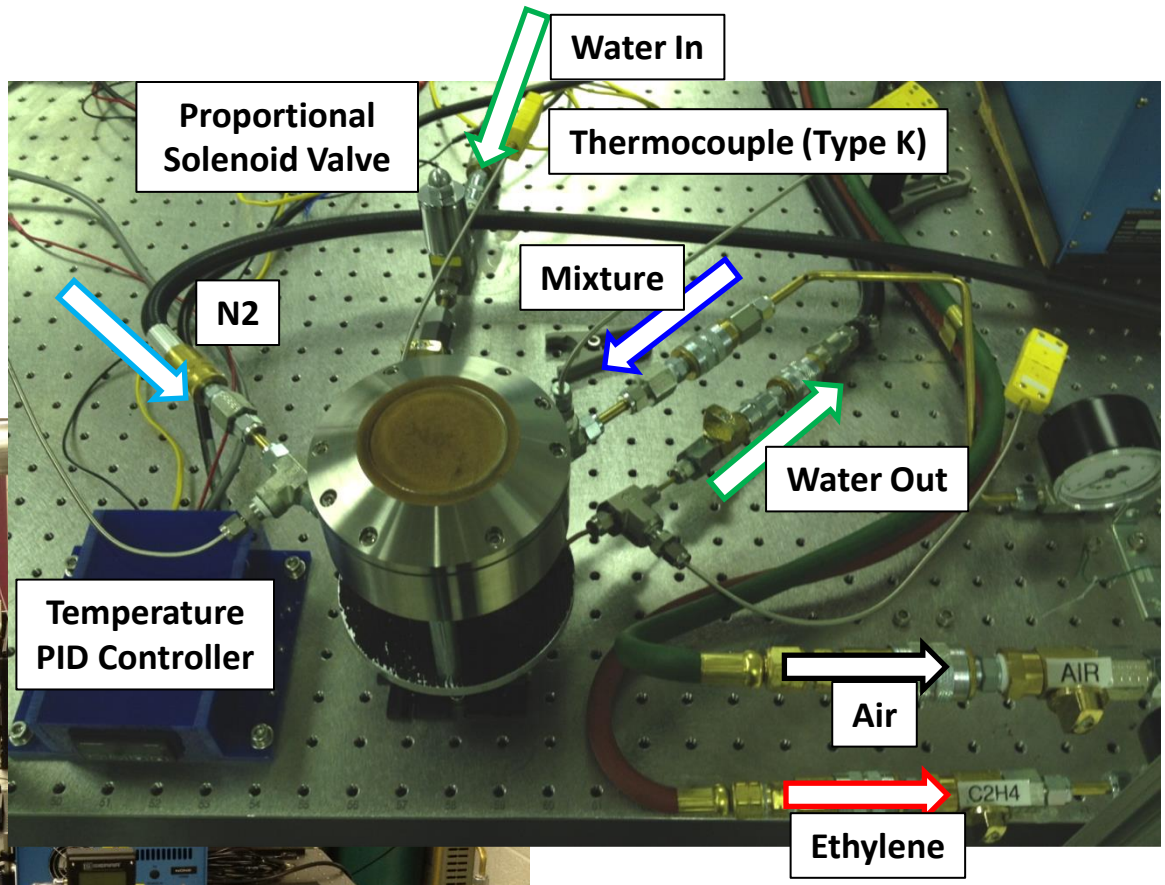

Flat flame standards [14].

[11] Schulz, C., Kock, B. F., Hofmann, M., Michelsen, H., Will, S., Bougie, B., Suntz, R. and Smallwood, G., 2006, "Laser-induced incandescence: recent trends and current questions", *Applied Physics B* 83(3), pp.333-354

Ethylene/air premixed flat flame is examined under the same conditions as by Olofsson and Bladh in Lund group [15][16].

Fuel: Ethylene + Air with ϕ=2.1

Total flow rate: 10 slpm @ 0° C and 1 atm

Co-flow shielding Gas: N2

Flame Stagnation Plate: Stainless steel, 60 mm diameter, 20 mm thick

Burner coolant temperature is 20° C

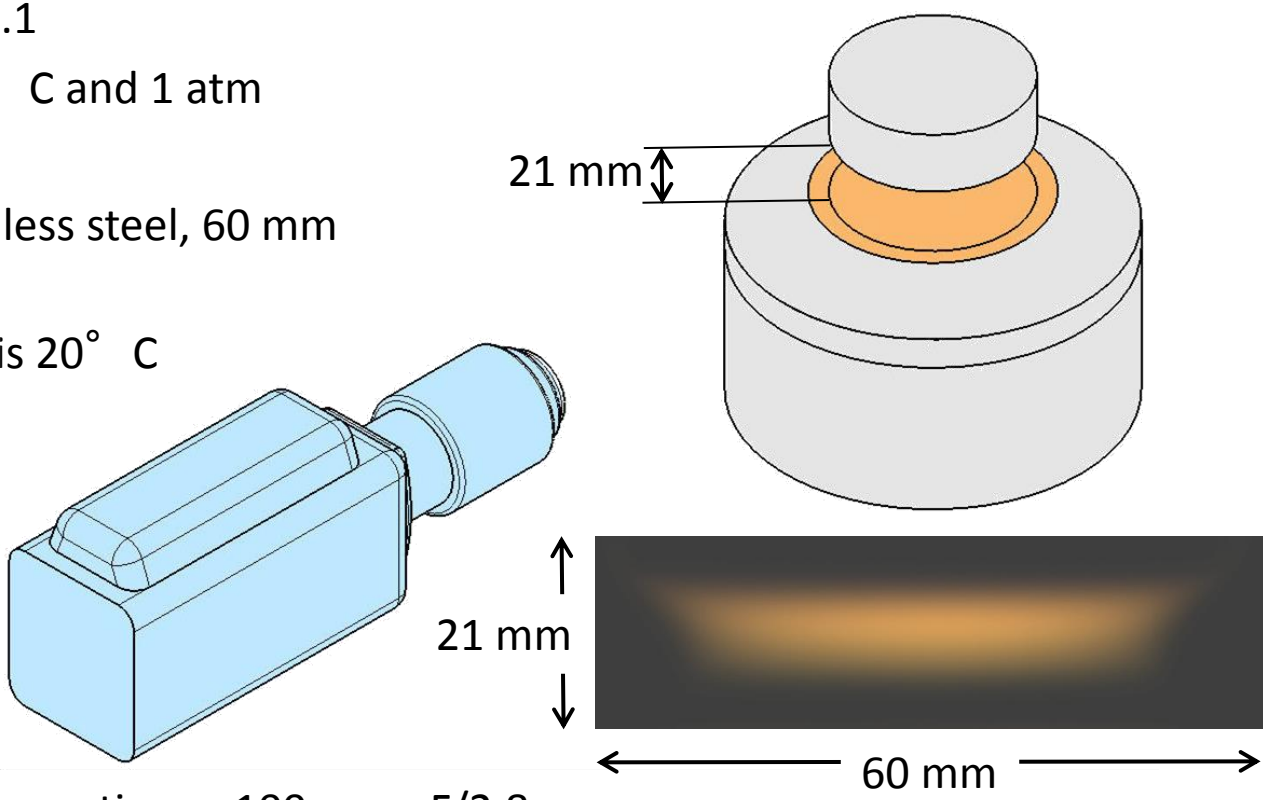

Exposure time = 100 µsec, F/2.8

[12] Olofsson, N.-E., Bladh, H., Bohlin, A., Johnsson, J., Bengtsson, P.-E., "ARE SOOTING PREMIXED POROUS-PLUG BURNER FLAMES ONE-DIMENSIONAL? A LASER-BASED EXPERIMENTAL INVESTIGATION" Combust. Sci. Technol., 185: 293-309, (2013)

[13] Bladh, H. Johnsson, J. Olofsson, N.-E., Bohlin, A., Bengtsson, P.-E., "Optical soot characterization using two-color laser-induced incandescence (2C-LII) in the soot growth region of a premixed flat flame" Proc. Combus. Inst. 33, 641-648 (2011)

Since soot particles in flat flame have radiative heat loss to the ambient environment, soot temperature is examined in a detailed analytical and numerical investigation.

$$\frac{1}{6}\pi d_p^3 \rho_s c_s \frac{dT_{soot}}{dt} = \dot{q}_{conduction} - \dot{q}_{radiation}$$

Soot diameter $d_p = 2a$

Soot conduction heat transfer rate $\dot{q}_{conduction}$ is expressed as [17]:

$$\dot{q}_{conduction} = \frac{1}{8}\alpha_T \pi d_p^2 p_g \sqrt{\frac{8k_B T_g}{\pi m_g}} \frac{\gamma_g + 1}{\gamma_g - 1}\left(1 - \frac{T_{soot}}{T_g}\right)$$

Soot radiative heat transfer rate $\dot{q}_{radiation}$ is expressed as:

$$\dot{q}_{radiation} = \int_{\Delta\lambda} \frac{\pi d_p^2 \cdot C_1}{\lambda^5 \left[\exp\left(\frac{C_2}{\lambda T_a}\right) - 1\right]} d\lambda$$

$\alpha_T = 0.48$ [16]

p_g Gas pressure [Pa]

k_B Boltzmann constant.

T_g Gas temperature [K]

m_g Average mass of gas molecules [kg]

γ_g Specific heat ratio of gas

[13] Bladh, H., Johnsson, J. Olofsson, N. E., Bohlin, A. and Bengtsson, P. E., 2011, "Optical soot characterization using two-color laser-induced incandescence (2C-LII) in the soot growth region of a premixed flat flame", **33**(1), pp.641-648

[14] Filippov, A. V. and Rosner, D. E., 2000, "Energy transfer between an aerosol particle and gas at high temperature ratios in the Knudsen transition regime", *International Journal of Heat and Mass Transfer* **43**(1), pp.127-38

Under thermal equilibrium condition, $\frac{dT_{soot}}{dt} = 0$, the following equation holds:

$$\frac{1}{8}\alpha_T p_g \sqrt{\frac{8k_B T_g}{\pi m_g}} \frac{\gamma_g + 1}{\gamma_g - 1}\left(1 - \frac{T_{soot}}{T_g}\right) = \int_{\Delta\lambda} \frac{C_1}{\lambda^5\left[\exp\left(\frac{C_2}{\lambda T_a}\right) - 1\right]} d\lambda$$

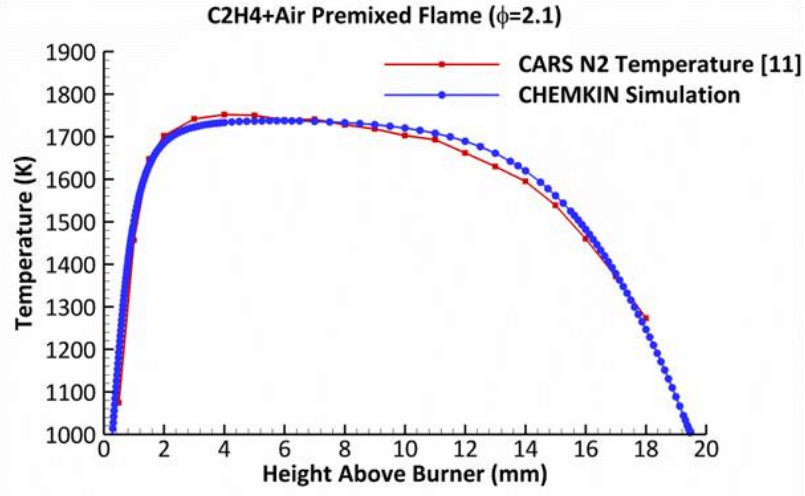

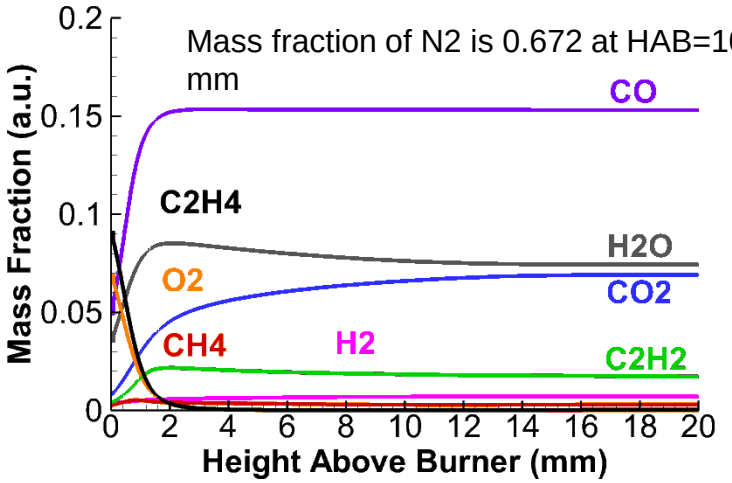

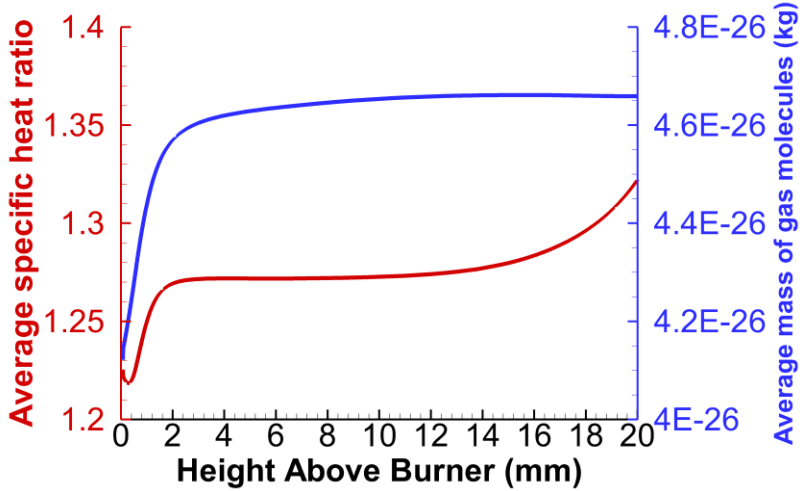

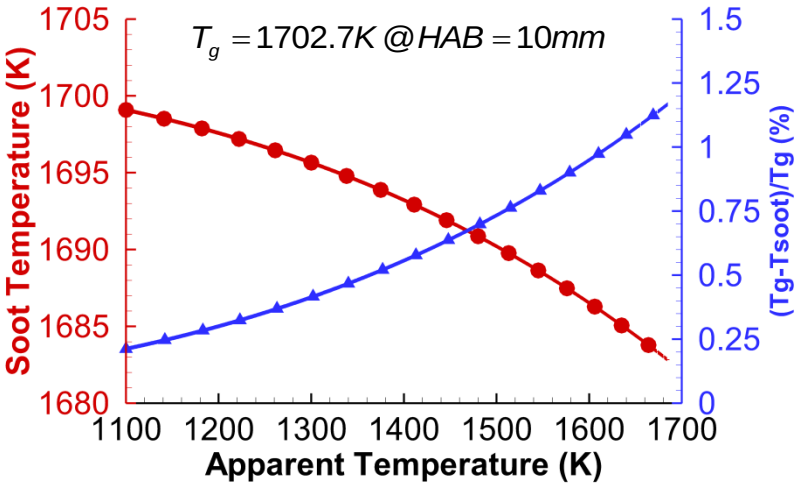

[13] Bladh, H., Johnsson, J. Olofsson, N. E., Bohlin, A. and Bengtsson, P. E., 2011, "Optical soot characterization using two-color laser-induced incandescence (2C-LII) in the soot growth region of a premixed flat flame", **33**(1), pp.641-648

Under thermal equilibrium condition, $\frac{dT_{soot}}{dt} = 0$, the following equation holds:

$$\frac{1}{8}\alpha_T p_g \sqrt{\frac{8k_B T_g}{\pi m_g}} \frac{\gamma_g + 1}{\gamma_g - 1}\left(1 - \frac{T_{soot}}{T_g}\right) = \int_{\Delta\lambda} \frac{C_1}{\lambda^5\left[\exp\left(\frac{C_2}{\lambda T_a}\right) - 1\right]} d\lambda$$

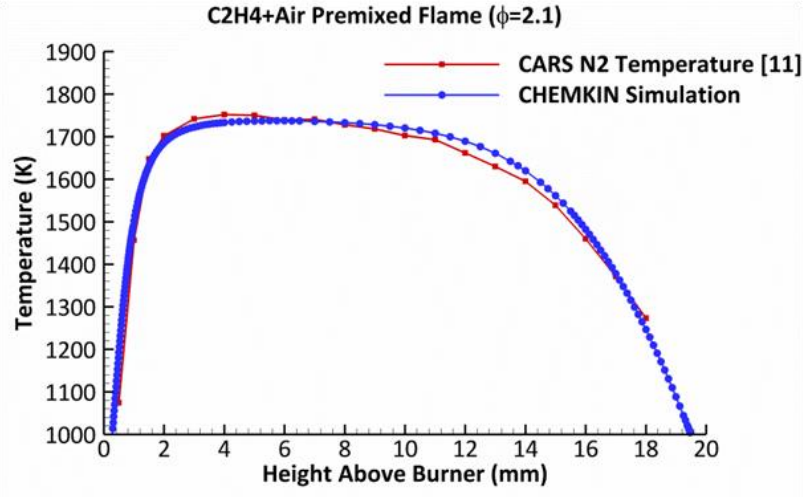

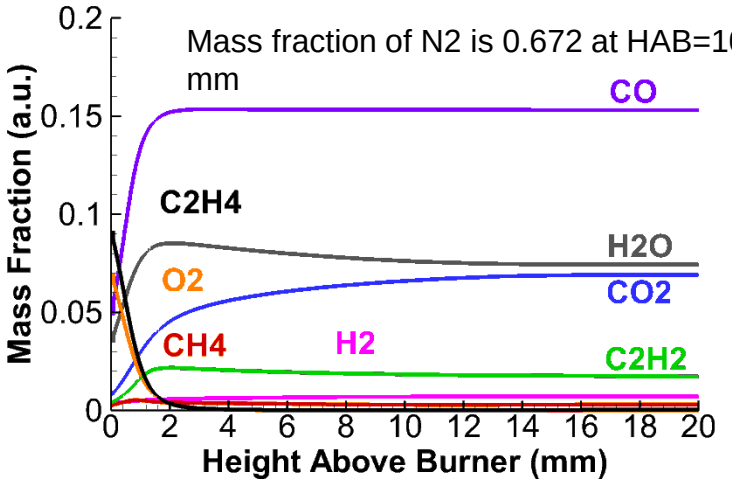

- The calculated soot temperature is close to the gas temperature (measured by CARS) with errors less than 1.25%.
- Soot temperature can be approximated by CARS gas temperature measurement.

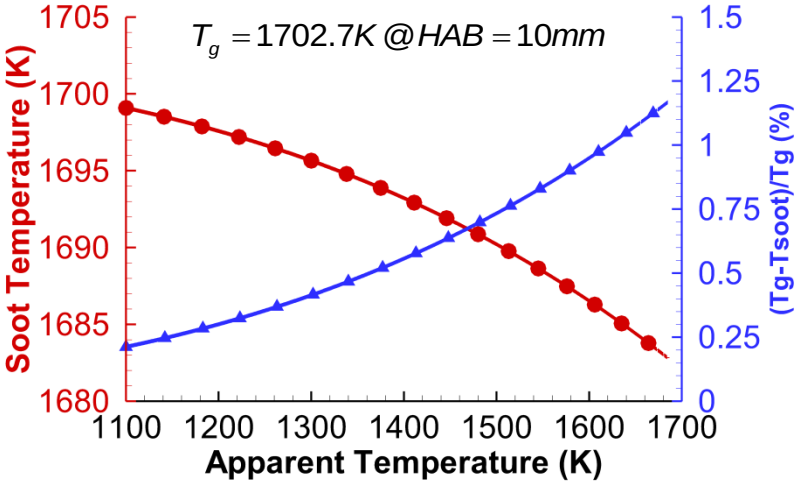

[13] Bladh, H., Johnsson, J. Olofsson, N. E., Bohlin, A. and Bengtsson, P. E., 2011, "Optical soot characterization using two-color laser-induced incandescence (2C-LII) in the soot growth region of a premixed flat flame", **33**(1), pp.641-648

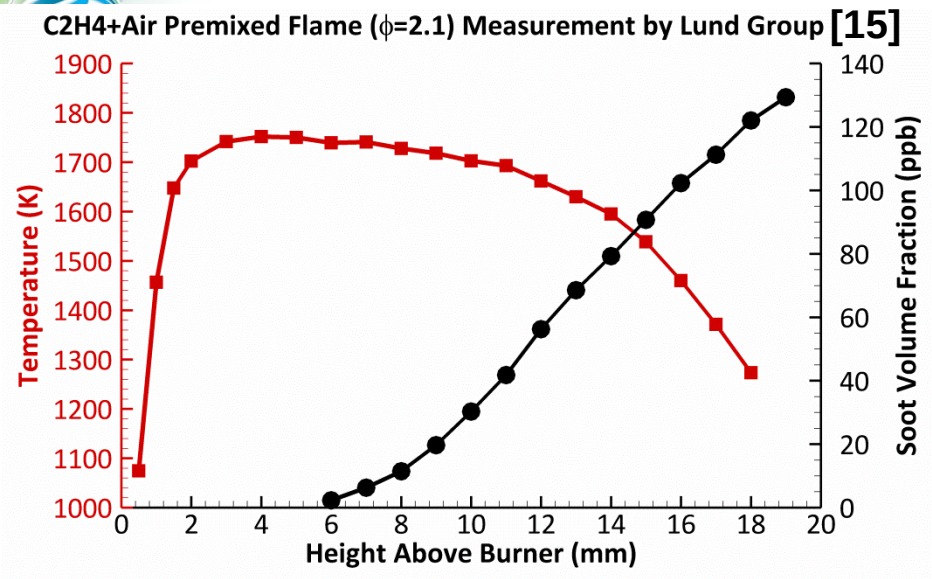

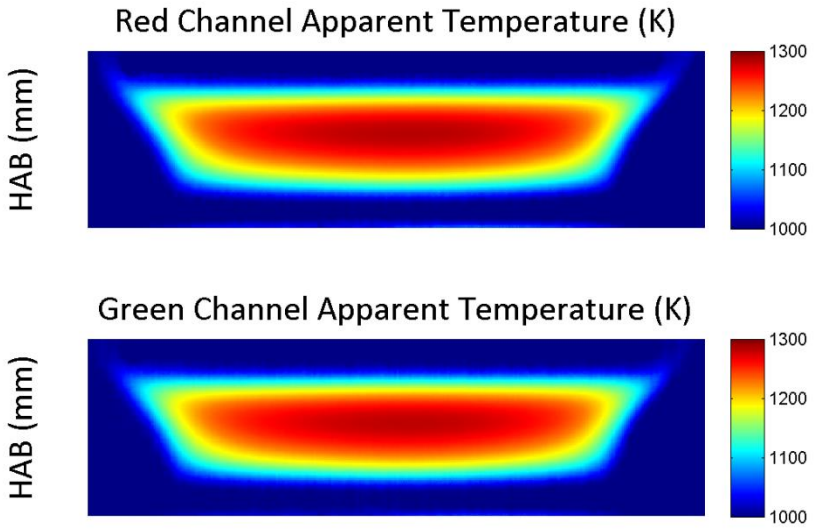

$$\int \frac{Q(red)\cdot C_1}{\lambda^5\left[\exp\left(\frac{C_2}{\lambda T_a(red)}\right)-1\right]}d\lambda = \int\left[1-\exp\left(-\frac{g_{red}\,f_v L}{\lambda^{\alpha}}\right)\right]\cdot\frac{Q(red)\cdot C_1}{\lambda^5\left[\exp\left(\frac{C_2}{\lambda T}\right)-1\right]}d\lambda$$

$$\int \frac{Q(green)\cdot C_1}{\lambda^5\left[\exp\left(\frac{C_2}{\lambda T_a(green)}\right)-1\right]}d\lambda = \int\left[1-\exp\left(-\frac{g_{green}\,f_v L}{\lambda^{\alpha}}\right)\right]\cdot\frac{Q(green)\cdot C_1}{\lambda^5\left[\exp\left(\frac{C_2}{\lambda T}\right)-1\right]}d\lambda$$

[15] Olofsson, N.-E., Bladh, H., Bohlin, A., Johnsson, J., Bengtsson, P.-E., “ARE SOOTING PREMIXED POROUS-PLUG BURNER FLAMES ONE-DIMENSIONAL? A LASER-BASED EXPERIMENTAL INVESTIGATION” Combust. Sci. Technol., 185: 293-309, (2013)

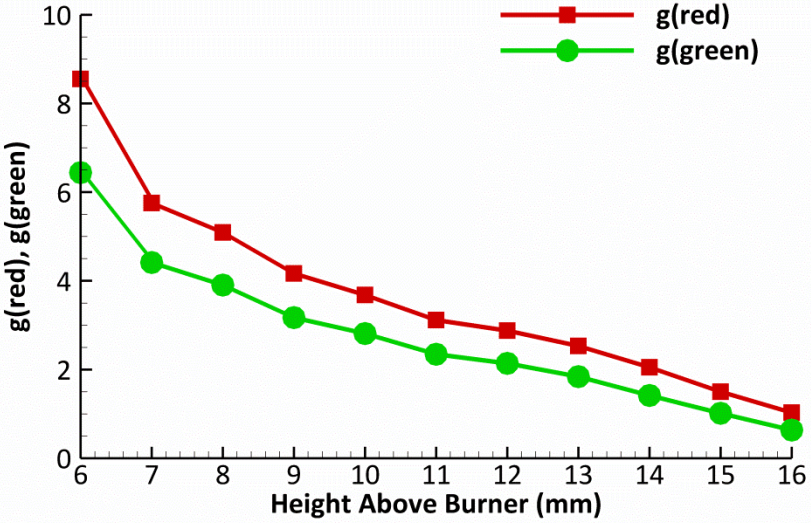

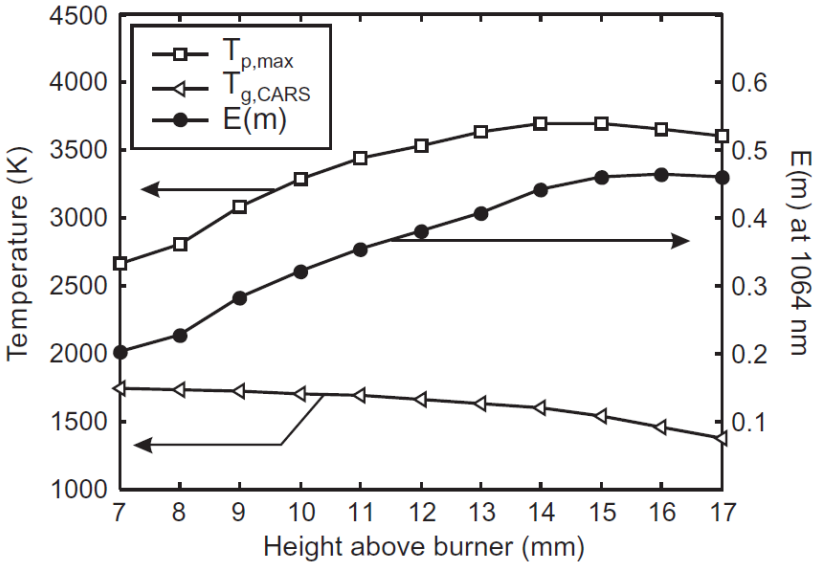

Evaluated maximum soot particle temperatures, Tp,max, flame temperatures, Tg,CARS, and the absorption function, E(m), as function of height above burner. [16]

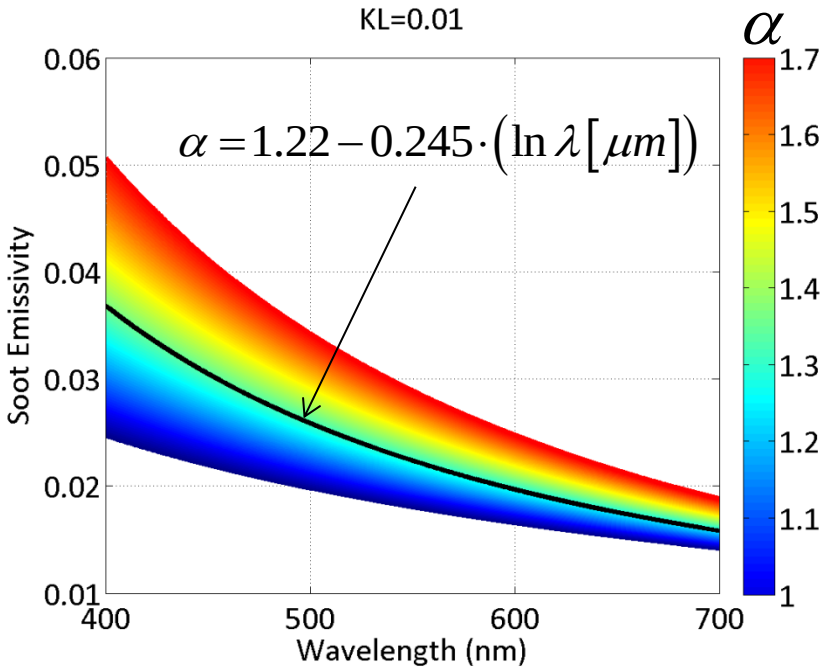

$$g_{red} \neq g_{green}$$

- Assumption of KL being wavelength-independent fails.
- g are decreasing when HAB increase is because α overestimate soot emissivity at longer wavelength for this application, because flat flame temperature gets lower with increasing HAB beyond 6 mm.

[13] Bladh, H. Johnsson, J. Olofsson, N.-E., Bohlin, A., Bengtsson, P.-E., “Optical soot characterization using two-color laser-induced incandescence (2C-LII) in the soot growth region of a premixed flat flame” Proc. Combus. Inst. 33, 641-648 (2011)

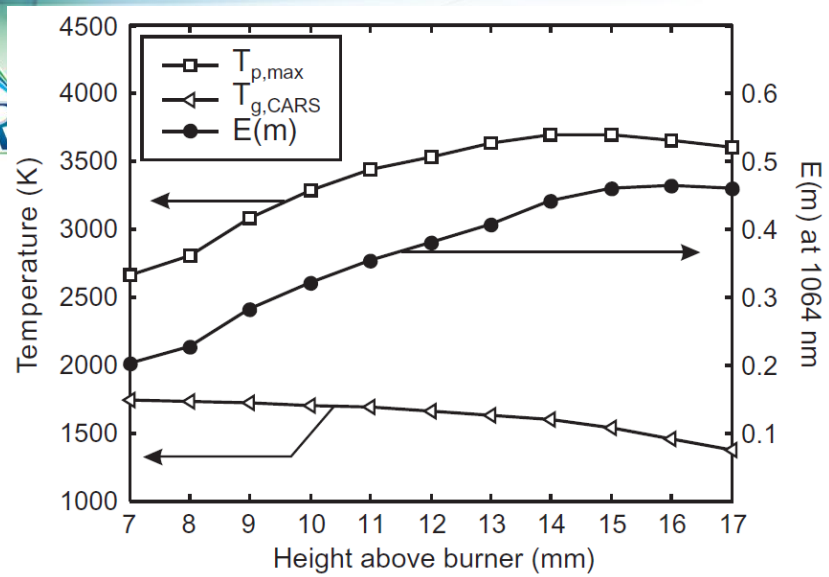

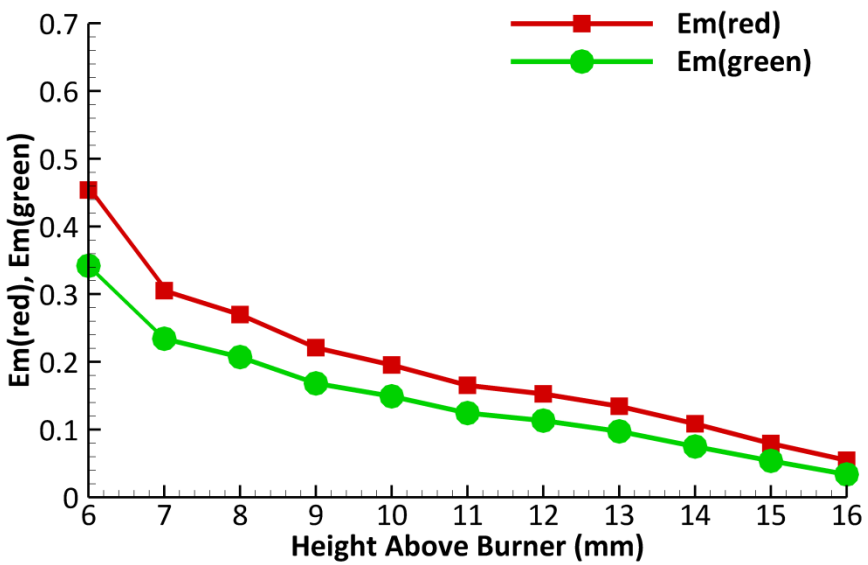

Evaluated maximum soot particle temperatures, Tp,max, flame temperatures, Tg,CARS, and the absorption function, E(m), as function of height above burner. [16]

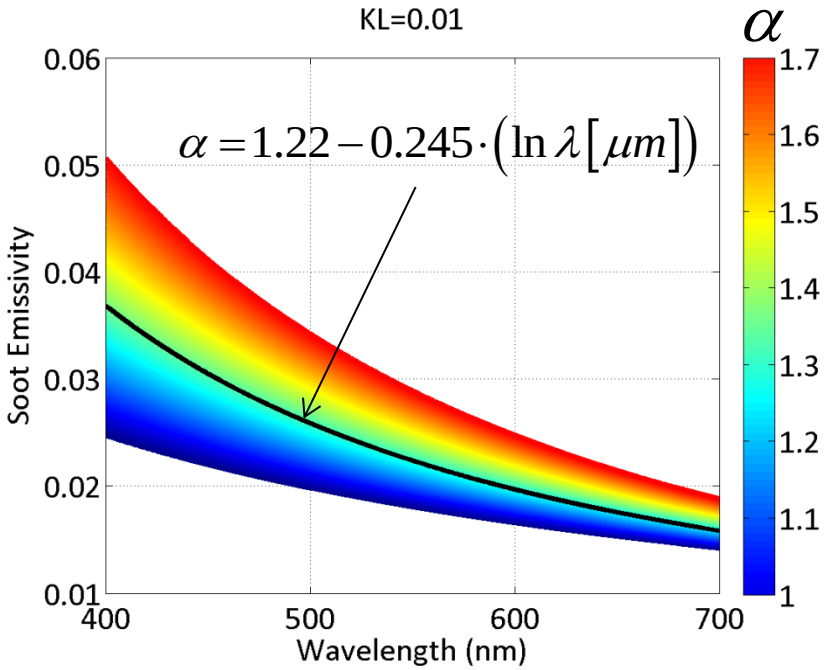

$$g = -6\pi\Im(m)$$

$$g_{red} \neq g_{green} \qquad e_{soot} = 1 - \exp\left(-\frac{g f_v L}{l^a}\right)$$

- KL is a function of wavelength.
- g are decreasing when HAB increase is because α overestimate soot emissivity at longer wavelength for this application, because flat flame temperature gets lower with increasing HAB beyond 6 mm.

[13] Bladh, H. Johnsson, J. Olofsson, N.-E., Bohlin, A., Bengtsson, P.-E., “Optical soot characterization using two-color laser-induced incandescence (2C-LII) in the soot growth region of a premixed flat flame” Proc. Combus. Inst. 33, 641-648 (2011)

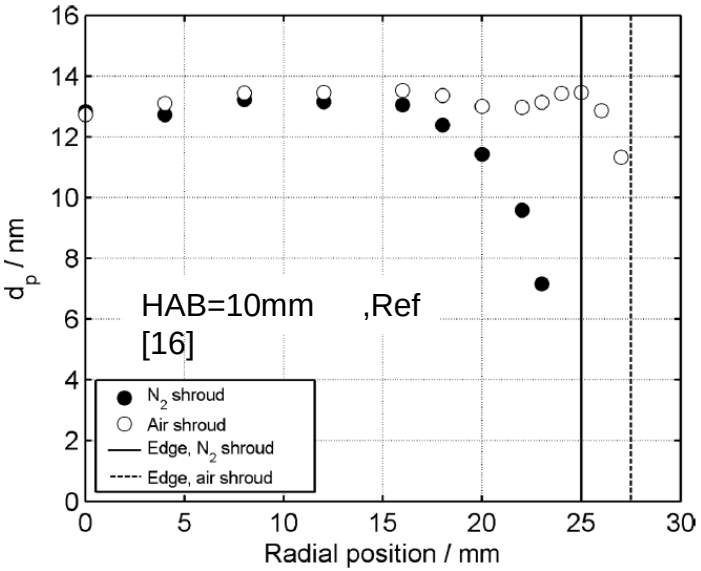

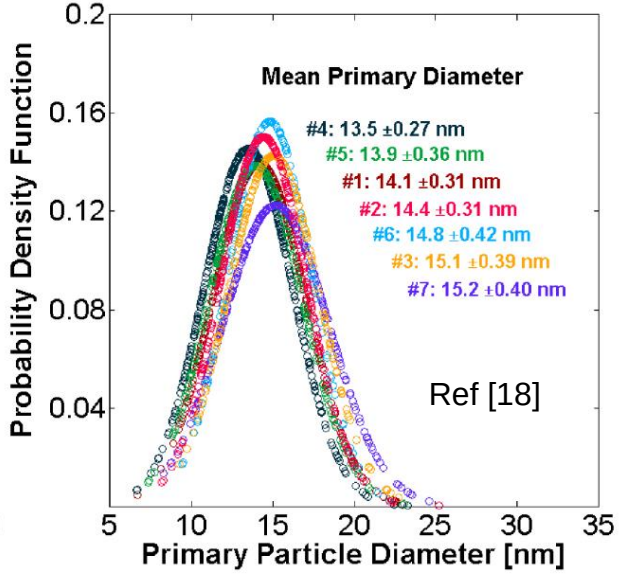

@ HAB=10 mm

$g_{red} = 3.681529$

$g_{green} = 2.810614$

Classic Two-Color Method

$$\varepsilon_{soot} = 1 - \exp\left(-\frac{KL}{\lambda^{\alpha}}\right)$$

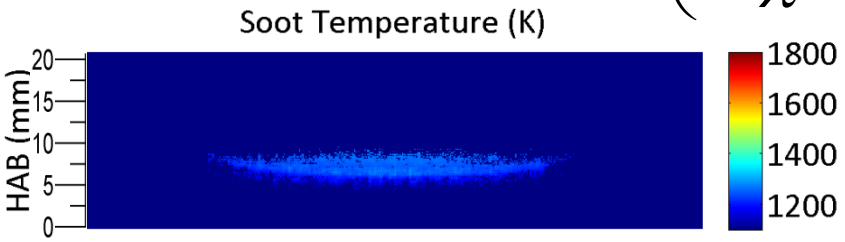

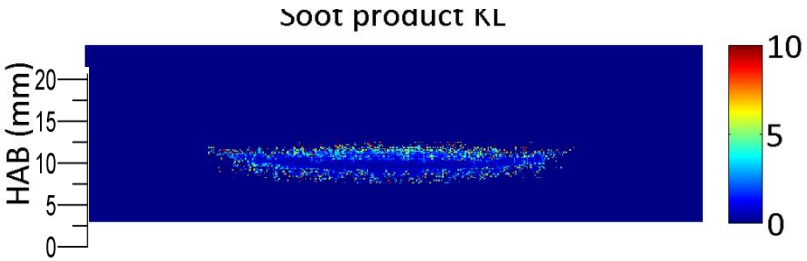

This Work

$$\varepsilon_{soot} = 1 - \exp\left(-\frac{gf_v L}{\lambda^{\alpha}}\right)$$

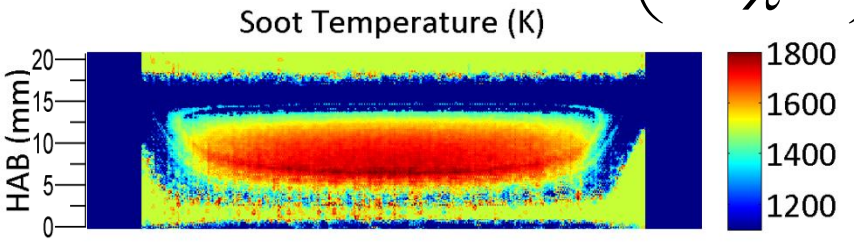

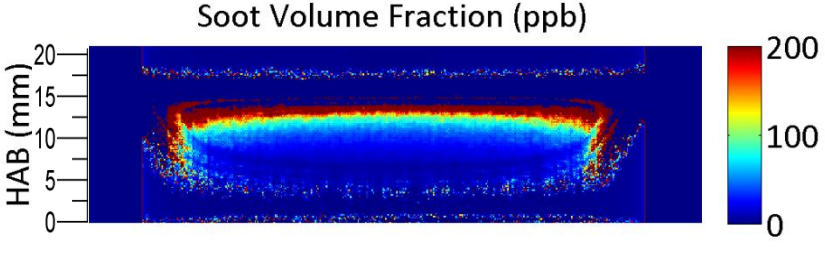

[15] Olofsson, N.-E., Bladh, H., Bohlin, A., Johnsson, J., Bengtsson, P.-E., "ARE SOOTING PREMIXED POROUS-PLUG BURNER FLAMES ONE-DIMENSIONAL? A LASER-BASED EXPERIMENTAL INVESTIGATION" Combust. Sci. Technol., 185: 293-309, (2013)

[16] Kook, S., Zhang, R., Szeto, K. Pickett, L. et al., "In-Flame Soot Sampling and Particle Analysis in a Diesel Engine"SAE Int. J. Fuels Lubr. 6(1):2013, doi: 10.4271/2013-01-0912

With flame-calibrated soot emissivity model, the discrepancy is resolved in a global perspective.

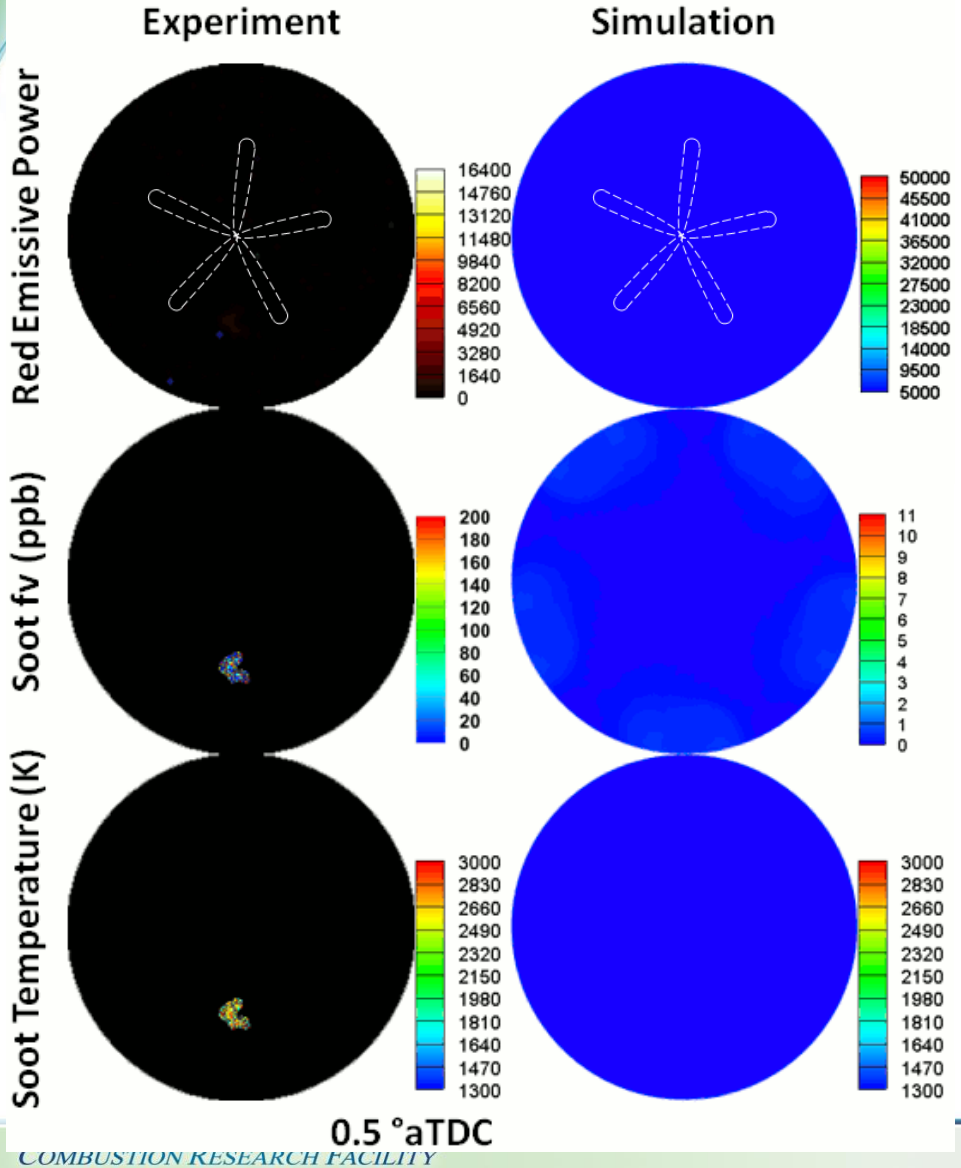

- With the flame-calibrated emissivity model, soot temperatures (both high-speed and simulation) are higher than previous results.
- Simulated two-color soot temperatures are close to the experimental two-color temperatures within ±5% from 3.5°aTDC to 44.5°aTDC.

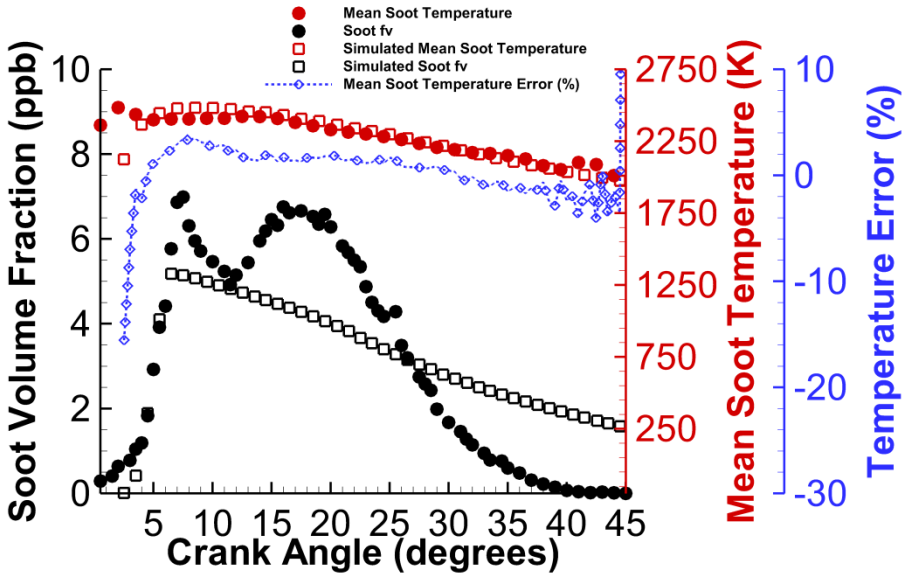

High-speed soot two-color pyrometry exhibits as a powerful tool assisting soot kinetic modeling

Soot two-step model [19]

Soot formation rate:

$$\frac{dm_{cf}}{d\theta} = \left(c_g \frac{dm_{fi}}{d\theta} + c_l m_{lt} \right) P \cdot \exp\left(-\frac{10000}{T} \right) \frac{1}{\omega}$$

Soot oxidation rate:

$$\frac{dm_{cb}}{d\theta} = c_b V_u \frac{6 m_{cf}}{\rho_c d_c} \cdot P_{O_2} \cdot \exp\left(-\frac{39300}{RT} \right) \frac{1}{\omega}$$

Net rate of soot formation:

$$\frac{dm_c}{d\theta} = \frac{dm_{cf}}{d\theta} - \frac{dm_{cb}}{d\theta}$$

Soot phenomenological model [20]

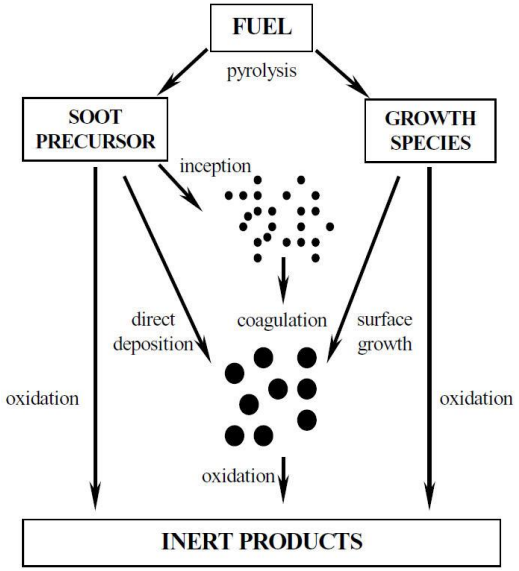

[17] Hiroyasu, H. and Kadota, T., 1976, "Models for Combustion and Formation of Nitric Oxide and Soot in Direct Injection Diesel Engines", *SAE Technical Paper* 760129, DOI:10.4271/760129

[18] Liu, Y., Tao, F., Foster, D. E. and Reitz, R. D., 2005, "Application of a Multiple-Step Phenomenological Soot Model to HSDI Diesel Multiple Injection Modeling", *SAE Technical Paper* 2005-01-0924, DOI:10.4271/2005-01-0924

Outline

- Motivation
- High-speed in-cylinder soot optical thermometry
- **Particle image velocimetry (PIV) inside an optical engine for swirl asymmetry quantification**
- Quantification of in-cylinder mixture preparation with fuel tracer planar laser-induced fluorescence (PLIF) technique
- Research outlook

Reduce spray asymmetry is considered as one strategy to reduce UHC emission in LTC regime.

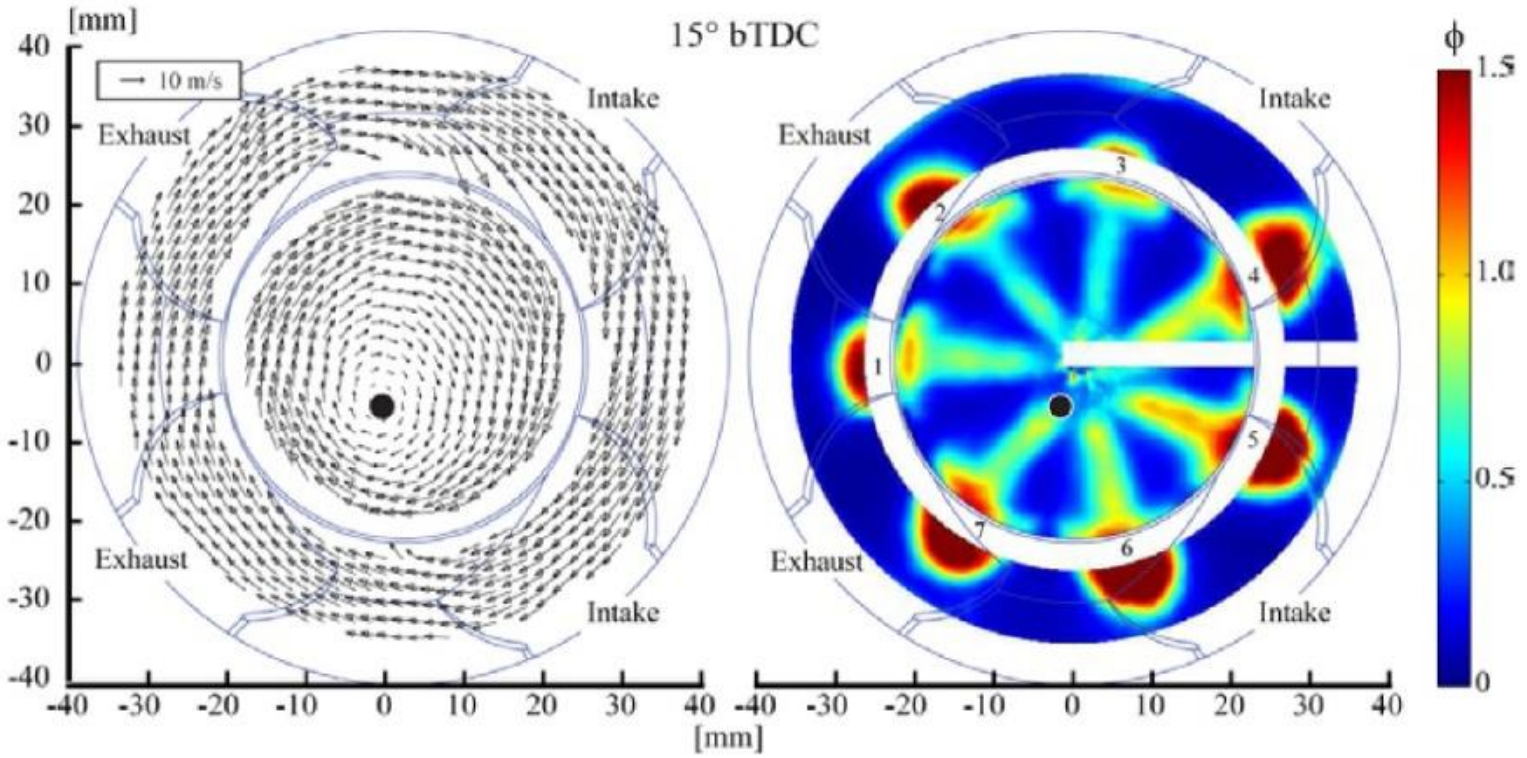

- In-cylinder mean flow asymmetry is initiated by the intake port orientation for twin-port design.
- The asymmetrical mean flow with realistic piston bowl geometry has been observed both in simulation and experiment.

[19] Petersen, B., Miles, P., and Sahoo, D., "Equivalence Ratio Distributions in a Light-Duty Diesel Engine Operating under Partially Premixed Conditions," *SAE Int. J. Engines* 5(2):526-537, 2012, doi:10.4271/2012-01-0692.

In-cylinder swirl is initiated by intake port geometry which generates jets with significant bore-scale angular momentum (twin-port type design).

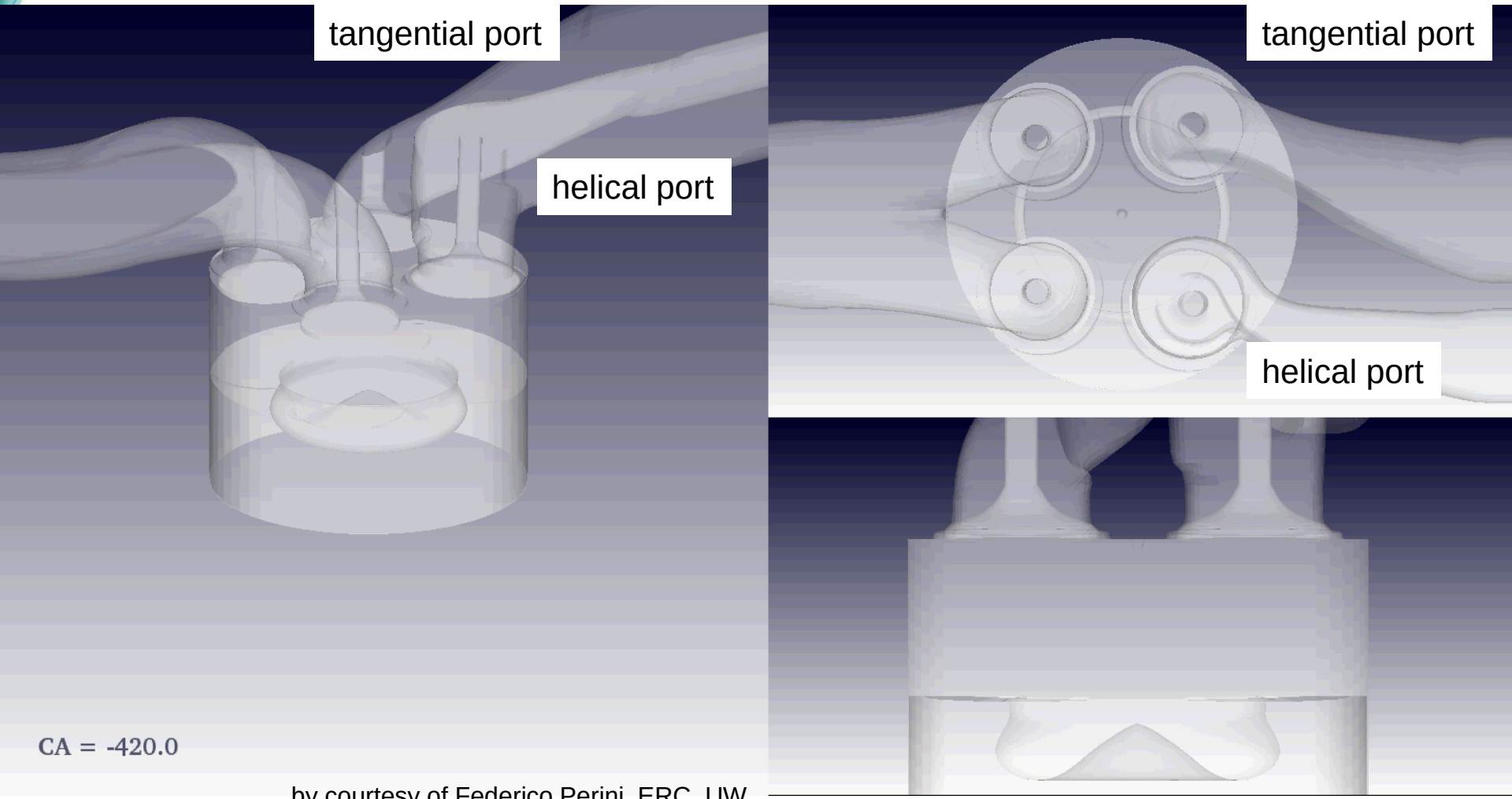

by courtesy of Federico Perini, ERC, UW

Resolving meaningful in-cylinder velocity measurements from a real combustion device is not easy because…

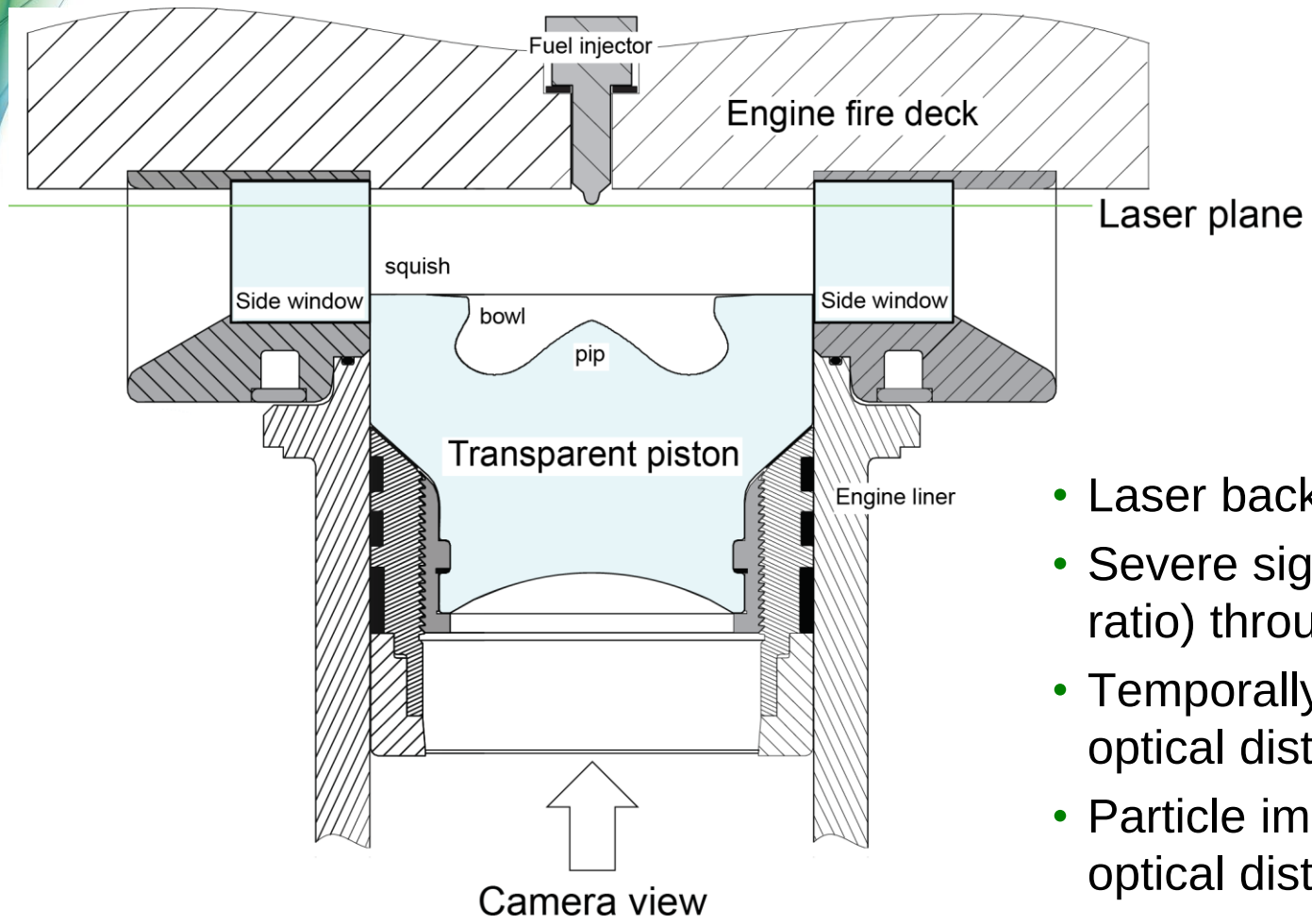

- Laser background scattering.
- Severe signal degradation (S/N ratio) through the piston.
- Temporally- and spatially-variant optical distortion.
- Particle image aberration due to optical distortion.
- Beam steering.

A demonstration of planar PIV experiments inside a swirl-supported light-duty optical Diesel engine with a realistic piston geometry

18µm SiO_2, -20°aTDC, z=2.5mm

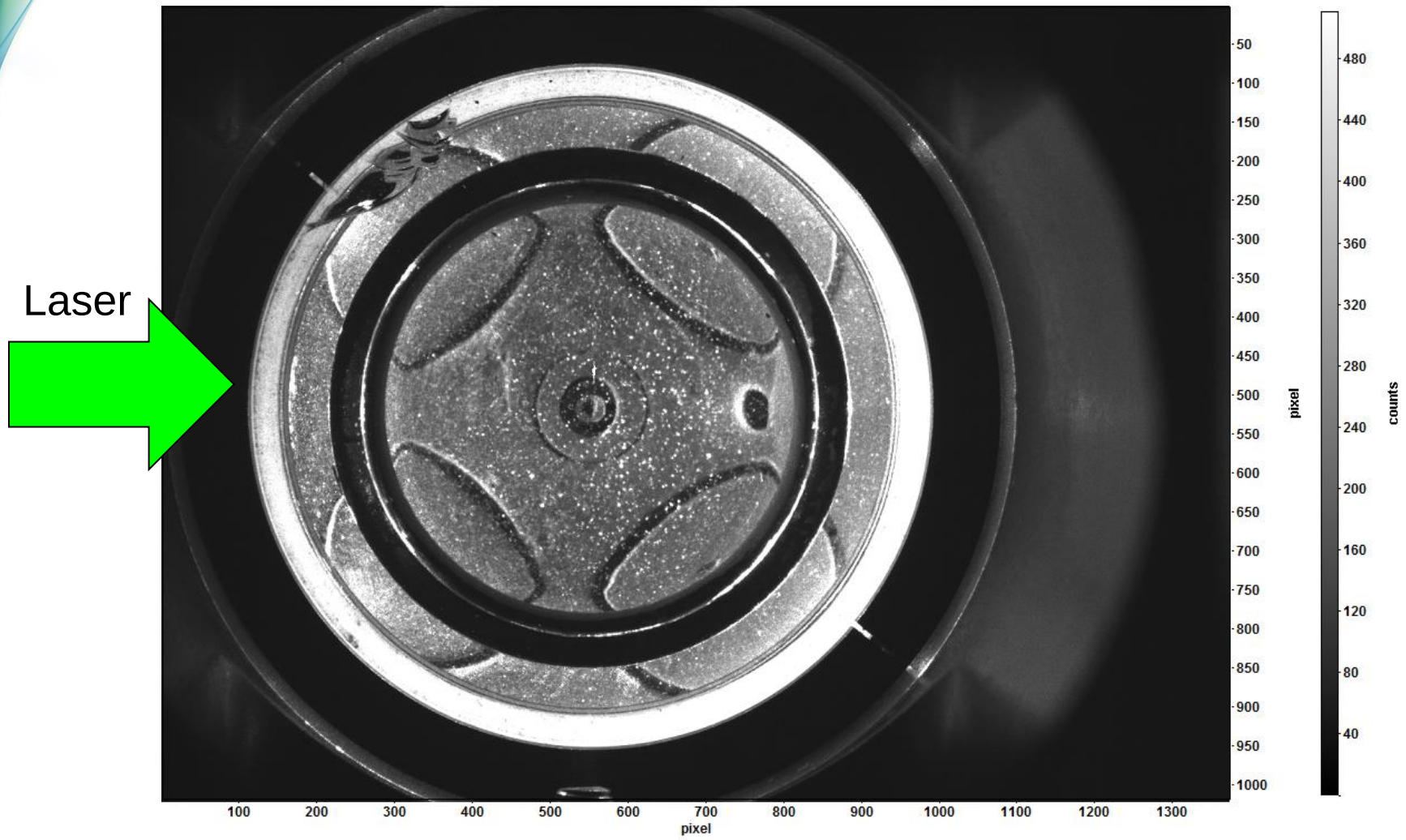

Strong beam steering effects create streaks in the laser sheet; PIV processing is unsuccessful for squish flow measurements

18µm SiO_2, -0°aTDC, z=0.67mm

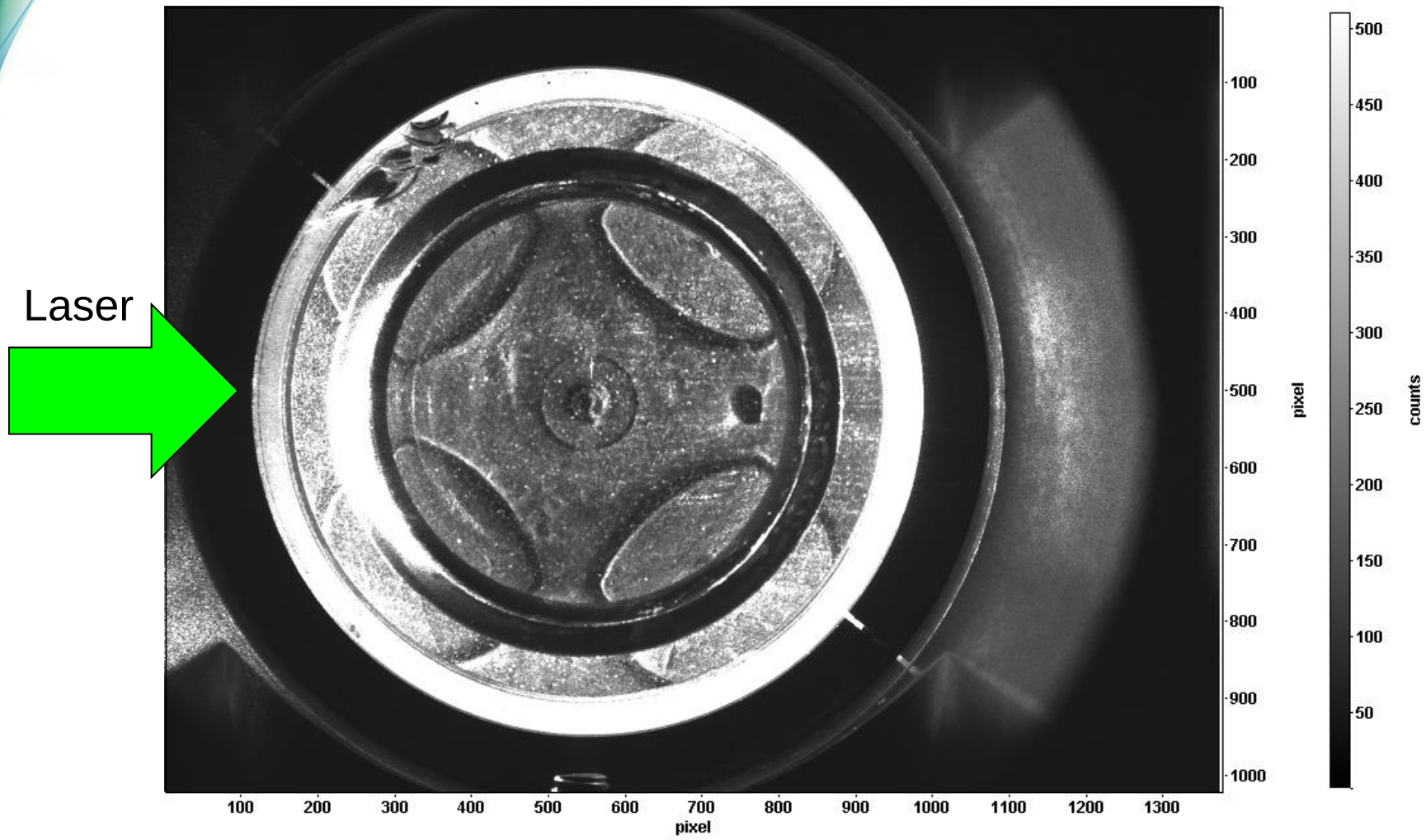

The proposed hybrid back-projection method accounts for the optical distortion change during the laser temporal interval.

Raw Target Image

Dewarped Target Image

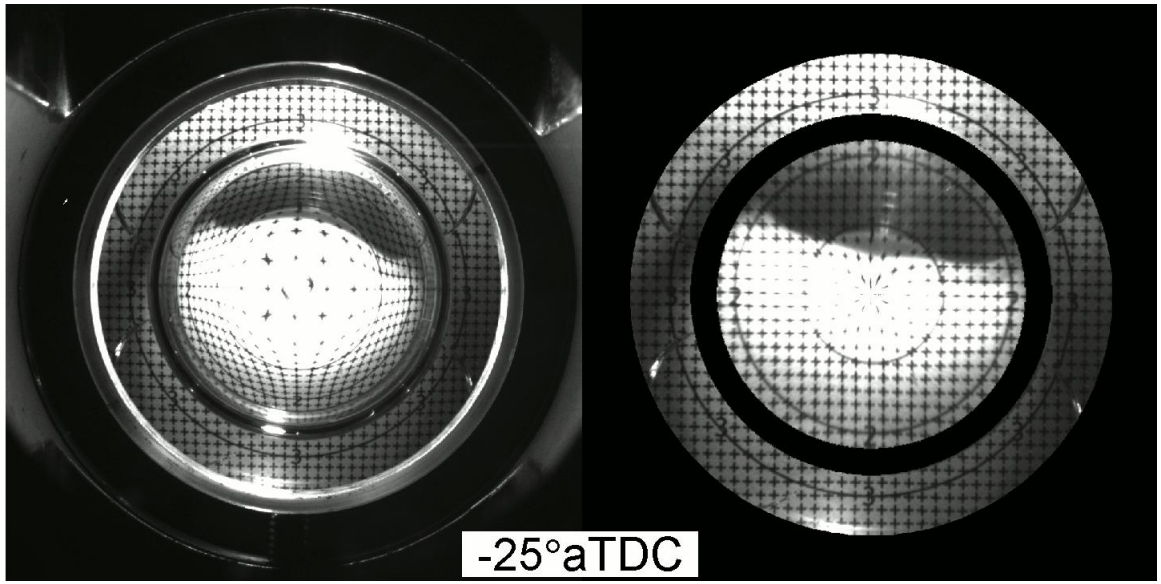

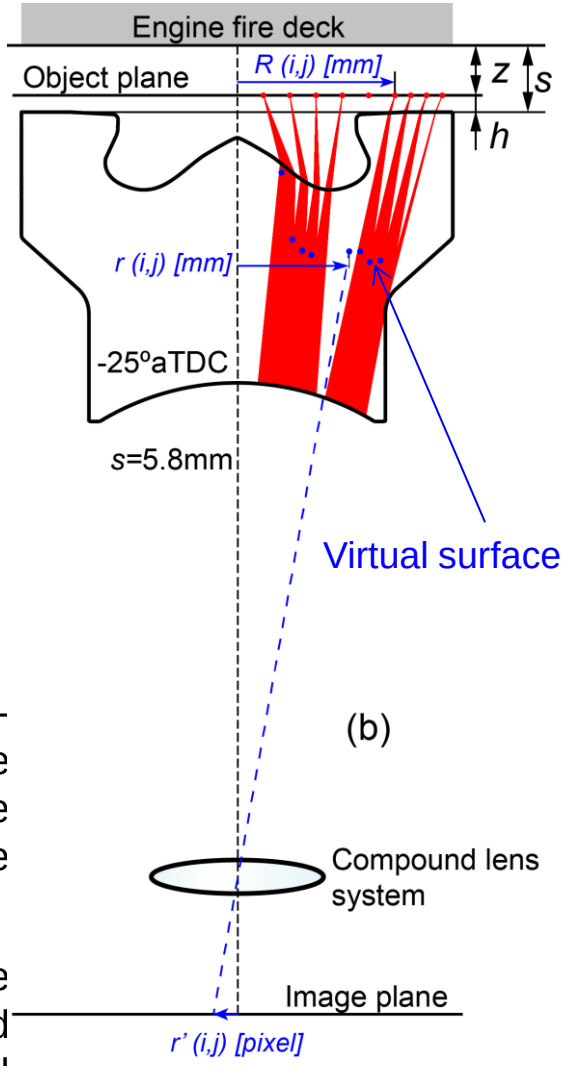

Artificial radial velocity @ -45^{0}aTDC

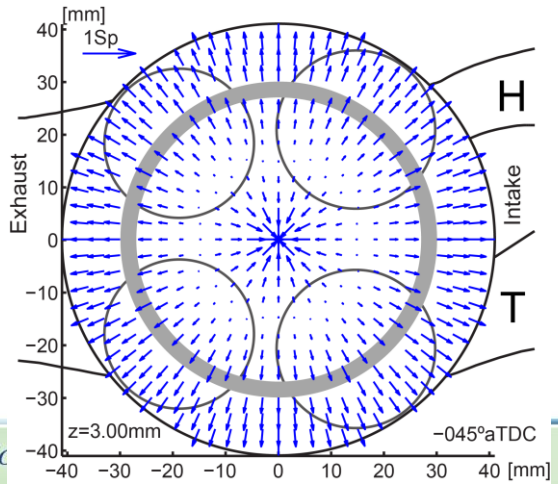

- Distorted particle images are two-dimensional projections of the virtual surface through the compound lens system in the image plane.
- Neglecting optical distortion change during laser temporal interval could results in significant artificial radial velocity components.

Ray tracing allows a full dewarping transformation with any given laser plane position and piston location.

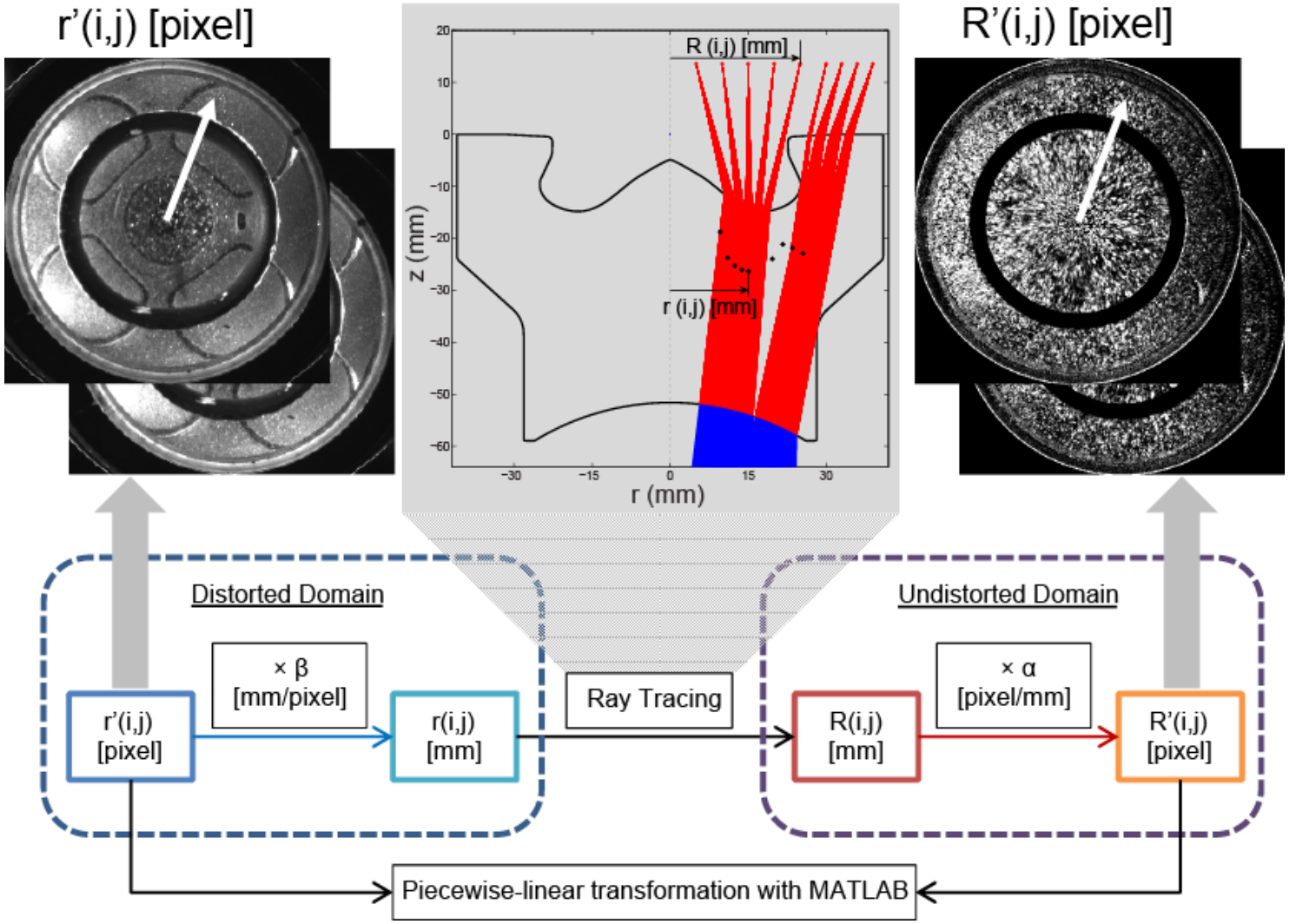

[20] Zha, K., Busch, S., Park, C. and Miles, P.C., 2016. A novel method for correction of temporally-and spatially-variant optical distortion in planar particle image velocimetry. *Measurement Science and Technology*, *27*(8), p.085201.

Uncertainty analysis of the hybrid back-projection method with simulated particle images (Method A).

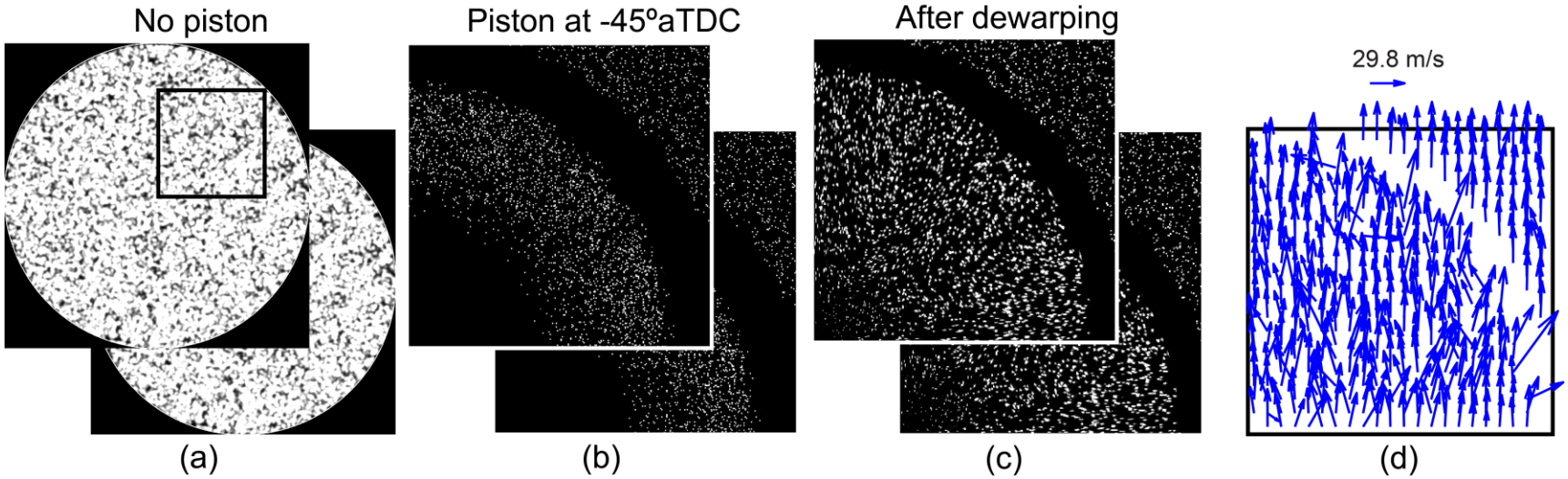

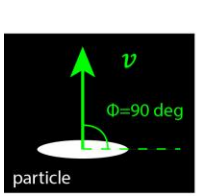

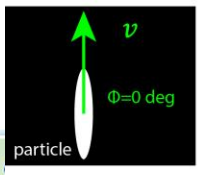

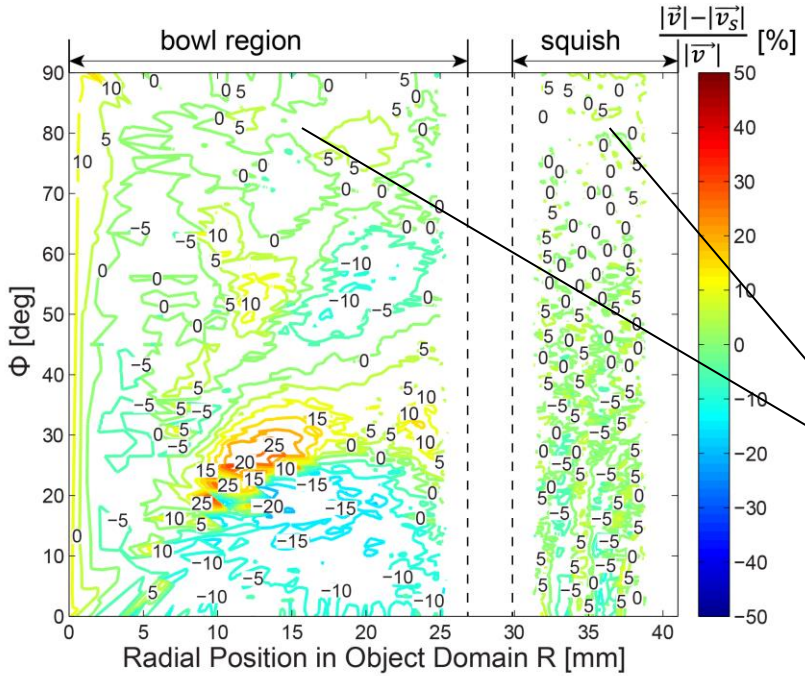

- Dewarping-induced systematic error is not only spatially dependent, but also has directional dependence.
- Systematic error in the squish region is smaller than in the bowl region due to less severe particle image deformation.
- For swirling flows with small radial velocity components, this error may not be significant (less than 6%).

Uncertainty analysis of the hybrid back-projection method with simulated particle images (Method B).

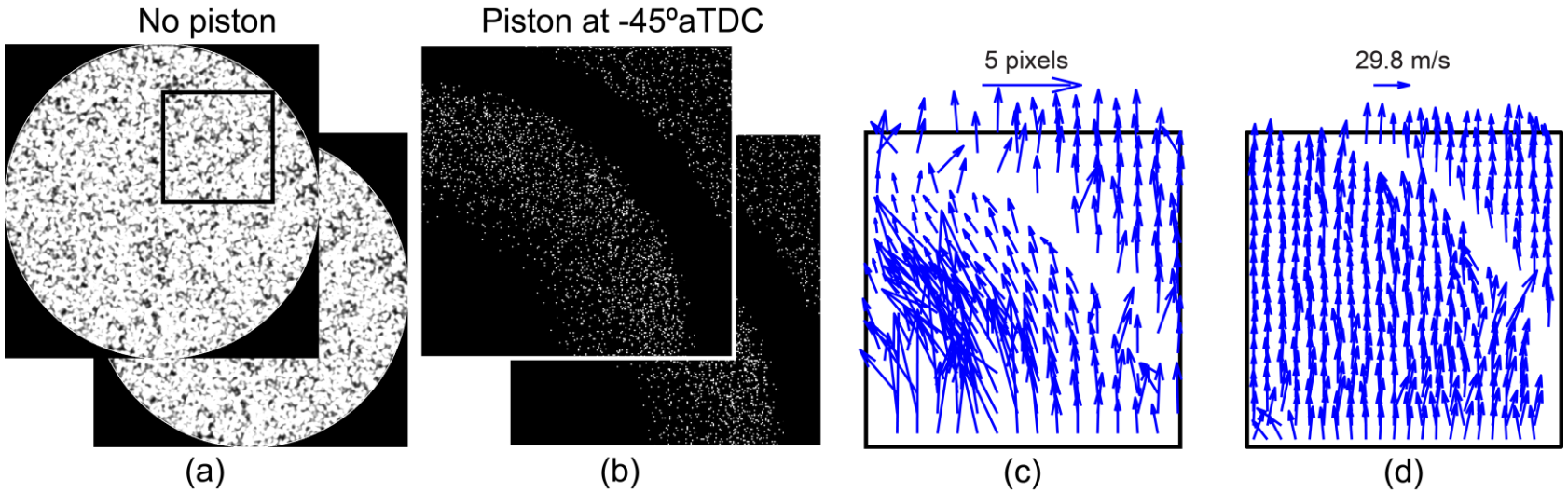

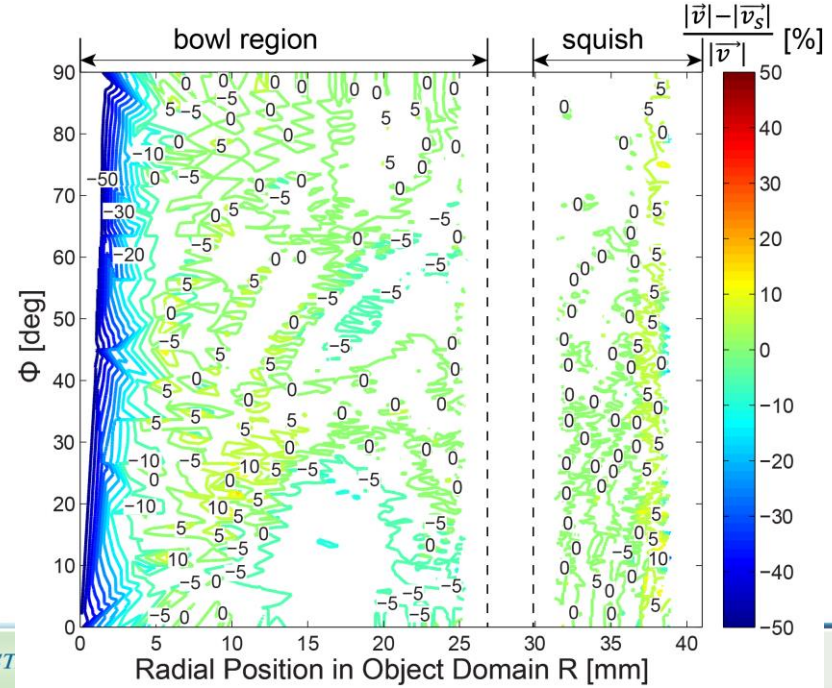

- Dewarping-induced systematic error is reduced if PIV interrogation is performed on undewarped particle image pairs (especially inside bowl area, except injector exit).
- Systematic error in the squish region is smaller than in the bowl region due to less severe particle image deformation.

Two optical pistons are compared to quantify piston-induced swirl asymmetry

- Two piston bowl geometries with the same bowl volume available for in-cylinder flow asymmetry comparison.

Re-entrant

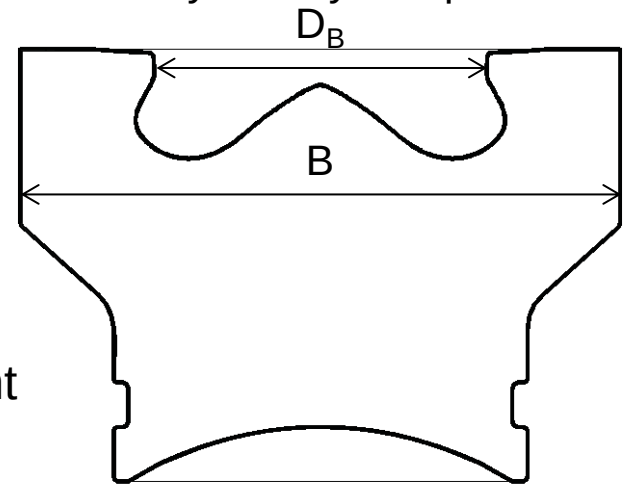

- Squish height (TDC) = 0.711 mm
- Compression ratio = 16.7
- With valve cut-outs
- Bowl to bore ratio: $D_B/B=0.55$
- Plenty of data available with this geometry matching fired LTC cases

Stepped-lip

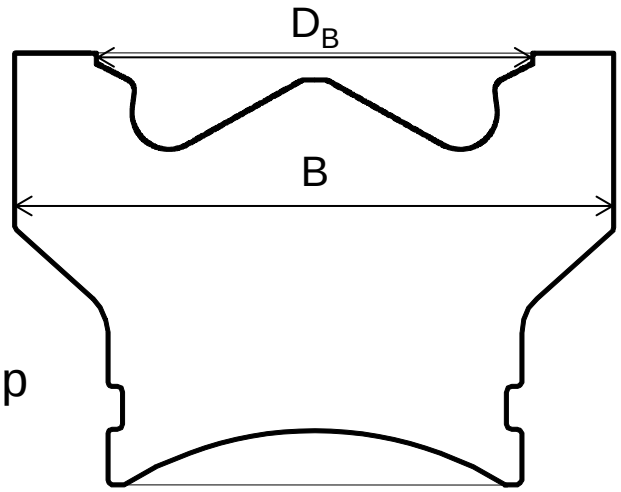

- Squish height (TDC) = 1.346 mm
- Compression ratio = 15.8
- Different optical distortion pattern
- No valve cut-outs
- Bowl to bore ratio: $D_B/B=0.73$
- 30% higher laser pulse energy
- Optimized laser sheet

Swirl-Plane PIV Measurement Setup and Test Cases

GM 1.9 L Diesel Engine	
Bore	82 mm
Stroke	90.4 mm
Displacement Volume	0.477 L
Geometries CR	16.7
Intake / Exhaust Valves	2 / 2
Swirl Ratio	2.2, 3.5
Engine Speed	1500 rpm
Intake Pressure	1.5 bar
Intake Temperature	99^0C
O2 Mole Fraction	10%
Constant total mass flow rate	8.936 g/s
Operating Condition	Motoring

Test cases:

- Swirl-plane vertical position (below fire deck) z=3mm, z=10mm and z=18mm.
- CAD of PIV measurement: every 15CAD through full intake and compression (until piston interferes with laser sheet).

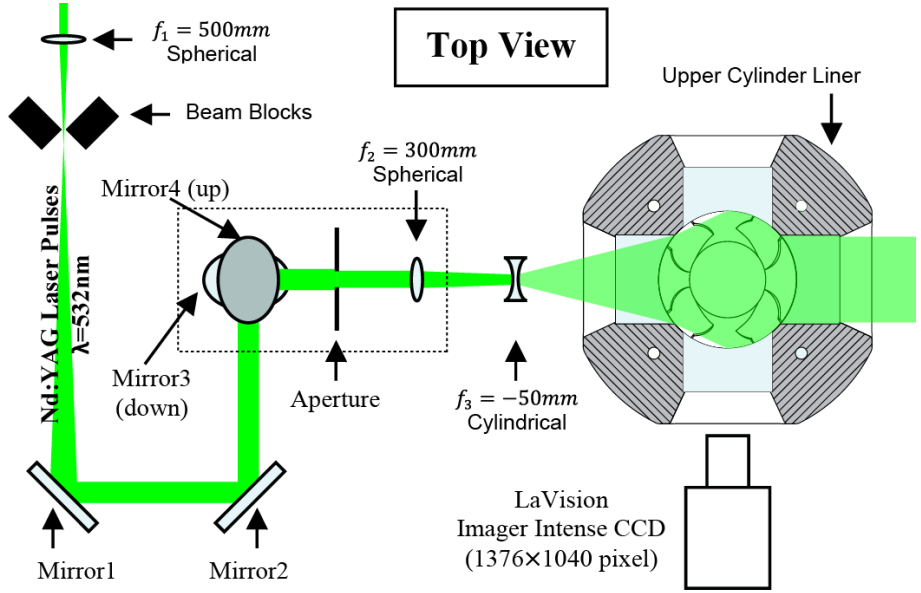

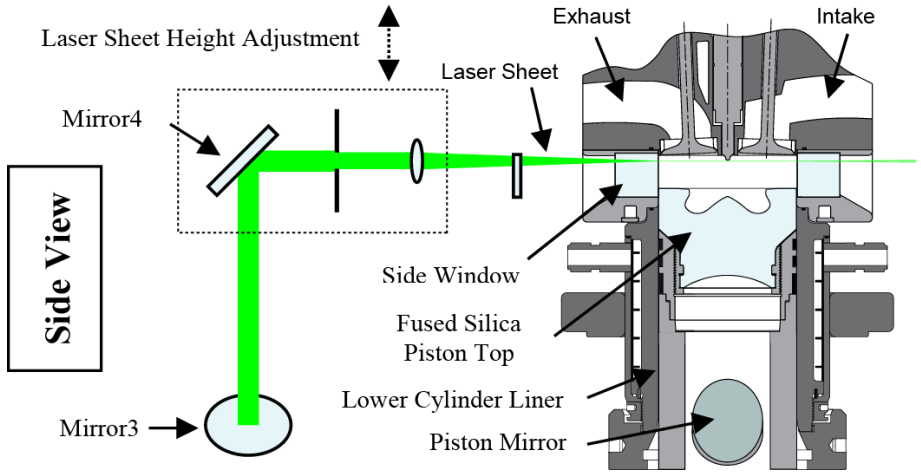

Instantaneous velocity results ($R_{s,steady}$=2.2) from swirl-plane PIV measurements

Re-entrant piston bowl

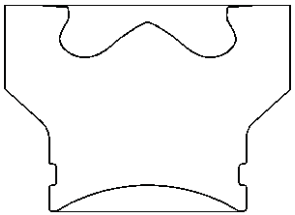

Stepped-lip piston bowl

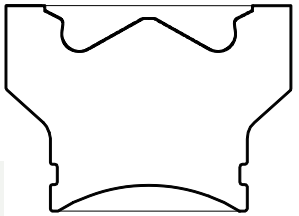

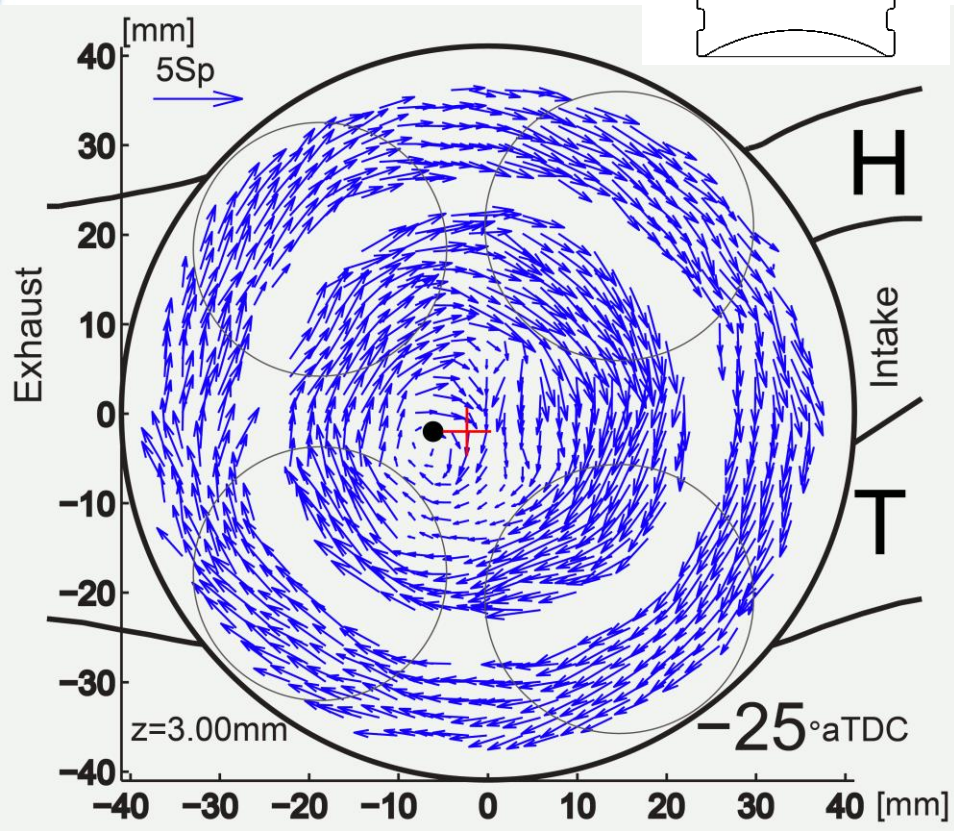

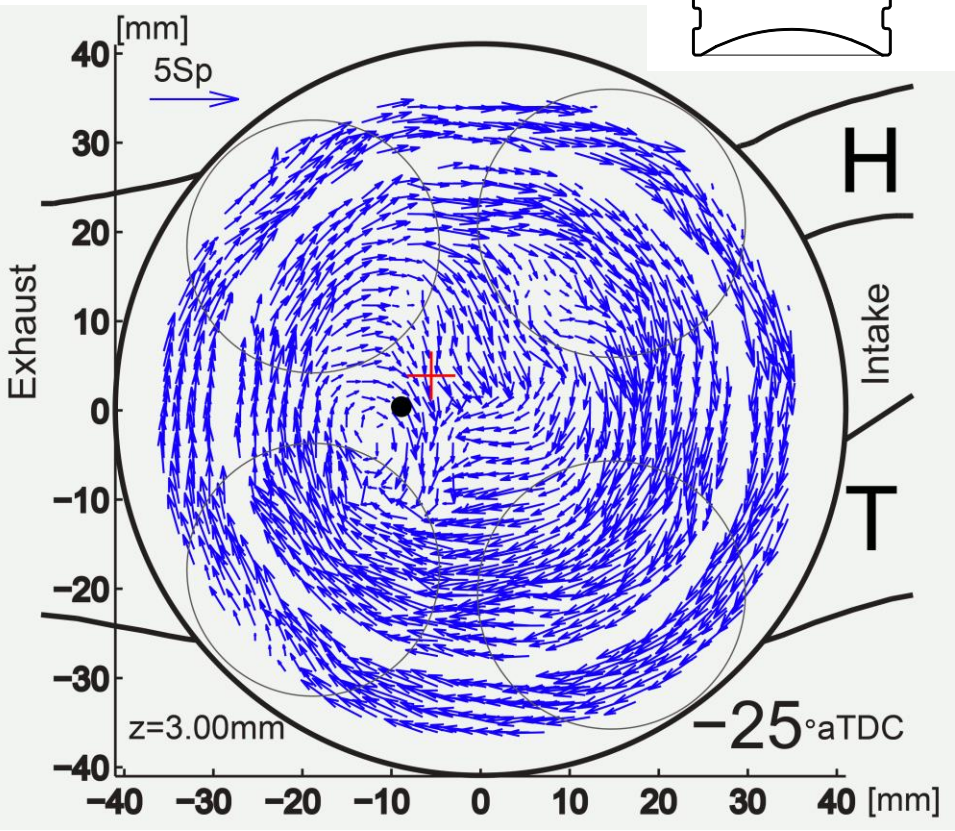

Black dots show the swirl center location for each instantaneous velocity field. Red crosses mark the swirl center mean locations. S_p stands for mean piston speed (4.51 m/s). "H": helical port, "T": tangential port.

In-cylinder swirl with stepped-lip piston is more eccentric.

Re-entrant piston bowl, $R_{s,steady}$=2.2

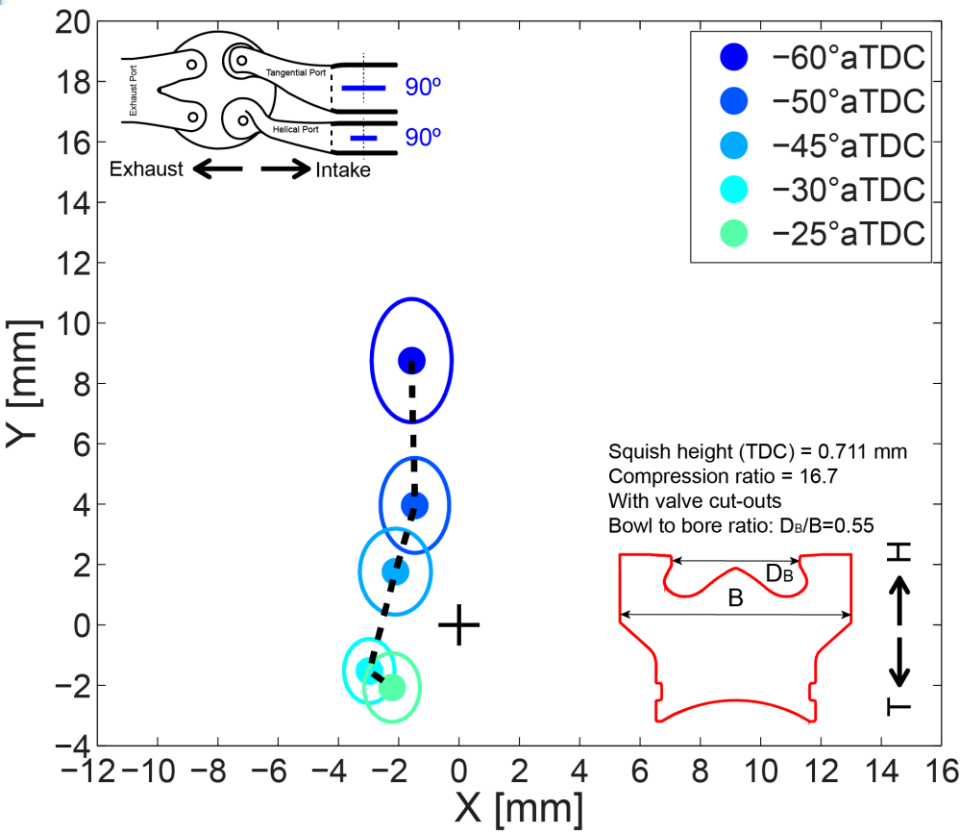

Stepped-lip piston bowl, $R_{s,steady}$=2.2

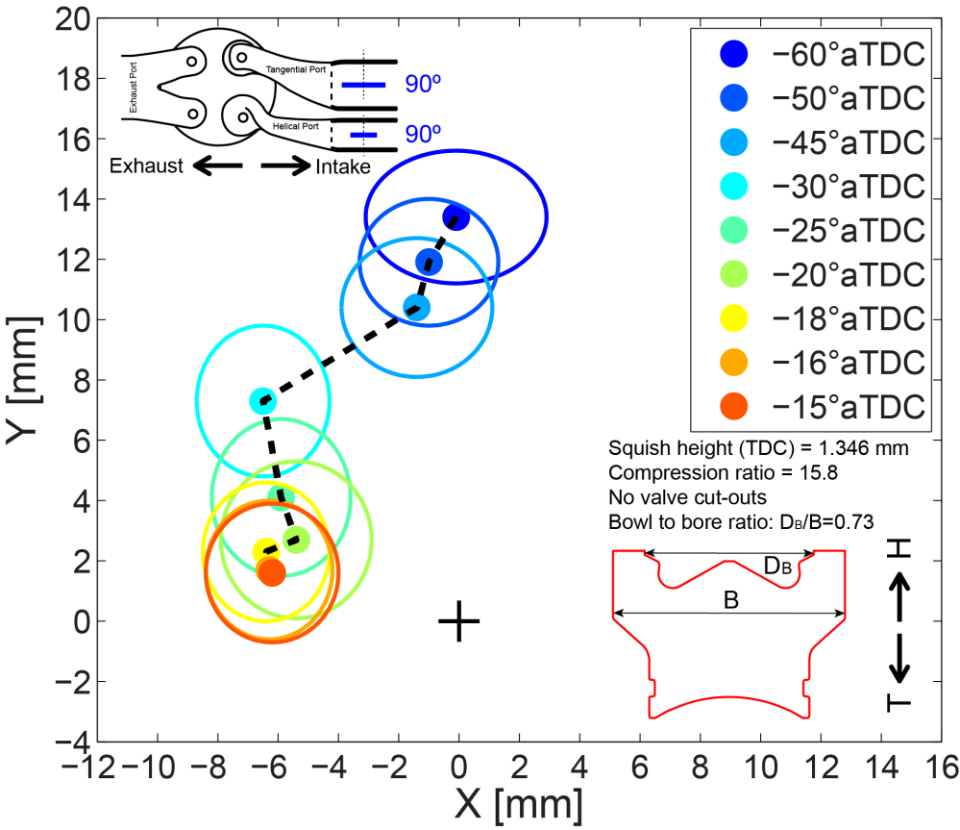

Each black ellipse indicates one σ of swirl center location away from the mean positions (out of 220 instantaneous velocity fields).

Outline

- Motivation
- High-speed in-cylinder soot optical thermometry
- Particle image velocimetry (PIV) inside an optical engine for swirl asymmetry quantification
- **Quantification of in-cylinder mixture preparation with fuel tracer planar laser-induced fluorescence (PLIF) technique**
- Research outlook

What makes the stepped-lip bowl more efficient than the conventional bowl?

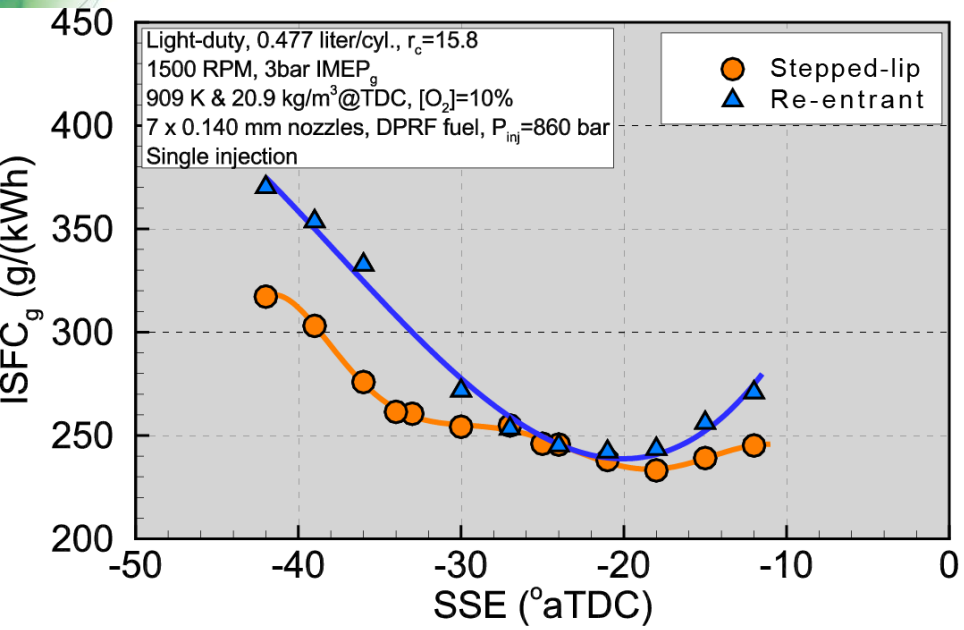

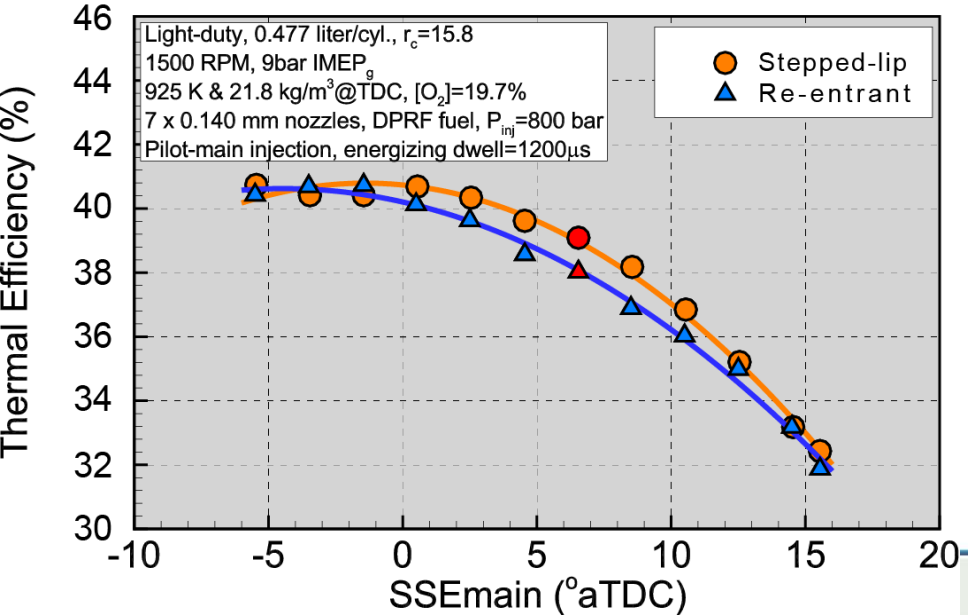

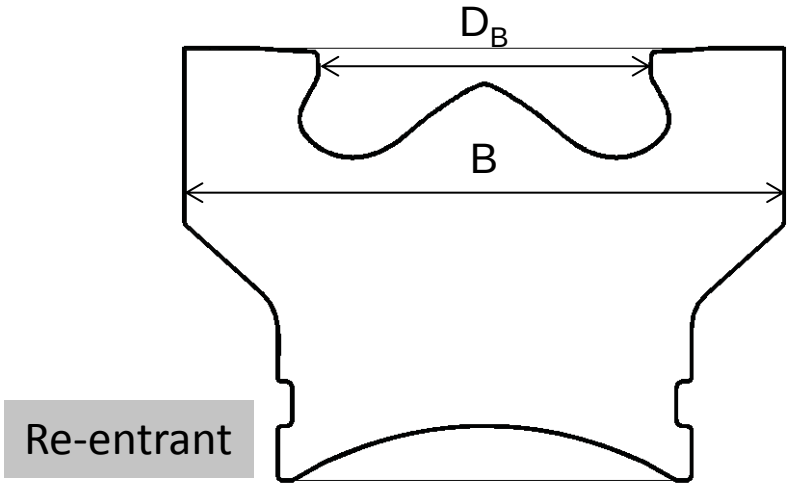

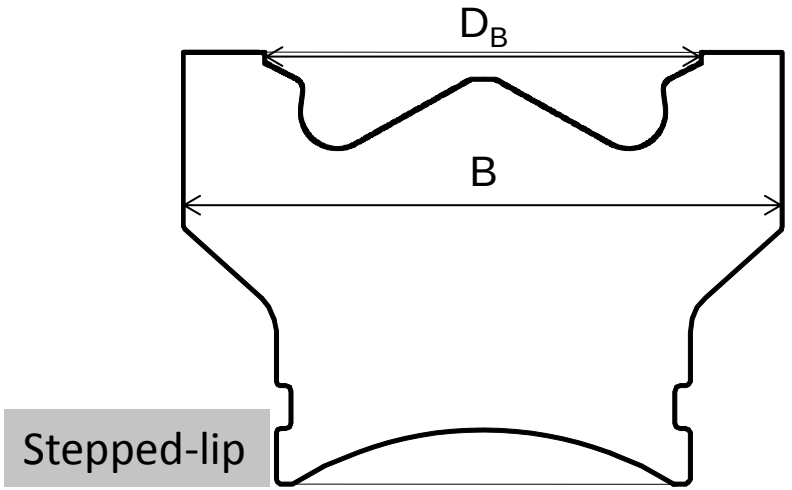

What makes the stepped-lip bowl more efficient than the conventional bowl?

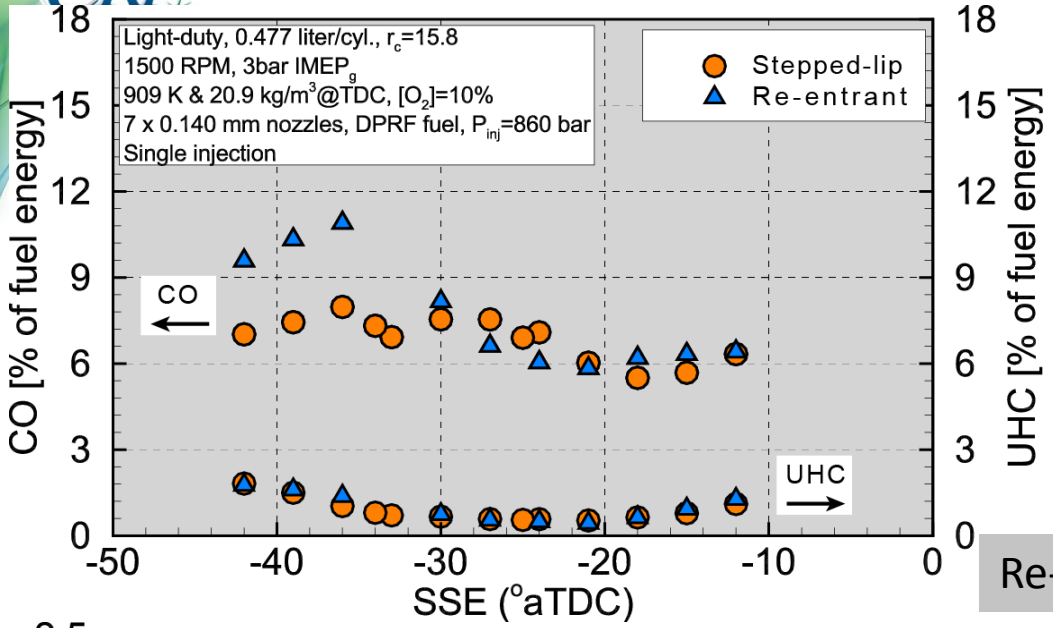

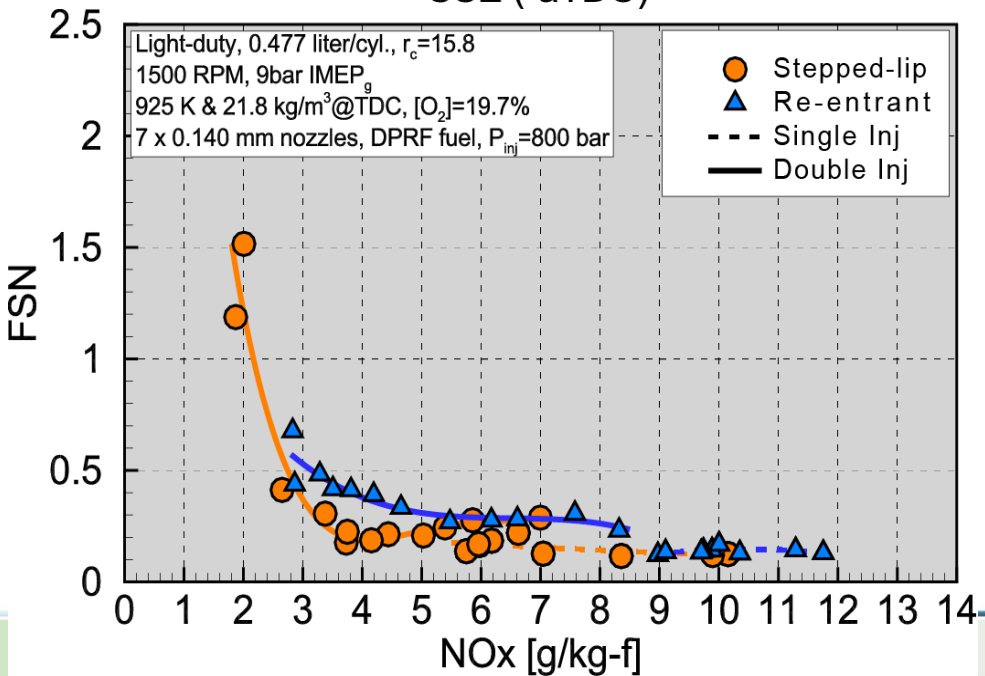

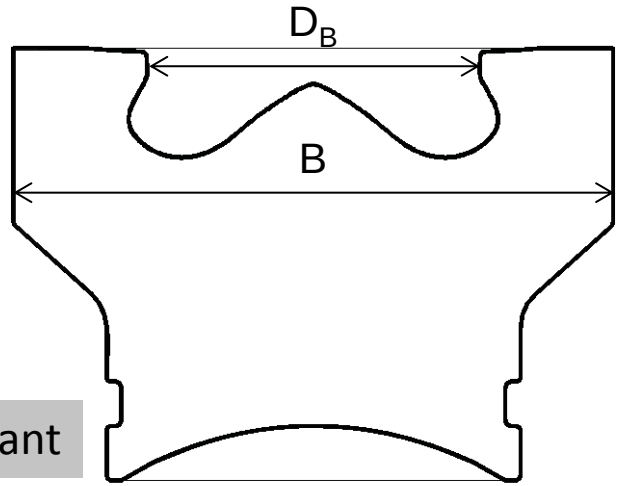

Re-entrant

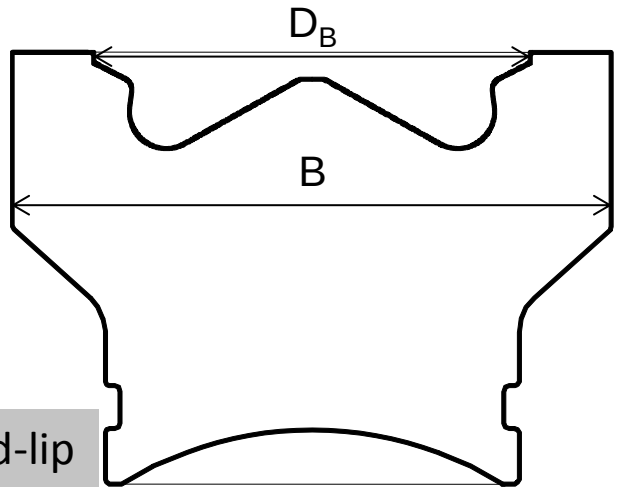

Stepped-lip

In order to understand the mechanism, piston geometry effects on in-cylinder mixture preparation is needed to investigate.

- Two quartz pistons have identical:
  - Bowl volume = 0.028 L
  - Squish height = 1.35 mm
  - Compression ratio = 15.8
  - No valve cut-outs
- Different bowl geometry result in different bowl-to-bore ratio:
  - Re-entrant: $D_B/B=0.55$
  - Stepped-lip: $D_B/B=0.73$
- Surface area of stepped-lip bowl is ~10% less than for the conventional bowl
- Injector tip penetration is set based on recommendations from OEM partners.

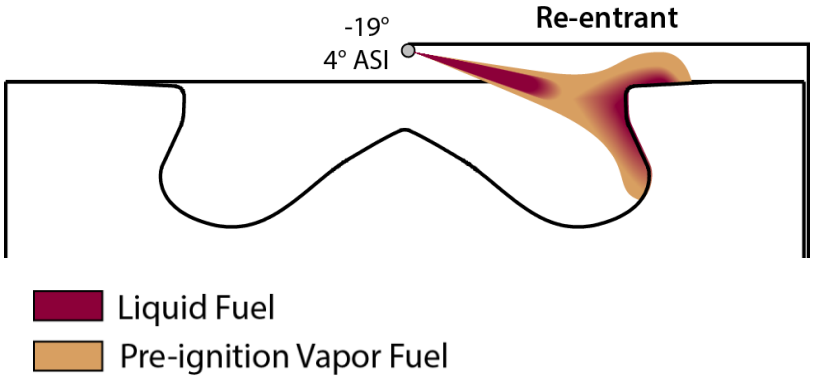

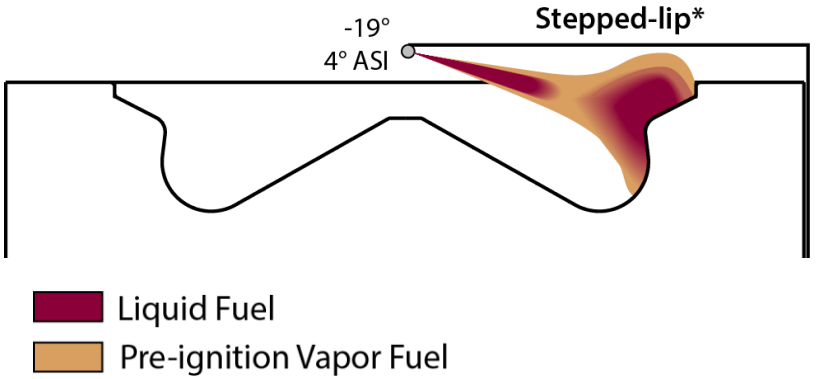

PLIF Experiments in the SNL 0.48L light-duty single-cylinder optical engine

- Engine operation
  - 1500 rpm
  - Non-combusting, 0% O_2
  - Fuel: 42 vol% n-hexadecane + 58 vol% heptamethylnonane
  - Tracer: 0.5 weight% 1-methylnaphthalene
  - Swirl ratio: 2.2
- Illumination source
  - Nd:YAG, 4th harmonic (266 nm)
  - ~ 30 mJ/pulse (relative intensity measured for each shot)
  - Laser sheet thickness < 1 mm
- Imaging
  - PI-MAX4 ICCD camera (gain = 15)
  - Nikon UV-105 lens (f/16)
  - WG-295 long pass filter

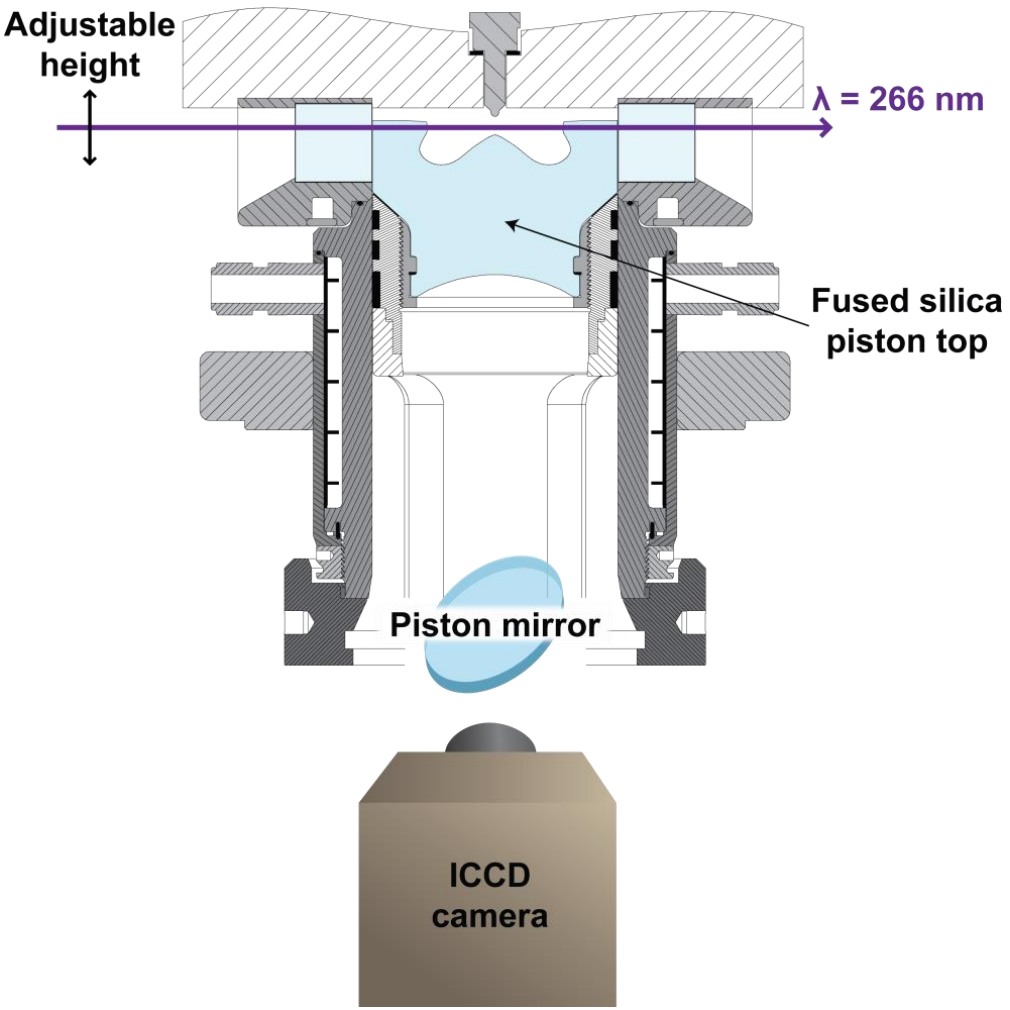

PLIF setup: laser plane locations

- Plane 1 (P1) is set half of squish height
- Plane 2 (P2) is empirically determined
  - Re-entrant: at rim of bowl where laser sheet passes through with minimal deflection
  - Stepped-lip: 1.37 mm above the piston top
- Plane 3 (P3) is set deep within bowl
  - Re-entrant: 9.88 mm below the piston top
  - Stepped-lip: 8.98 mm below the piston top
- P2 and P3 move with the piston as crank angle changes.

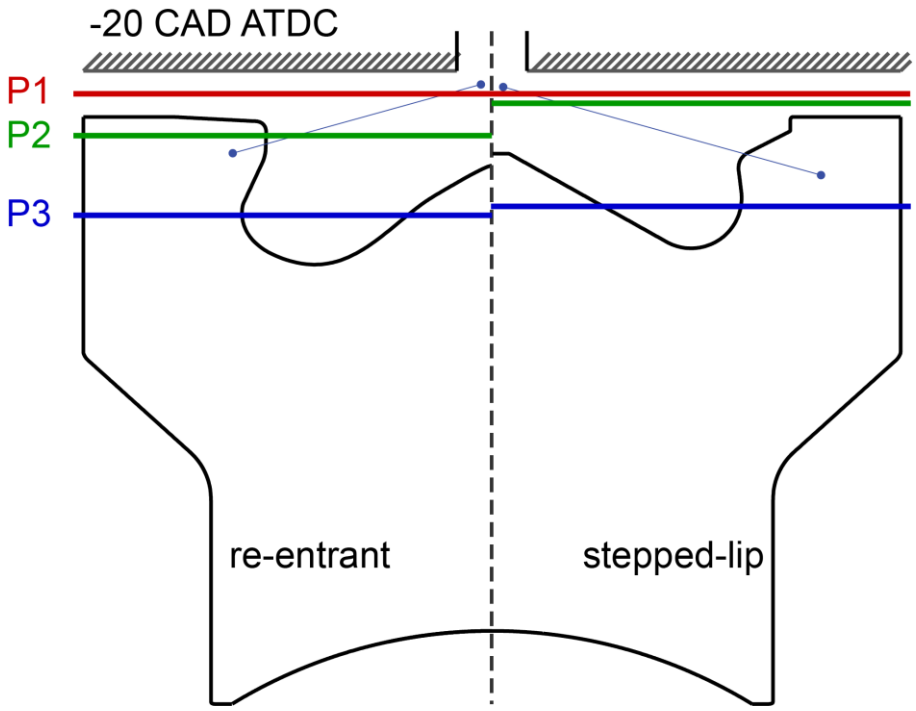

PLIF: data collection and processing

- Three sets of images for a given crank angle, plane, and operating point (51 images per set)
  - Background (no fuel injection)
  - Flat-field (6/8 injections in intake stroke)
  - Fuel injection image (desired operating point)
  - Fuel injection Image sets taken over range starting from injection ending prior to SOC.
- 9:15min's measurement schedule to maintain temperatures and pressures
- Distortion correction according to established ray-tracing routine

$$\chi_{fuel,d} = \chi_{fuel,cal} \frac{S_d}{S_{cal}} \frac{E_{cal}}{E_d} \frac{T_d}{T_{cal}} \frac{P_{cal}}{P_d} \frac{\sigma\eta(T_{cal})}{\sigma\eta(T_d)}$$

- $\chi_{fuel,d}$ = (moles nC16H34 + moles iC16H34 + moles 1MN) / (total moles of CO2, N2, nC16H34, iC16H34, and 1MN).

Uncertainties of PLIF measurements

- Dewarping-induced error in radial locations: measurements near chamber center (R<~7mm) is not reliable.
- Camera nonlinearity at high intensities.
- Beam steering effects start to show up in squish region when piston is within ±15 CAD around TDC.
- Plumes facing the coming laser produce more reliable measurements.
  - Injector shadow caused by the laser interference.
  - Out-of-plane fluorescence signal from liquid brought by laser scattering and background reflections.
  - Signal trapping, fluorescence from laser light reflected off chamber surfaces.

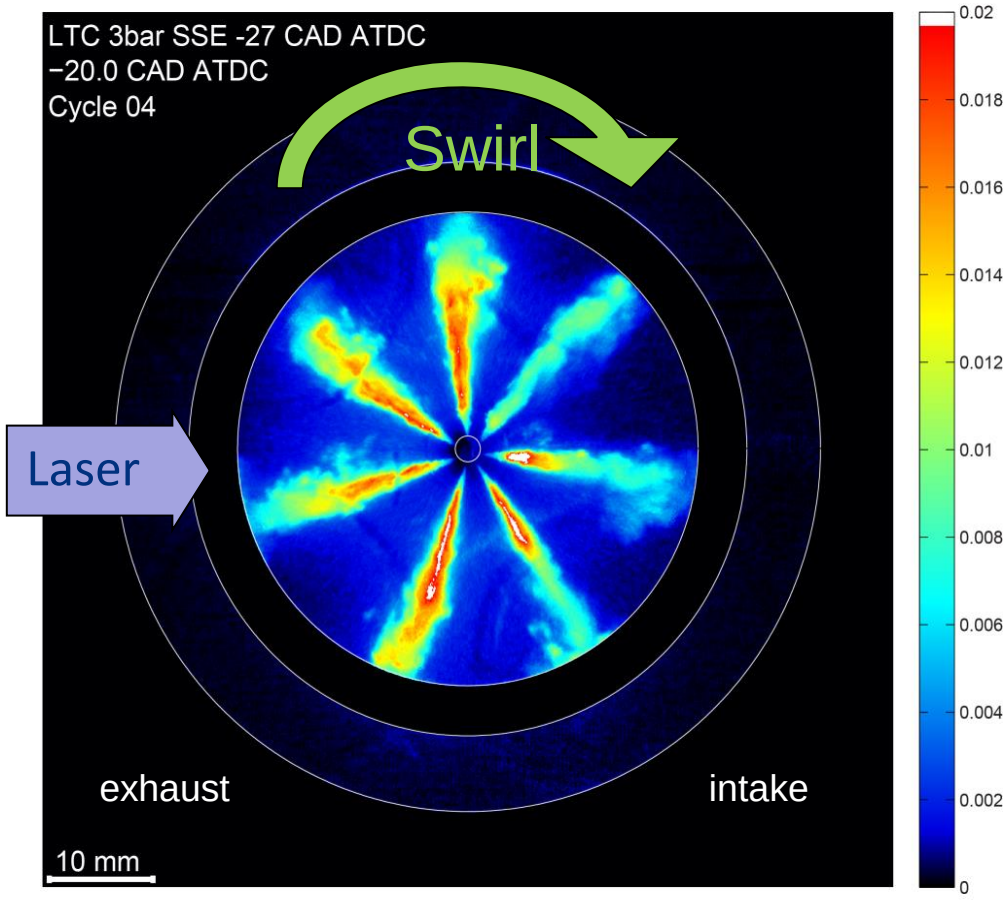

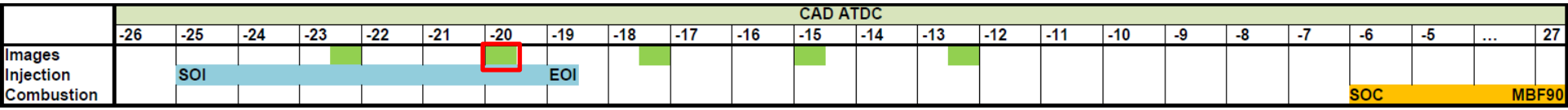

Points of interest for optical investigation

Single-injection, EGR-diluted LTC regime

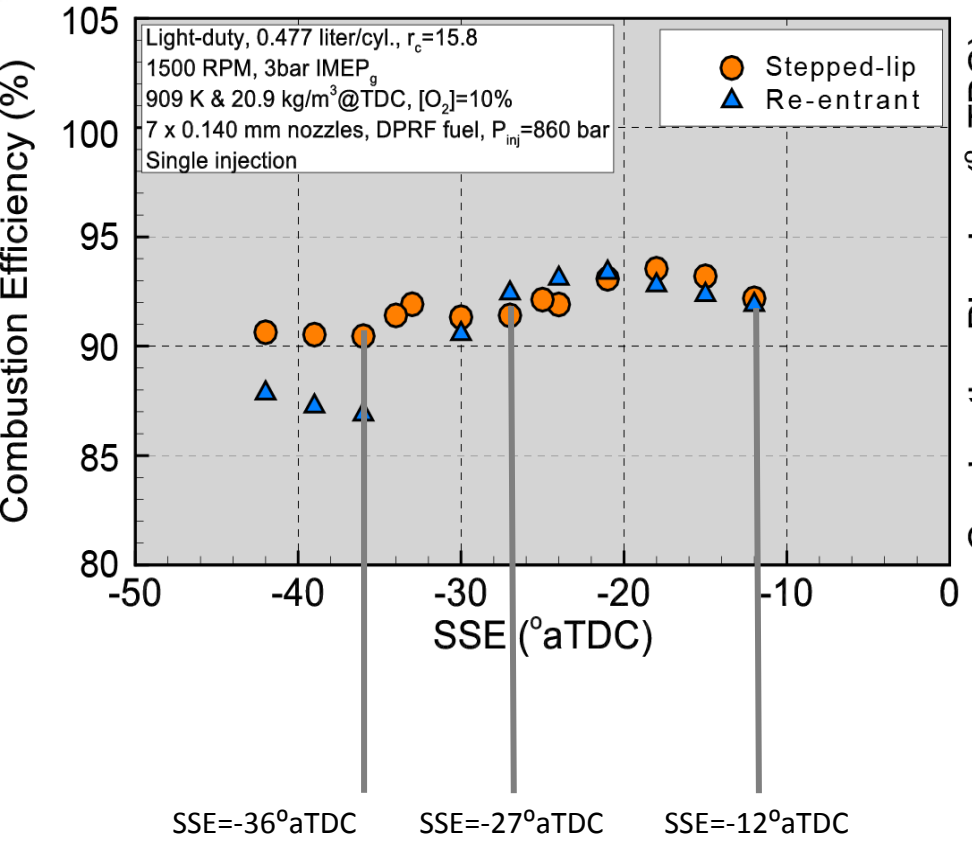

Double-injection, conventional combustion

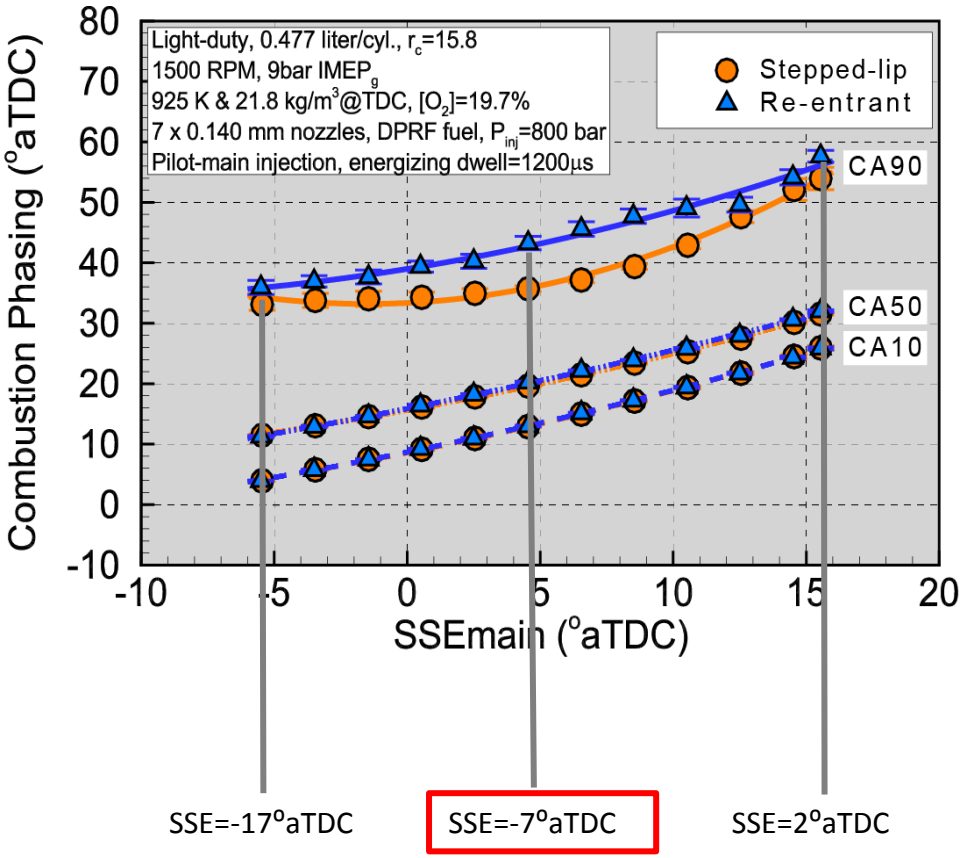

Is there a simple metric to quantify piston geometry impact on in-cylinder mixture preparation?

Re-entrant Bowl

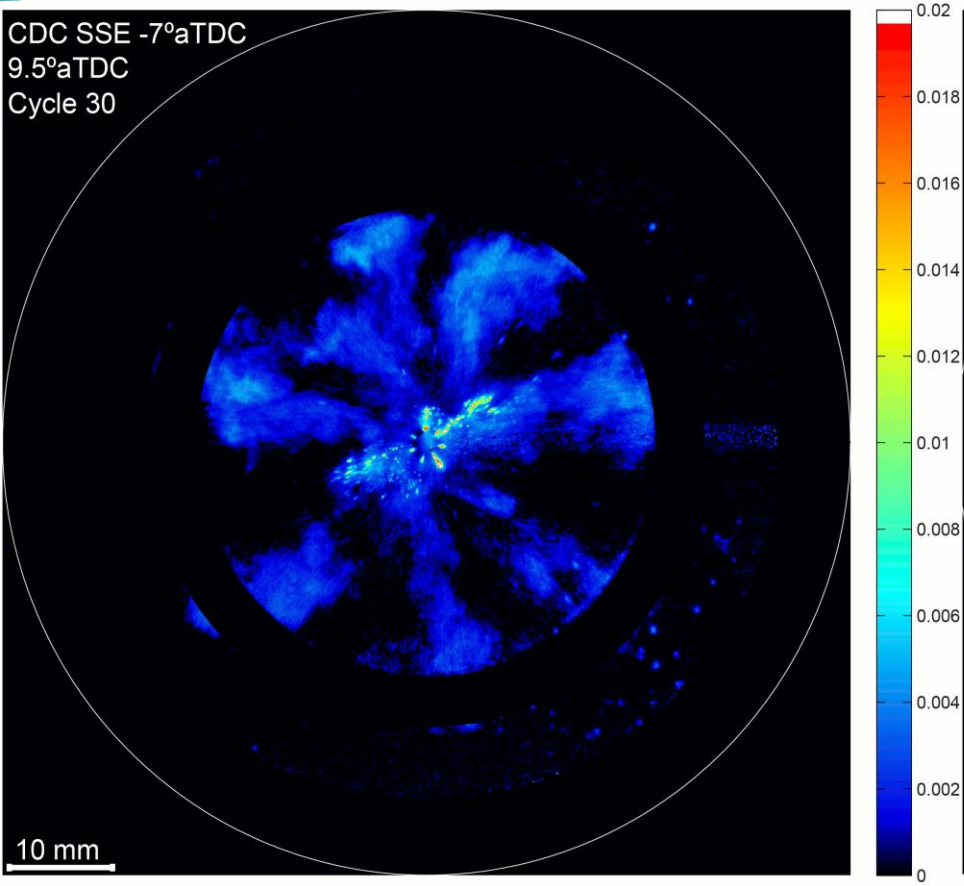

Stepped-lip Bowl

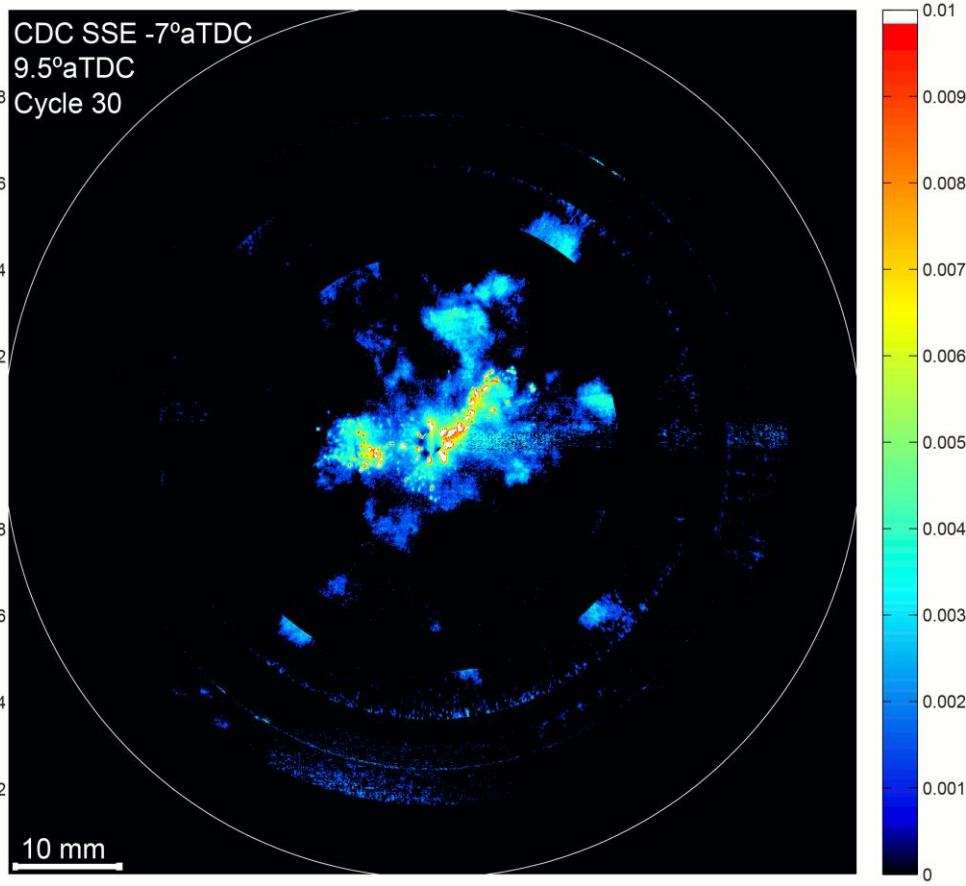

Area-averaged fuel mole fraction is calculated in polar coordinates to quantify spray-dominated mixture preparation pattern.

$\chi_{fuel,d}$

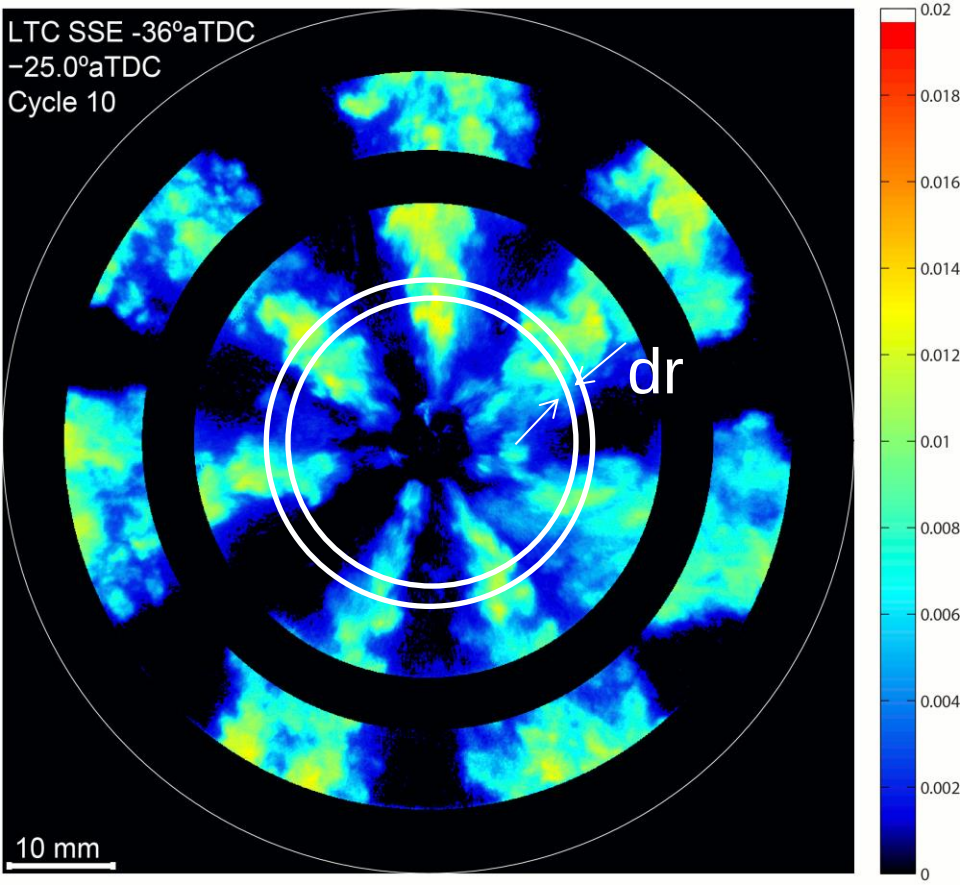

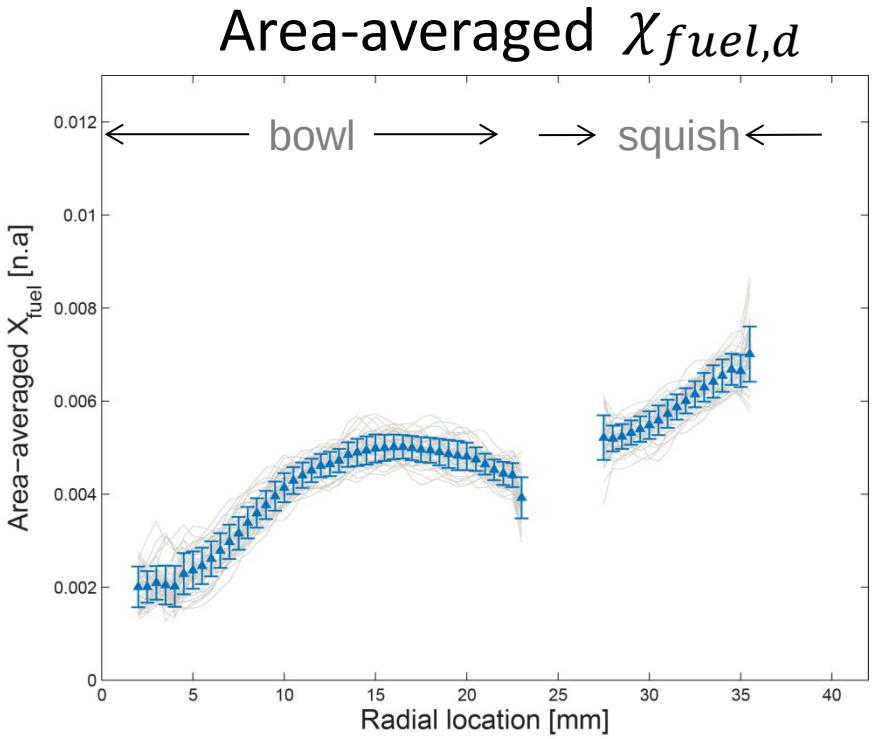

Error bar marks ±σ out of 50 realizations

High $\chi_{fuel,d}$ observed in lip region implies better air utilization with stepped-lip piston geometry.

$\chi_{fuel,d}$

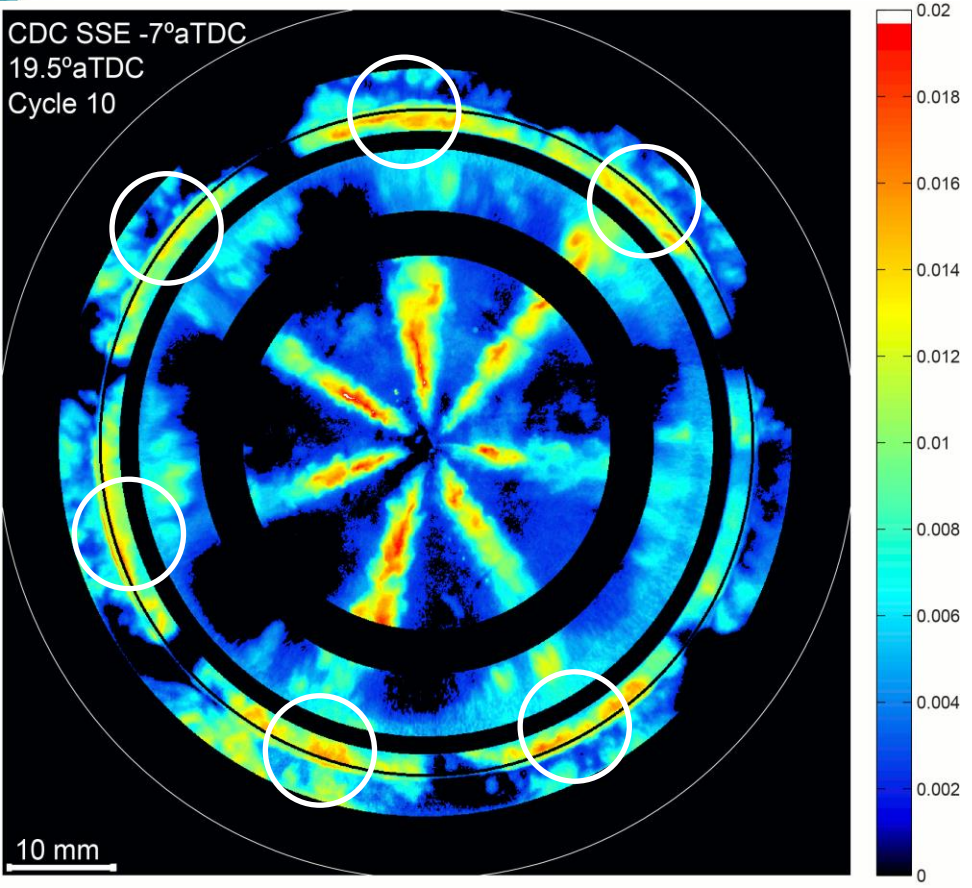

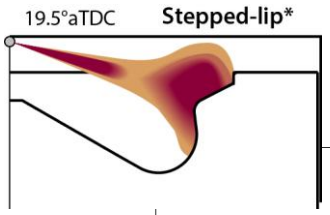

Area-averaged $\chi_{fuel,d}$

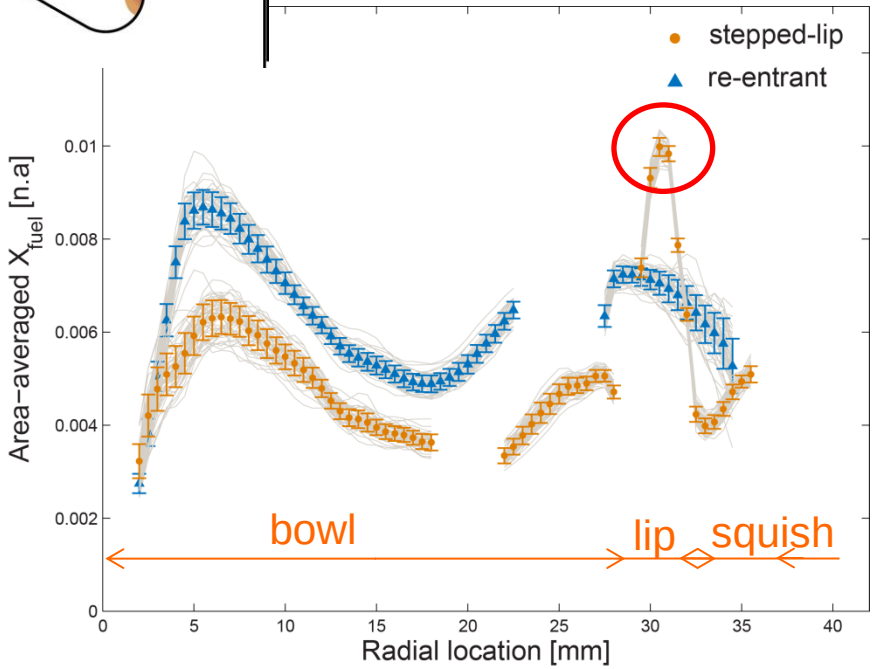

Error bar marks ±σ out of 50 realizations

Area-averaged fuel mole fraction with re-entrant bowl under CDC regime

Re-entrant Bowl $\chi_{fuel,d}$

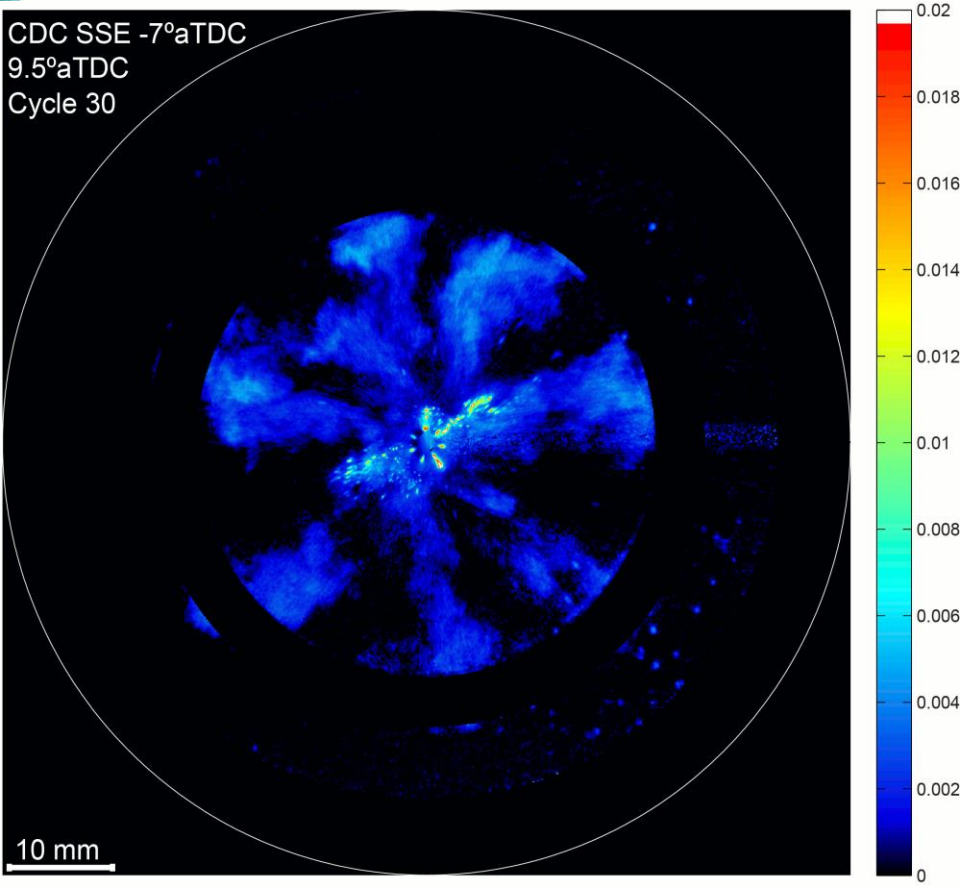

Area-averaged $\chi_{fuel,d}$

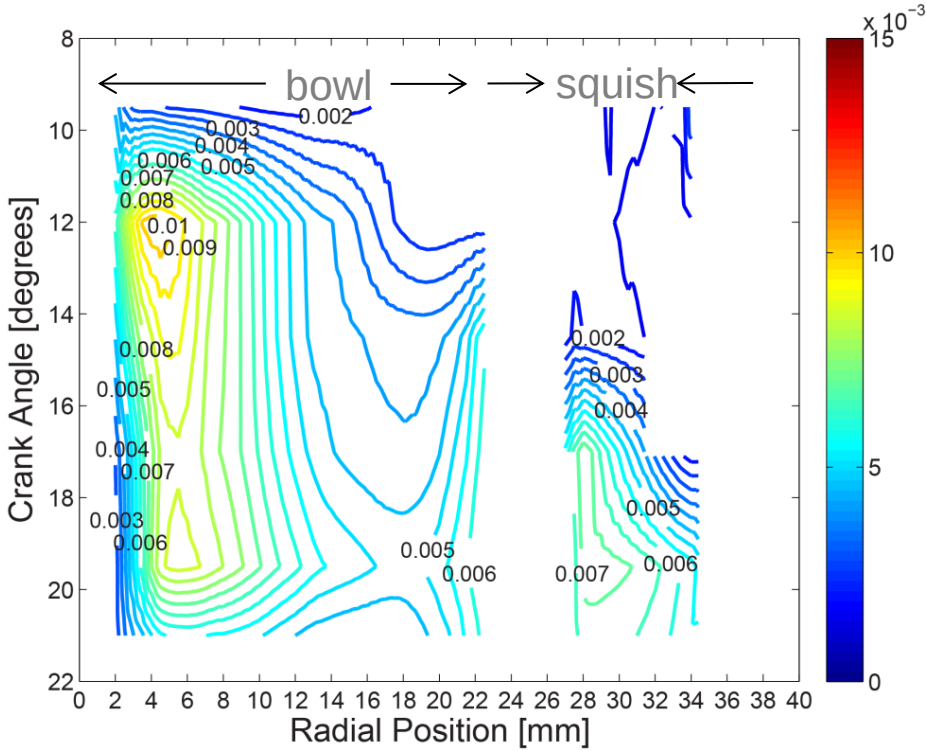

Area-averaged fuel mole fraction with stepped-lip bowl under CDC regime

Stepped-lip Bowl $\chi_{fuel,d}$

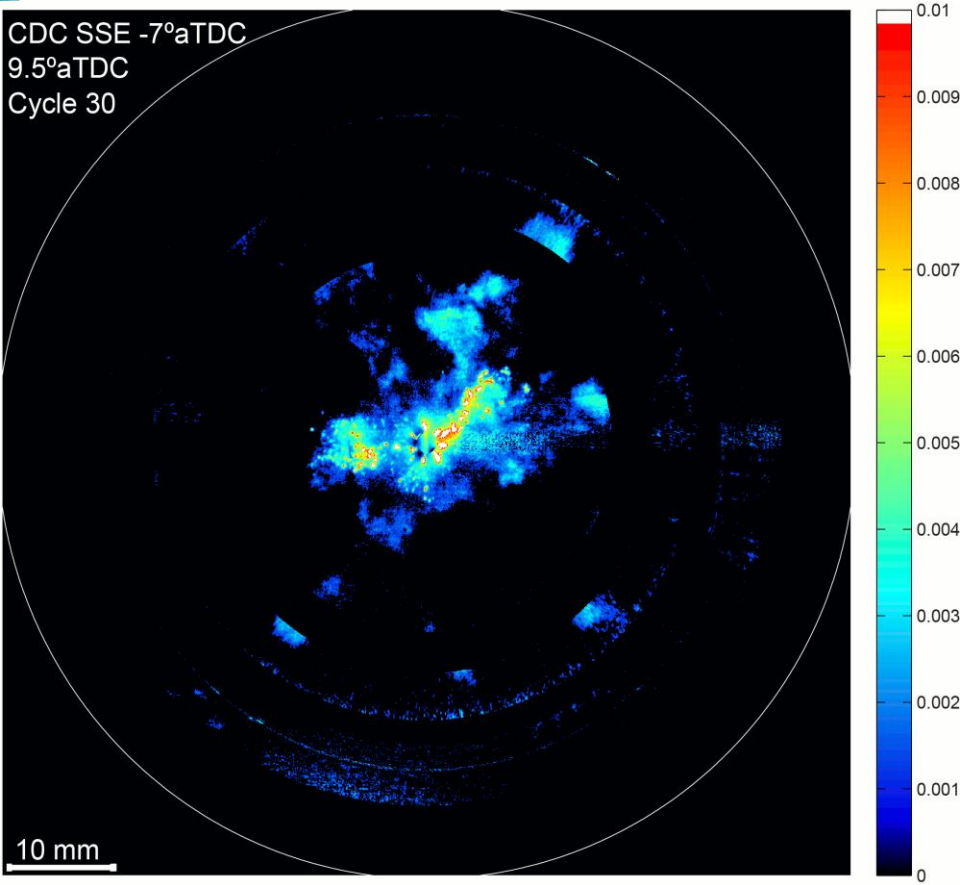

Area-averaged $\chi_{fuel,d}$

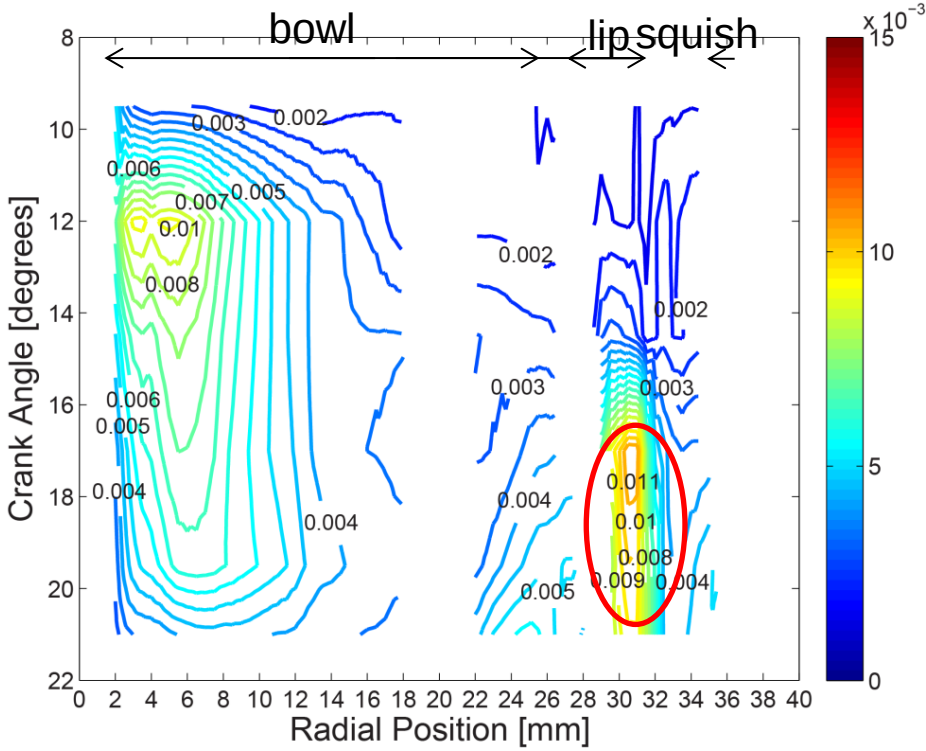

High $\chi_{fuel,d}$ is observed in lip region!

Conclusion - Stepped-lip geometry results in localized high fuel concentration on lip shoulder, which implies better air utilization.

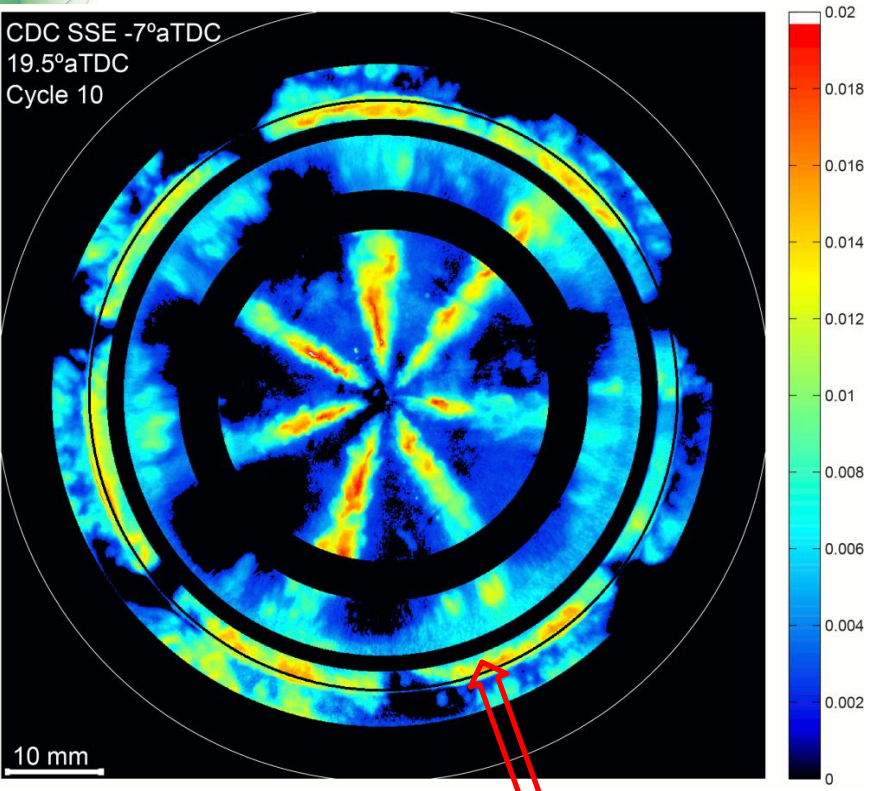

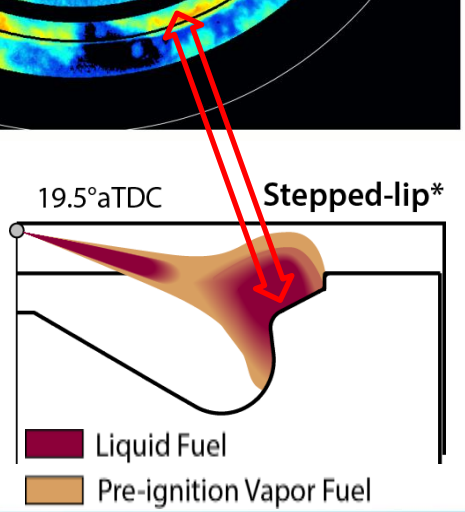

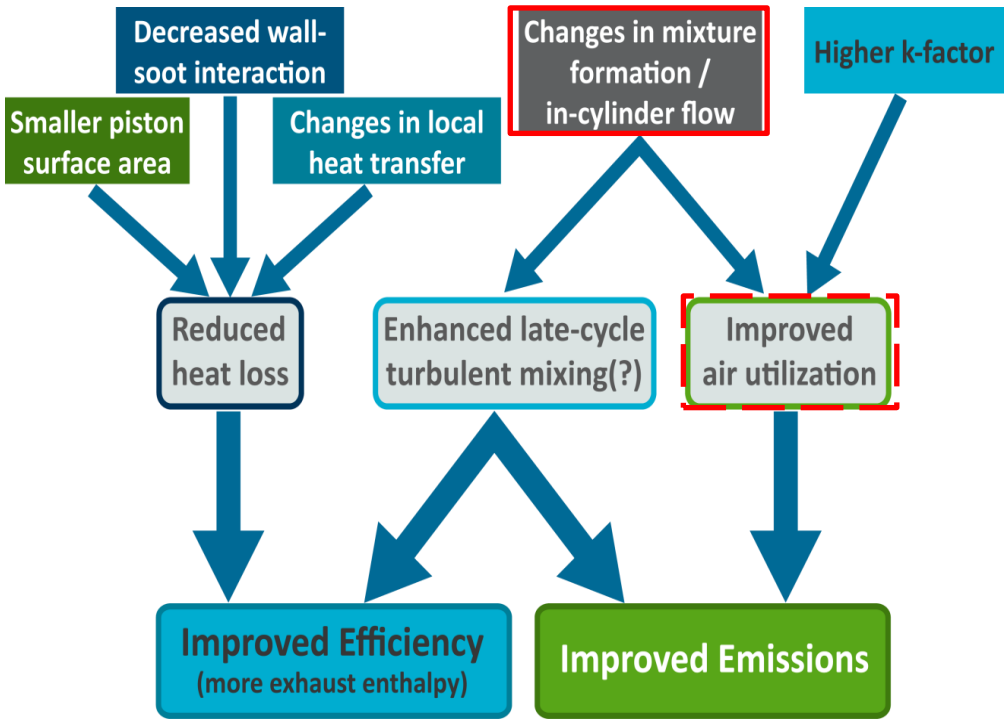

Outline

- Motivation
- High-speed in-cylinder soot optical thermometry
- Particle image velocimetry (PIV) inside an optical engine for swirl asymmetry quantification
- Quantification of in-cylinder mixture preparation with fuel tracer planar laser-induced fluorescence (PLIF) technique
- **Research outlook**

Advanced ICEs Efficiency Scientific & Engineering Challenges

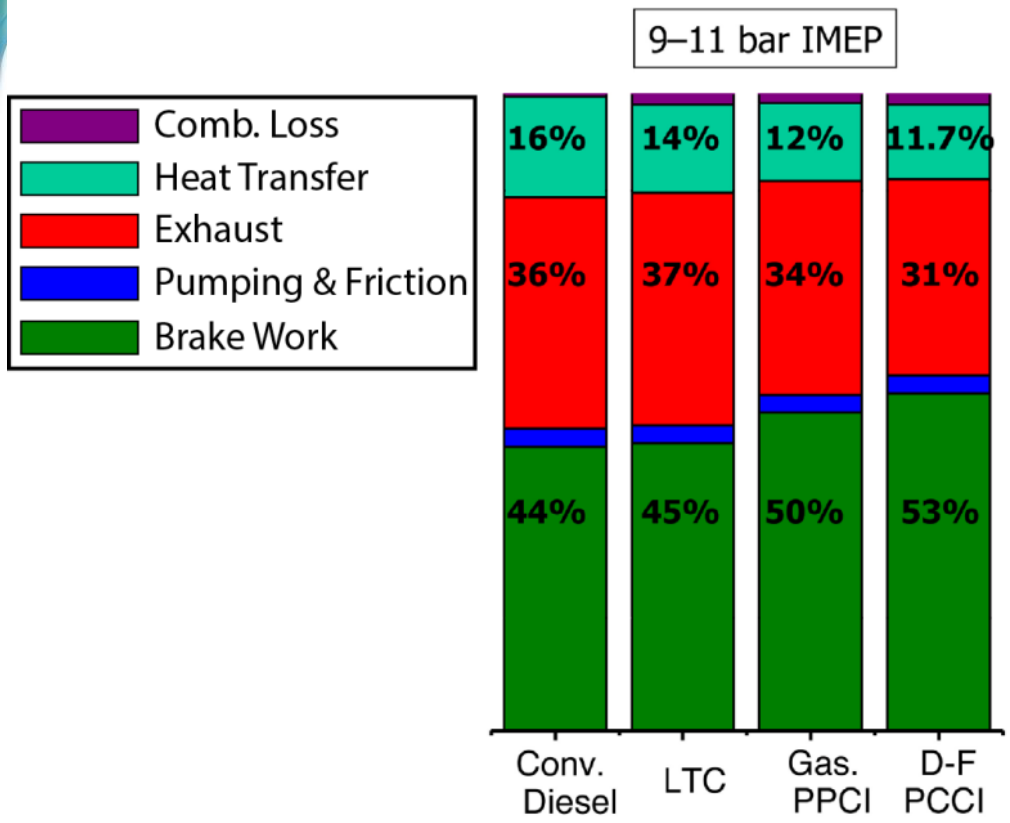

[2] Adapted from David Foster (UW), Transportation Combustion Engine Efficiency Colloquium, 2010 and Paul C. Miles (Sandia), SAND2013-7374c

Heat Transfer

Flow
- Mean flows (Swirl, Tumble)
- Turbulence

Temperature & Composition
- CR
- Lambda
- EGR
- Combustion Phasing/Duration
- Soot radiation

Chamber Geometry
- Chamber shape
- Bowl shape (re-entrant, shallow bowl)

Exhaust Losses

Work Extraction
- Combustion Phasing/Duration
- Charge Composition (lean, EGR)

Linked to Heat Transfer
- Interacts with gas properties to impact work extraction

Low-temperature combustion systems achieve greater premixing and lower peak temperatures.

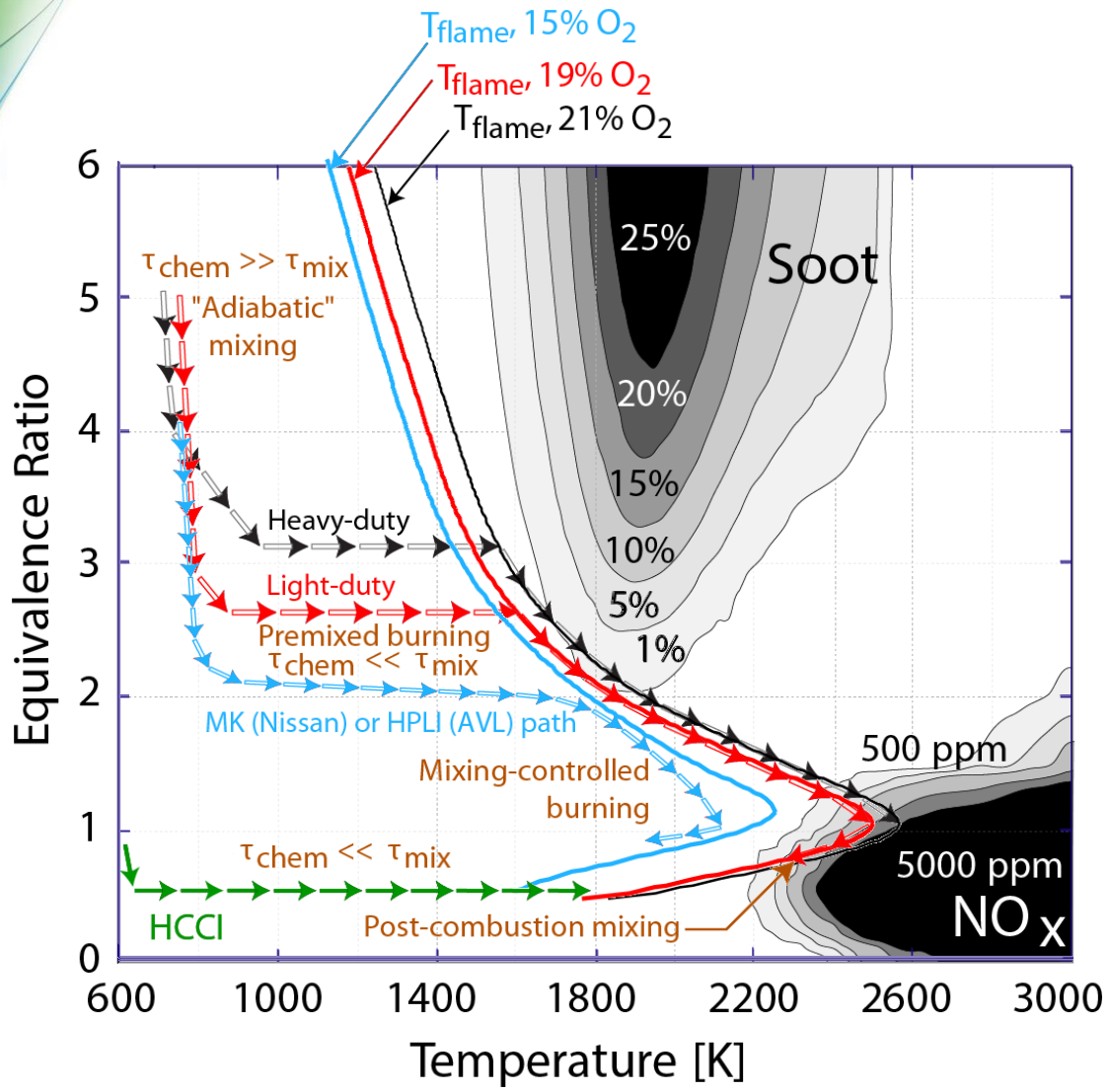

- Mixing processes influence the combustion path.
- Large path changes are obtained when the mixing time scales less than the chemical time scales.
- Greater premixing is achieved using:
  - High injection pressure
  - Boost
- Lower peak temperature are achieved with low ambient temperatures (low CR, late-injection) and high EGR rates.

[4] Adapted from Paul Miles (Sandia), 3rd International Symposium on Homogeneous Charge Compression Ignition (HCCI), 2006

Acknowledgements

Financial support from DOE Office of Vehicle Technology and U.S. Army TARDEC are greatly acknowledged.

Acknowledgements

DOE Office of Vehicle Technologies, Gurpreet Singh, Leo Breton

U.S. Army TARDEC, Peter Schilh

Sandia combustion scientists, Paul C. Miles and Stephen Busch

Sandia post-docs and visiting scholars, W. Ethan Eagle, Louis-Marie Christian Malbec, Julien Luc Manin, Brian Riley Peterson, Wei Zeng; Cheolwoong Park, Xu He.

Sandia R&D Technologist, Ken St. Hilaire and Tim Gilbertson

University of Wisconsin-Madison, Federico Perini, Rolf D. Reitz

General Motors, Alok Warey, Dick Peterson

Ford Motor Company, Benjamin Petersen

Convergent Science, Inc. Sameera Wijeyakulasuriya, Saurav Mitra, P. K. Senecal

Wayne State University, Xin Yu, Xi Luo, Ming-Chia Lai, Marcis Jansons

Lund University, N.-E. Olofsoon, Henrik Bladh, Per-Erik Bengtsson

University of New South Wales, Sanghoon Kook

Thank you for your attention !
Any questions?

BACKUP SLIDES

Petroleum-fueled IC engines are important solutions for *propulsion* purpose in Industrial and Transportation sectors.

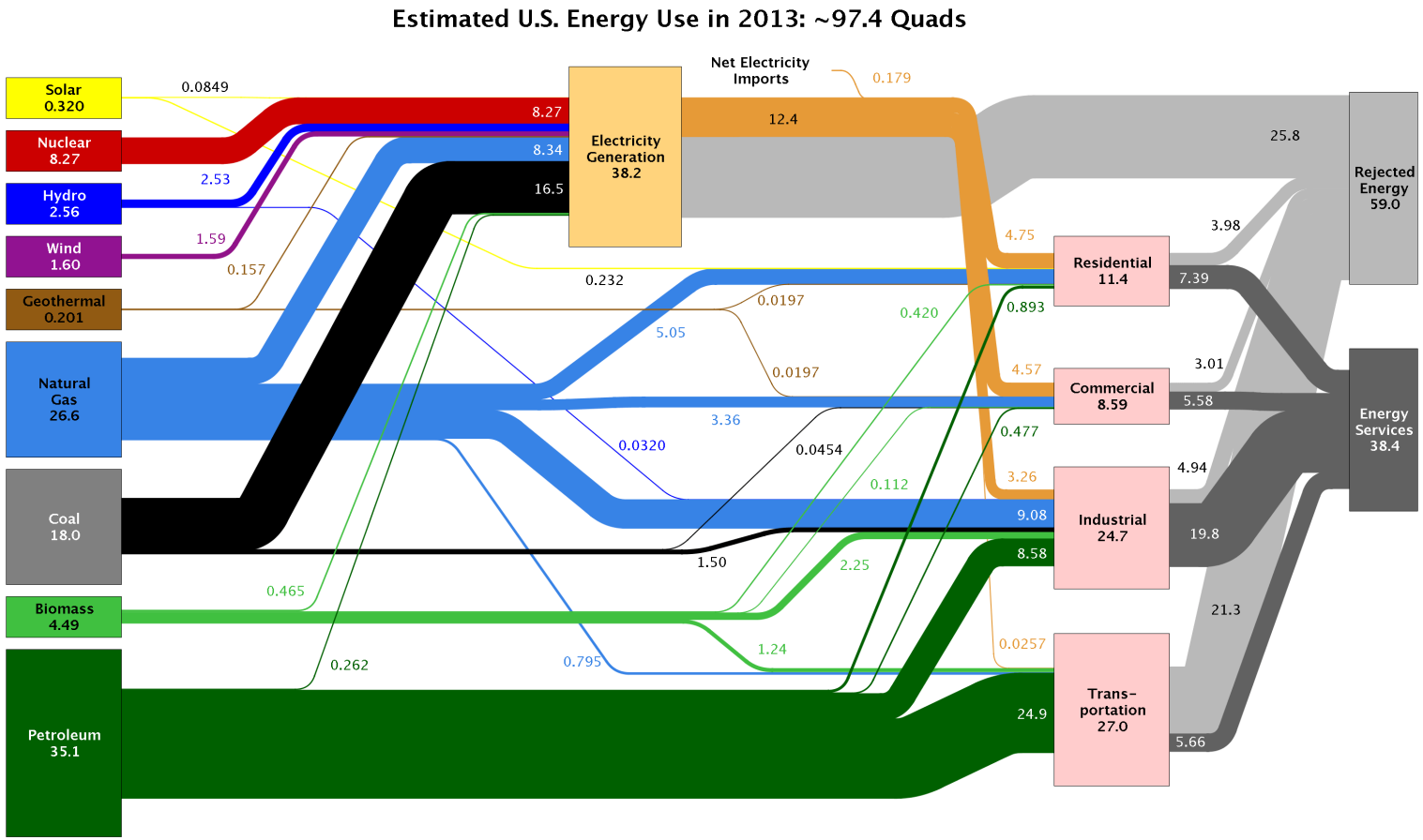

Source: LLNL 2014. Data is based on DOE/EIA-0035(2014-03), March, 2014. If this information or a reproduction of it is used, credit must be given to the Lawrence Livermore National Laboratory and the Department of Energy, under whose auspices the work was performed. Distributed electricity represents only retail electricity sales and does not include self-generation. EIA reports consumption of renewable resources (i.e., hydro, wind, geothermal and solar) for electricity in BTU-equivalent values by assuming a typical fossil fuel plant "heat rate." The efficiency of electricity production is calculated as the total retail electricity delivered divided by the primary energy input into electricity generation. End use efficiency is estimated as 65% for the residential and commercial sectors 80% for the industrial sector, and 21% for the transportation sector. Totals may not equal sum of components due to independent rounding. LLNL-MI-410527

PIV Particle Fidelity Check

- Aerosol → size ~= 1 µm, Mie-scattering signal is too weak to image through the piston
- Lycopodium spores → size =32 µm, low ring friction, but induces large lag error
- Porous SiO_2
- 2 µm, small lag error, but creates ring friction problems
- 18 µm, lag error during early intake, and ring friction problems
- **<u>2 µm Porous SiO_2</u>** yields an acceptable flow tracing accuracy with errors < 1%.

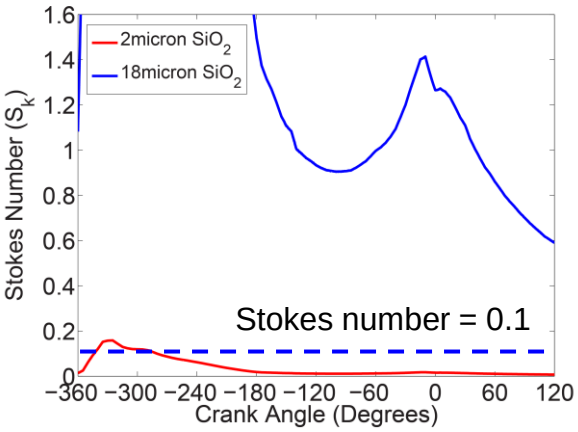

Porous SiO_2 (**18 µm**)

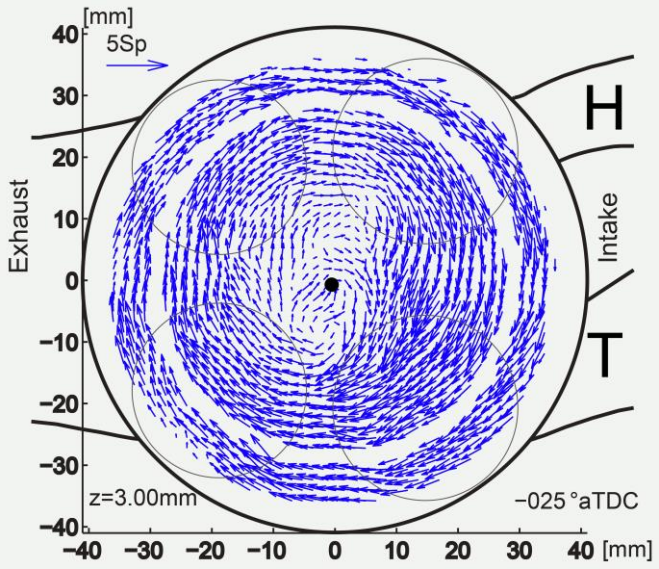

Porous SiO_2 (**2 µm**)

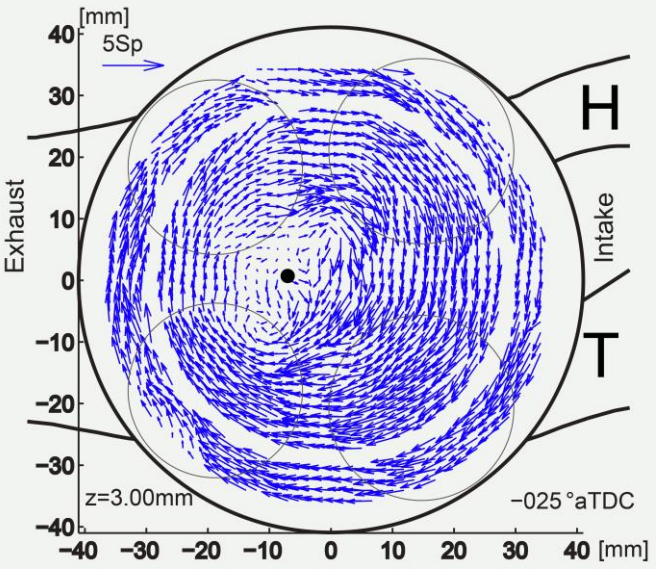

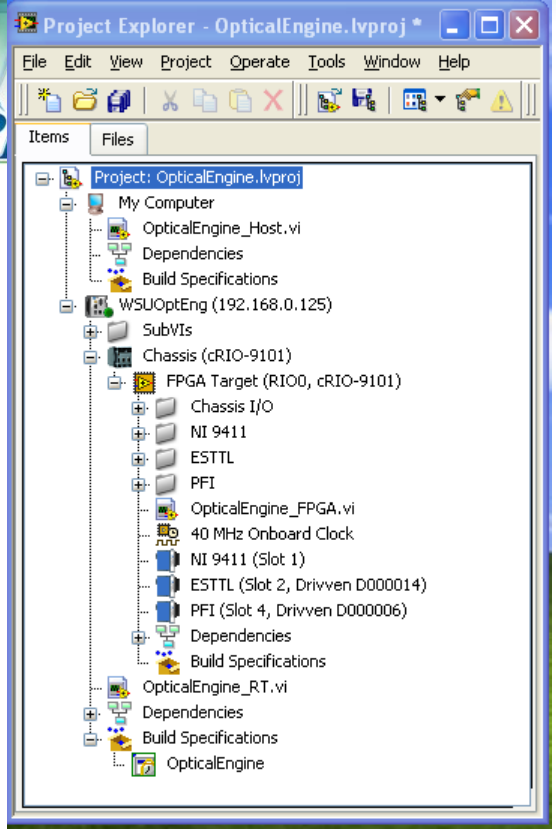

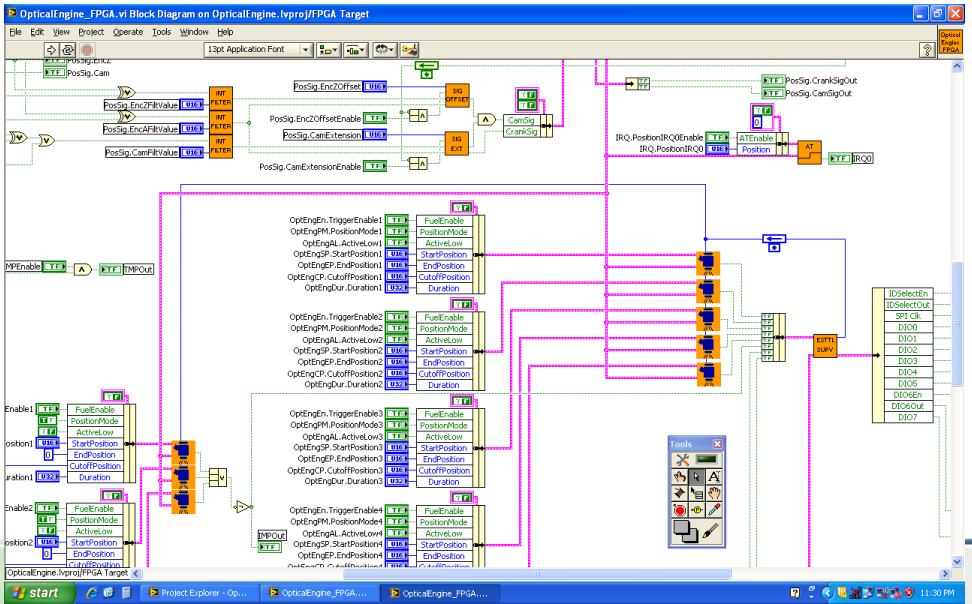

NI cRIO FPGA Controller

In-cylinder Injection (Solenoid, Piezo-electric)

Cameras (PI-MAX2/3, Phantom)

PFI Injection

Pulse Generator (Stanford DG535)

Nd: YAG Laser

Dye Laser

Laser Beam Shutter (Thorlabs, SH05)

Chopper Wheel

Fuel Wall Impingement and Temperature-Controlled Evaporation Rates

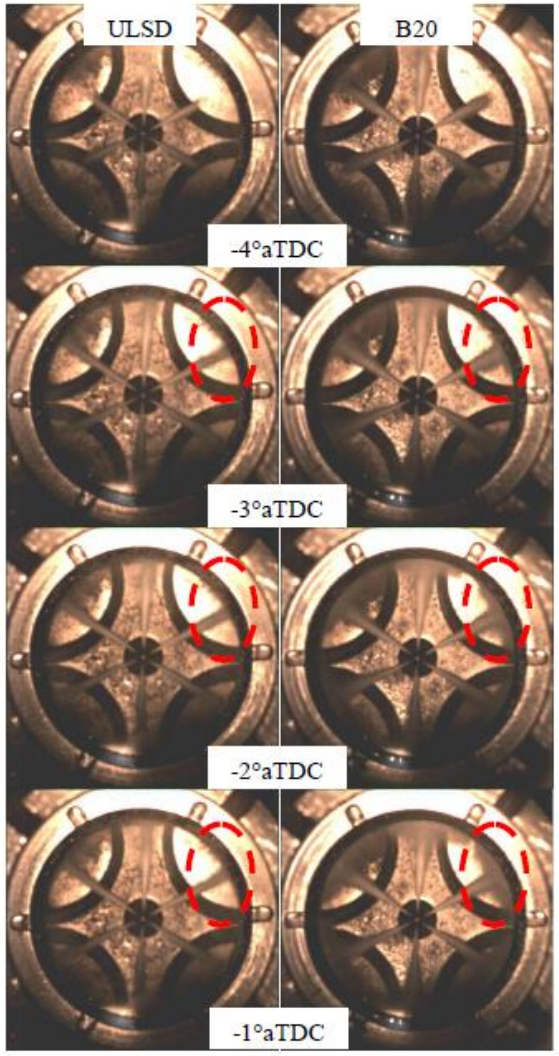

ULSD Fuel

B20 Biodiesel

24°aTDC

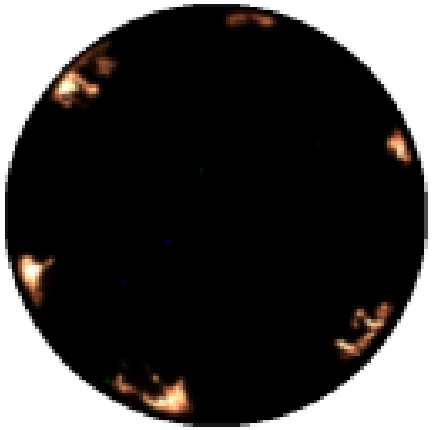

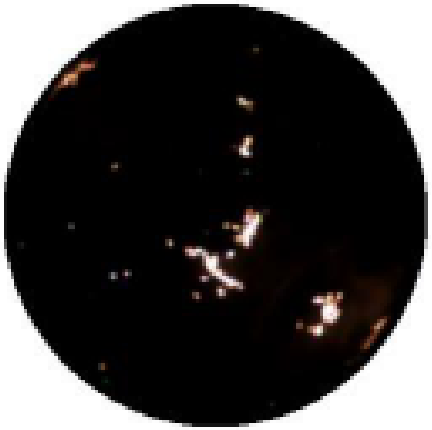

- Wall fuel impingement results in sooty pool burning
- Wall film evaporation controlled by surface temperature
- The ratio of splash mass to impinging mass increases with Weber number (Grover *et al*. "A spray wall impingement Model Based Upon Conservation Principles.")

$$We = \frac{\rho v^2 D}{\sigma}$$

Biodiesel has higher SMD [8]
Biodiesel has higher surface tension [9]

[8] Lee, Chang Sik; Park, Sung Wook; Kwon, Sang Il "An Experimental Study on the Atomization and Combustion Characteristics of Biodiesel-Blended Fuels" Energy & Fuels, **19**, pp. 2201-2208, 2005

[9] McCrady, Johnathon P.; Stringer, Valerie L.; Hansen, Alan C. and Lee, Chia-fon F. "Computational Analysis of Biodiesel Combustion in a Low-Temperature Combustion Engine" SAE Technical Paper, 2007-01-0617, 2007

Apparent Rate of Heat-Release Analysis

The First Law Thermodynamics for open system:

$$dU = \delta Q - \delta W + h_f dm_f - h_{cr} dm_{cr}$$

m_f mass of injected fuel

m_{cr} mass of gas lose to crevices

$$\delta Q = \delta Q_{ch} - \delta Q_{ht}$$

$$\delta W = pdV$$

$$dU = mc_v dT + u \cdot dm = mc_v dT + u\left(dm_f - dm_{cr}\right)$$

$$\delta Q_{ch} = mc_v dT + \left(u - h_f\right) dm_f - \left(u - h_{cr}\right) dm_{cr} + pdV + \delta Q_{ht}$$

$$\delta Q_{ch} - \delta Q_{ht} - \left(u - h_f\right) dm_f + \left(u - h_{cr}\right) dm_{cr} = mc_v dT + pdV$$

From the ideal gas law, if R is constant,

$$pV = mRT \quad \Rightarrow \quad \frac{dp}{p} + \frac{dV}{V} = \frac{dT}{T}$$

$$\delta Q_{ch} - \delta Q_{ht} - \left(u - h_f\right) dm_f + \left(u - h_{cr}\right) dm_{cr} = \frac{\gamma}{\gamma - 1} p \frac{dV}{d\theta} + \frac{1}{\gamma - 1} V \frac{dp}{d\theta}$$

$$\delta Q_{ch} - \delta Q_{ht} - \left(u - h_f\right) dm_f + \left(u - h_{cr}\right) dm_{cr} = \frac{\gamma}{\gamma - 1} p \frac{dV}{d\theta} + \frac{1}{\gamma - 1} V \frac{dp}{d\theta}$$

Gas loses to crevices

Fuel delivered into chamber

Heat-transfer rate to the walls

Gross heat-release rate

γ approximation is made by fit exponent n for
the compression of the unburned mixture prior to combustion
and
the expansion of burned gases following the end of combustion,
assuming these two are isentropic processes.

$$pV^n = constant \quad [7]$$

[7] Heywood, John B., "INTERNAL COMBUSTION ENGINE FUNDAMENTALS", McGraw-Hill Science/Engineering/Math, 1988